

Reliability of structures exposed to traffic and environmental loads

Mariia Nesterova

► To cite this version:

Mariia Nesterova. Reliability of structures exposed to traffic and environmental loads. Civil Engineering. Université Paris-Est, 2019. English. NNT : 2019PESC2056 . tel-02438396v2

HAL Id: tel-02438396

<https://hal.archives-ouvertes.fr/tel-02438396v2>

Submitted on 18 Feb 2020 (v2), last revised 27 Feb 2020 (v3)

HAL is a multi-disciplinary open access archive for the deposit and dissemination of scientific research documents, whether they are published or not. The documents may come from teaching and research institutions in France or abroad, or from public or private research centers.

L'archive ouverte pluridisciplinaire **HAL**, est destinée au dépôt et à la diffusion de documents scientifiques de niveau recherche, publiés ou non, émanant des établissements d'enseignement et de recherche français ou étrangers, des laboratoires publics ou privés.

Reliability of structures exposed to traffic and environmental loads

THÈSE

pour obtenir le grade de

Docteur de l'Université Paris-Est

présentée par

Mariia NESTEROVA

le 25 octobre 2019

JURY

| | | |
|-----------------------------|-----------------------------|-------------------|
| <i>Président du jury :</i> | Professeur, IFMA | Maurice LEMAIRE |
| <i>Examineur :</i> | Professeur, EPFL | Eugen BRÜHWILER |
| <i>Rapporteur :</i> | Professeur, ULiège | Vincent DENOËL |
| <i>Rapporteur :</i> | Maître de conférences, INSA | Béatrice FAVERJON |
| <i>Encadrant :</i> | Dr, IFSTTAR | Franziska SCHMIDT |
| <i>Directeur de thèse :</i> | Professeur, UPEM | Christian SOIZE |



« There's nothing I believe in more strongly than getting young people interested in science and engineering, for a better tomorrow, for all humankind. »

Bill Nye

A handwritten signature in blue ink that reads "Bill Nye". The signature is written in a cursive, flowing style with a large initial 'B' and a stylized 'N'.

University Paris-Est Marne-la-Vallée

Doctoral School of Science, Engineering and Environment

Reliability of structures exposed to traffic and environmental loads

Mariia NESTEROVA

Abstract

The Thesis is dedicated to reliability analysis of the deck of Millau viaduct, a cable-stayed bridge located in Southern France. The main interest is the extrapolation in time of loads and load effects affecting the bridge in order to observe the reliability of chosen elements during the operational life of the structure.

Millau viaduct is a complex unique bridge of French road infrastructure in the early stage of its life. It is important to be able to predict possible extreme loads on the deck of the bridge due to traffic growing in volume or weight. Such predictions require data from monitored actions or load effects in elements of the bridge. Large-scale structures need an enormous amount of data, that is not easy to obtain, to store and to analyze. It leads to another challenge - predictions based on limited time and accessible monitoring data.

In the current work, predictions for traffic loads are done using provided data from bridge Weigh-in-Motion (BWIM) traffic monitoring for the case of the the ultimate limit state (ULS). For load extrapolation in time, several methods of Extreme Value Theory (EVT) are compared, with the most attention to the Peaks Over Threshold (POT) approach. Moreover, a contribution to existing methods for threshold choice, as the main challenge of POT approach, is made.

In large cable-stayed bridges, not necessarily traffic is the leading action, but environment loads can have similar or superior effect. The focus of this work is on the deck of Millau viaduct, therefore, static wind loads obtained from structural health monitoring (SHM) of the viaduct are considered in combination with queues of traffic lorries. A probabilistic model is made to observe probabilities of extreme cases for both actions and their combination. As well, the influence of monitoring duration on confidence intervals for return levels of loads is studied.

For the steel orthotropic deck of the bridge, both, local effects caused by passing vehicles and global effects, contribute to values of stresses. Global effects are coming from traffic queues on both lanes and static wind in a perpendicular direction. In this Thesis, finite element model (FEM) of the deck is performed in order to assess stresses in the deck. That brings a possibility to make predictions for the fatigue limit state too.

Usually, fatigue damage accumulated in a chosen part of the deck during a monitoring period is extrapolated in time linearly. The current work proposes a methodology to extrapolate numbers of fatigue cycles in time with the POT approach, which accounts for a change in traffic in volume and weight with time. Comparison of the proposed approach with the classical method is made and used in the fatigue reliability analysis.

Reliability analysis is made as well for the ULS in order to compare the results obtained from several EVT approaches, to observe the importance of wind actions on the reliability of the deck, and to compare EVT-based predictions with design load models of European Norms (EN) for traffic and wind.

Keywords :

Reliability, traffic loads, wind loads, fatigue, extreme effects, combination, Millau, viaduct, bridge, operational life, EVT, Extreme Value Theory, WIM, Weigh In Motion

Université Paris-Est Marne-la-Vallée

L'école doctorale Sciences, Ingénierie et Environnement

Fiabilité de structures soumises aux actions du trafic et aux sollicitations naturelles

Mariia NESTEROVA

Résumé

Cette thèse est consacrée à l'analyse de la fiabilité du tablier du viaduc de Millau, un pont à haubans situé dans le sud de la France. Le but principal est d'extrapoler dans le temps les charges et les effets de charges sur le pont afin d'observer la fiabilité de différentes parties de la structure pendant sa durée de vie.

Le viaduc de Millau est une infrastructure routière française, complexe et unique, qui est en début de vie. Il est important de pouvoir prévoir les charges extrêmes possibles sur le tablier du pont en raison de l'augmentation du volume ou du poids des véhicules. De telles prévisions nécessitent des données mesurées sur l'ouvrage, soit les charges ou actions, soit les effets de celles-ci. Les structures à grande échelle ont besoin d'une grande quantité de données, qu'il est difficile d'obtenir, de stocker et d'analyser. Cela pose un autre défi : les prévisions basées sur un temps limité et des données de surveillance accessibles.

Les prévisions de charges de trafic dans ce travail sont effectuées à l'aide des données fournies par la surveillance du trafic du système BWIM pour le cas d'état limite ultime. Pour l'extrapolation de charge dans le temps, plusieurs méthodes de la théorie des valeurs extrêmes (EVT) sont comparées, une attention particulière étant accordée à l'approche POT. De plus, une contribution aux méthodes existantes pour le choix du seuil, en tant que principal défi de l'approche de POT, est apportée.

Dans les grands ponts à haubans, le trafic n'est pas nécessairement l'action principale, mais les charges climatiques peuvent avoir un effet similaire ou supérieur. Le centre de ce travail est le tablier du viaduc de Millau. Par conséquent, la charge de vent statique obtenue à partir du système de surveillance de la santé structurelle du viaduc est considérée en combinaison avec les files de camions de circulation. Un modèle probabiliste est créé pour observer les probabilités de cas extrêmes pour les actions et leur combinaison.

De même, l'influence de la durée de surveillance sur les intervalles de confiance pour les niveaux de retour de charges est étudiée.

Dans le détail du tablier orthotrope en acier, les effets locaux causés par le passage de véhicules et les effets globaux contribuent à la valeur des contraintes. Les effets globaux proviennent des files des véhicules sur les deux voies de tablier et du vent statique dans une direction perpendiculaire. Dans cette thèse, un modèle d'éléments finis du pont est créé afin d'évaluer les contraintes dans le pont. Cela offre également la possibilité de prévoir l'état limite de fatigue.

Habituellement, les dommages de fatigue accumulés dans un détail pendant la période de surveillance sont extrapolés linéairement. Le travail actuel propose une méthodologie pour extrapoler le nombre de cycles de fatigue dans le temps avec l'approche POT, qui prend en compte une variation du trafic en volume et en poids avec le temps. Une comparaison de l'approche proposée avec la méthode classique est effectuée et utilisée dans l'analyse de fiabilité en raison de fatigue.

Une analyse de fiabilité est également effectuée pour l'état limite ultime afin de comparer les résultats obtenus avec plusieurs approches de EVT, d'observer l'importance des actions du vent sur la fiabilité du tablier et de comparer les prévisions basées sur EVT avec les modèles de charge de calcul des normes Européennes pour le trafic et le vent.

Mots clef :

Fiabilité, actions du trafic, actions du vent, fatigue, les effets extrêmes, combinaison, Millau, viaduc, pont, durée de vie, Théorie des Valeurs Extrêmes, WIM, charges en mouvement

Contents

| | |
|--|-------------|
| Abstract | iii |
| Résumé | v |
| Contents | vii |
| List of Figures | xi |
| List of Tables | xv |
| Abbreviations | xvii |
| Glossary | xix |
| List of Symbols | xxi |
| 1 Introduction | 1 |
| 1.1 Motivation | 2 |
| 1.2 Research objectives | 4 |
| 1.3 Literature review | 7 |
| 1.3.1 Studies on the reliability of existing bridges | 7 |
| 1.3.2 Traffic and wind loads in bridges, and their combination | 9 |
| 1.3.3 From measurements to predictions | 10 |
| 1.3.4 Extreme value theory for extrapolation of load effects | 11 |
| 1.3.5 The use of the Peaks-Over-Threshold approach | 15 |
| 1.4 Methodology | 17 |
| 1.5 Scientific contributions | 18 |
| 1.6 Plan of manuscript | 19 |
| 2 Methodology | 21 |
| 2.1 Applied reliability method for extrapolated load effects | 22 |
| 2.2 POT approach with the updated methodology for a threshold choice | 23 |

| | | |
|----------|---|-----------|
| 2.2.1 | Peaks Over Threshold approach | 23 |
| 2.2.2 | Confidence Intervals | 24 |
| 2.2.3 | POT for the reliability analysis | 25 |
| 2.2.4 | Threshold choice | 25 |
| 2.3 | Combination of load effects caused by live and environmental actions . . . | 27 |
| 2.4 | Comparison between different approaches for load extrapolation | 29 |
| 2.4.1 | Block maximum method | 29 |
| 2.4.2 | Rice formula | 30 |
| 2.5 | POT approach for numbers of fatigue cycles | 31 |
| 3 | Millau viaduct | 35 |
| 3.1 | Overview | 36 |
| 3.2 | Object description | 37 |
| 3.2.1 | Location of the viaduct | 37 |
| 3.2.2 | Geometry of the viaduct | 37 |
| 3.2.3 | Monitoring of traffic | 39 |
| 3.2.4 | Data collection for wind | 40 |
| 3.3 | Analysis of monitored traffic actions on the deck of the viaduct | 45 |
| 3.3.1 | Amount and stationarity of traffic | 45 |
| 3.3.2 | Vehicles types | 48 |
| 3.3.3 | Amplitude of load effects | 49 |
| 3.3.4 | Invalid input data and assumptions made in the current work | 52 |
| 3.3.5 | Extrapolating of monitored traffic actions in time with the POT ap- proach | 53 |
| 3.4 | Combination of traffic and wind actions | 60 |
| 3.4.1 | Computational model for global load effects | 60 |
| 3.4.2 | Probabilistic model | 62 |
| 3.4.3 | Return levels for wind and traffic actions and load effects | 63 |
| 3.4.4 | Combination of actions and comparison with load models from Eu- ropean standards | 64 |
| 3.5 | Extrapolation in time of the load effects in the deck | 67 |
| 3.5.1 | Finite Element Model | 67 |
| 3.5.2 | Return levels for local and global load effects based on several EVT approaches | 70 |
| | POT approach applied for stresses | 72 |
| | Block maximum approach for daily and weekly stresses | 73 |
| | Fitting Rice formula using the number of up-crossings | 75 |

| | | |
|----------|--|------------|
| 3.6 | Generalized Pareto Distribution for fatigue life estimation | 78 |
| 3.6.1 | Cycles counting based on BWIM data | 78 |
| 3.6.2 | Fatigue load model according to standards | 80 |
| 3.6.3 | Peaks over threshold approach for the number of stress cycles | 81 |
| 3.6.4 | Estimated fatigue damage and comparison with standards | 85 |
| 3.7 | Reliability of the deck of the viaduct | 86 |
| 3.7.1 | Comparison of reliability indexes based on several EVT approaches | 86 |
| 3.7.2 | Reliability for wind and traffic actions and their combination | 87 |
| 3.7.3 | Fatigue limit state | 92 |
| 3.7.4 | Conclusions | 94 |
| 4 | Conclusions and perspectives | 99 |
| 4.1 | Summary of conclusions | 99 |
| 4.2 | Short-term perspectives | 101 |
| 4.3 | Long-term perspectives | 102 |
| 4.4 | Scientific production | 103 |
| | References | 105 |
| A | Adapted methodologies | 113 |
| A.1 | Wind load model according to European Standards | 113 |
| A.2 | Traffic load model according to European Standards | 115 |
| A.3 | Fatigue load model according to European Standards | 116 |

List of Figures

| | | |
|------|---|----|
| 1.1 | From monitoring to predictions | 1 |
| 1.2 | General algorithm representing objectives of work | 5 |
| 1.3 | Illustration of a tail distribution method | 13 |
| 1.4 | Illustration of a periodic maximum method | 13 |
| 2.1 | Plan of methodology | 21 |
| 2.2 | General algorithm, case of combination of actions | 28 |
| 2.3 | General algorithm, case of local load effects, comparison of approaches . . . | 29 |
| 2.4 | Relation between stress and number of cycles: (I) - no any damage, (II) - fatigue damage, (III) - extreme load effects | 31 |
| 2.5 | General algorithm, case of fatigue | 32 |
| 2.6 | Extrapolation of number of fatigue cycles, schematic graph | 33 |
| 3.1 | Perspective view of the Millau Viaduct | 35 |
| 3.2 | Location of the Millau viaduct in France, G | 37 |
| 3.3 | Scheme of the Millau Viaduct | 38 |
| 3.4 | Cross section of the deck of the Millau Viaduct | 38 |
| 3.5 | gross vehicle weight (GVW) recorded with bridge Weigh-in-Motion (BWIM) system, four periods of monitoring | 39 |
| 3.6 | BWIM system, scheme and photo inside the deck of the viaduct | 40 |
| 3.7 | Recorded wind speeds at the top of P2 of the Millau viaduct | 42 |
| 3.8 | Wind roses for the top of the pylon P2 and for the weather station | 42 |
| 3.9 | Wind speeds at different levels based on different recorded data for Millau viaduct | 43 |
| 3.10 | Histogram of the wind speeds at different levels for the period Oct 2016 – June 2017 | 44 |
| 3.11 | Wind load collection from wind speed at four different levels of considered part of the viaduct | 45 |
| 3.12 | Relative frequency of occurrence of vehicles per day of week, four periods of monitoring | 46 |

| | | |
|------|--|----|
| 3.13 | Relative frequency of types of recorded vehicles per day of week | 46 |
| 3.14 | Relative frequency of masses of recorded vehicles per day of week | 47 |
| 3.15 | Evidence of weekly stationarity, vehicle type "113" | 48 |
| 3.17 | Common numbers of axles for different types of vehicles | 48 |
| 3.16 | Axles configuration types of vehicles on the Millau viaduct | 49 |
| 3.18 | The most common type "113" of heavy vehicles in France | 50 |
| 3.19 | Histograms of total vehicles mass per vehicle type | 50 |
| 3.20 | PDFs of total vehicle mass and allowed mass per vehicle type | 51 |
| 3.21 | Histograms of vehicles on slow and fast lanes | 54 |
| 3.22 | Steps to be taken from monitoring to predictions of traffic actions and load effects | 55 |
| 3.23 | Representation of the POT approach | 55 |
| 3.24 | Threshold choice (a) by mean residual life plot (MRLP) for the mass of traffic | 56 |
| 3.25 | Threshold choice (b) depending on confidence intervals and the probability of exceedance | 57 |
| 3.26 | Analysis of the quality of the estimation, example, vehicle type "1111" | 57 |
| 3.27 | Analysis of the quality of the estimation for all the vehicles types | 59 |
| 3.28 | Schematic view of one of the deformation modes of the deck for the considered part of the bridge, [29] | 60 |
| 3.29 | Part of the bridge considered for the 2D computational model (left), scheme of the pile with its pylon P2 (middle), 2D computational model (right) | 61 |
| 3.30 | Geometry for the FE model analyzed with ANSYS software, [67] | 67 |
| 3.31 | Position of the studied cross-section and applied loads on the part of the deck | 68 |
| 3.32 | Deformation from a single load of 1000kN | 68 |
| 3.33 | Axle position on the slow lane of FEM \mathcal{M}_1 for "113" | 69 |
| 3.34 | Steps to be taken from monitoring to predictions of traffic actions and load effects | 71 |
| 3.35 | Studied detail, deck of Millau viaduct | 71 |
| 3.36 | PDF in log-scale of the stresses, MPa, in the studied detail | 72 |
| 3.37 | Threshold choice for stresses in the studied detail | 72 |
| 3.38 | POT approach for stresses in the studied detail | 73 |
| 3.39 | PDF in log-scale of stresses, MPa, considering global load effects (traffic on both lanes) | 74 |
| 3.40 | Threshold choice for updated stresses in the structural detail | 74 |
| 3.41 | POT approach for updated stresses in the structural detail | 74 |
| 3.42 | BM approach for stresses in the structural detail | 75 |

| | | |
|------|---|-----|
| 3.43 | Fitting the GEV distribution to maximum stresses: top - block = 1 week, bottom - block = 1 weekday | 76 |
| 3.44 | Example of fitting Rice formula using the number of levels out-crossings . . | 77 |
| 3.45 | Main types of axles groups and stresses from them | 78 |
| 3.46 | Bending moment from a 3-axles group, [70] | 79 |
| 3.47 | Histogram of stress cycles, studied detail, deck of Millau viaduct | 80 |
| 3.48 | Stress cycles histogram | 81 |
| 3.49 | Algorithm for the use of POT for the FLS | 83 |
| 3.50 | Histogram of stress cycles with equivalent stresses of 65.7 MPa and 37.9 MPa | 84 |
| 3.51 | Example of POT results for the range dS_2 : (i) fitting GPD to histogram of $C^{(2)}$, (ii) probability plot, (iii) return level plot | 84 |
| 3.52 | Fatigue damage accumulation during the operational life of the viaduct, comparison of two methods | 85 |
| 3.53 | Convergence of the reliability index by FORM, POT approach | 88 |
| 3.54 | Convergence of the reliability index, BM approach, daily | 88 |
| 3.55 | Convergence of the reliability index, BM approach, weekly | 88 |
| 3.56 | Convergence of the reliability index, LCC approach | 89 |
| 3.57 | Steps to be taken to access reliability based on data from monitoring | 89 |
| 3.58 | Convergence of the reliability index by FORM, wind actions | 91 |
| 3.59 | Convergence of the reliability index by FORM, wind + traffic | 92 |
| 3.60 | Convergence for the reliability index β , fatigue by EN | 94 |
| 3.61 | Convergence for the reliability index β , fatigue by POT | 94 |
| 3.62 | Evaluation of reliability index with time, EVT approaches | 95 |
| 3.63 | Evaluation of reliability index with time, traffic and wind | 95 |
| 3.64 | Evaluation of reliability index with time, fatigue | 97 |
| A.1 | EN 1993-2 : 2003. 4.3.2 (3) Figure 4.2a. Application of load Model 1 | 115 |
| A.2 | EN 1993-1-9 : 2005. 7.1 (3) Figure 7.1. Fatigue strength curves for direct stress ranges | 116 |

List of Tables

| | | |
|------|---|----|
| 1.1 | Examples of load combinations in standards of several countries | 10 |
| 1.2 | Advantages and drawbacks of several extreme value approaches | 14 |
| 3.1 | Monitored data for different types of trucks | 41 |
| 3.2 | Example of vehicles types | 41 |
| 3.3 | Wind load as a function of wind speed | 44 |
| 3.4 | Proportion of number of axles of each axles type | 49 |
| 3.5 | Permitted in France masses of vehicles for axle distances d [m] | 51 |
| 3.6 | Errors from BWIM measurements | 52 |
| 3.7 | Errors in axles types definition in input BWIM data | 53 |
| 3.8 | Return levels with confident intervals based on bridge Weigh-in-Motion (BWIM) of 43 days | 57 |
| 3.9 | Updated return level with confidence interval based on BWIM-II of 180 days with same thresholds | 58 |
| 3.10 | Wind speed, associated wind force applied to the 2D computational model, and computed bending moments | 62 |
| 3.11 | Occurrence of five-axles trucks | 62 |
| 3.12 | Bending moments (BM) for the traffic actions and their occurrence | 63 |
| 3.13 | Wind force associated with the predicted wind speed in 120 years and computed bending moments | 64 |
| 3.14 | Results for the return levels and confidence interval for the wind data collected at Creissels, $\text{Pr}(\text{NW})$ is the probability of occurrence of the wind NW direction, for 4 possible directions | 64 |
| 3.15 | Combination of extreme wind action with extreme traffic action, and probability to their simultaneous occurrence | 65 |
| 3.16 | Computational time and example of stress values for different mesh sizes of a simplified FEM and chosen mesh for the main FEM | 70 |
| 3.17 | Validation of the finite element model | 70 |
| 3.18 | Parameters found from up-crossing rate histogram (URH) for the fitted Rice formula | 77 |

| | | |
|------|---|-----|
| 3.19 | Values of return level for daily number of fatigue cycles $C^{(1)}$ and $C^{(2)}$ | 82 |
| 3.20 | Fatigue damage obtained with linear extrapolation of D_0 and POT | 85 |
| 3.21 | Random Variables for reliability modeling | 87 |
| 3.22 | Reliability index β for different studied cases | 89 |
| 3.23 | Random variables for the reliability analysis | 91 |
| 3.24 | Results of the reliability analysis | 92 |
| 3.25 | Random variables for the fatigue reliability analysis | 93 |
| 3.26 | Results of the fatigue reliability analysis | 94 |
| 3.27 | Summary of reliability indexes β and probabilities of failure P_f | 97 |
| A.1 | EN 1993-2 : 2003. Table 4.2. Load model 1 : characteristic values | 115 |
| A.2 | EN 1993-1-9 : 2005. Table 8.8. Orthotropic decks - closed stringers | 116 |

Abbreviations

| | |
|---------------|--|
| BM | Block Maximum |
| BMS | bridge management system |
| BWIM | bridge Weigh-in-Motion |
| CAFL | Constant Amplitude Fatigue Limit |
| CDF | cumulative distribution function |
| EN | European Norms |
| EVT | Extreme Value Theory |
| FE | finite element |
| FEM | finite element model |
| FLS | fatigue limit state |
| FORM | First Order Reliability Method |
| FORM and SORM | First and Second Order Reliability Methods |
| GEV | generalized extreme value |
| GEVD | generalized extreme value distribution |
| GPD | generalized Pareto distribution |
| GVW | gross vehicle weight |
| I | confidence interval |
| IS | Importance Sampling |
| LCC | Level Crossing Counting |
| LE | load effect |
| LSF | limit state function |

| | |
|------|-----------------------------------|
| MCS | Monte-Carlo simulation |
| MRLP | mean residual life plot |
| PDF | probability distribution function |
| PE | probability of exceedance |
| POT | Peaks Over Threshold |
| RL | return level |
| SHM | structural health monitoring |
| SLS | serviceability limit state |
| TH | threshold |
| ULS | ultimate limit state |
| URH | up-crossing rate histogram |
| WIM | Weigh-in-Motion |

Glossary

collapse – development of failure mechanisms in a structure to a degree involving disintegration and falling (parts of) structural members, [10]

design service life – assumed period for which a structure or a structural member is to be used for its intended purpose with anticipated maintenance, but without substantial repair being necessary, [10]

failure – insufficient load-bearing capacity or inadequate serviceability of a structure or structural member, or rupture or excessive deformation of the ground, in which the strengths of soil or rock are significant in providing resistance, [10]

fatigue – process of initiation and propagation of cracks through a structural part due to action of fluctuating stress, [8]

orthotropic – deck that comprises a structural steel deck plate stiffened either longitudinally or transversely, or in both directions

quantile – each of any set of values of a variate which divide a frequency distribution into equal groups, each containing the same fraction of the total population

reliability – ability of a structure or structural member to fulfill the specified requirements, during the working life, for which it has been designed, [10]

List of Symbols

| | | |
|--------------|--|---|
| A | S-N curve coefficient for the first slope | $\text{m s}^2 / 10^6 \text{ kg}$ |
| A_{ref} | reference area | m^2 |
| B | S-N curve coefficient for the second slope | $\text{m s}^2 / 10^6 \text{ kg}$ |
| C | daily number of cycles that is counted for each stress range | |
| C_r | return level for daily number of cycles | |
| C_t | given interval for traffic actions | |
| C_w | given interval for wind actions | |
| D_0 | initial damage accumulation during the monitoring period | |
| D_{cr} | critical damage accumulation | |
| D_f, D_f^* | accumulated fatigue damage | |
| d | axle distance | m |
| d_m | monitoring period considered for fatigue analysis | day |
| d_{ref} | reference block size | day |
| d_{return} | return period with a respect to a block size | day |
| d_x | chosen interval (block size) of a load effect | |
| E_d | design combination of loads | $\text{kN} (10^3 \text{ kg m/s}^2)$ |
| F_t | design traffic action | $\text{kN} (10^3 \text{ kg m/s}^2)$ |
| F | cumulative distribution function | |
| F_{TS} | concentrated axle load | $\text{kN} (10^3 \text{ kg m/s}^2)$ |
| F_{UDL} | uniformly distributed load | $\text{kN} (10^3 \text{ kg m/s}^2)$ |
| F_w | design wind action | $\text{kN} (10^3 \text{ kg m/s}^2)$ |
| G | limit state function | |
| I | confidence interval for return level of load effect | |
| K | category of a detail exposed to fatigue | $\text{MPa} (10^6 \text{ kg/m s}^2)$ |
| L_{span} | length of the span | m |
| L^{max} | extreme random load | |
| M | bending moment caused by the entire vehicle under an axle | $\text{kNm} (10^3 \text{ kg m}^2/\text{s}^2)$ |
| M_{ax} | value of bending moment under an axle alone | $\text{kNm} (10^3 \text{ kg m}^2/\text{s}^2)$ |
| M_t | bending moment induced by extreme traffic actions | $\text{kNm} (10^3 \text{ kg m}^2/\text{s}^2)$ |
| M_w | bending moment induced by extreme wind actions | $\text{kNm} (10^3 \text{ kg m}^2/\text{s}^2)$ |
| m_t, m_w | deterministic functions | |

| | | |
|------------------------|---|--|
| m_x | parameter of the Rice formula | |
| m, n | slopes of S-N curve | |
| N | number of occurrences of vehicles | |
| N_{sim} | number of simulations in reliability analysis | |
| N_e | number of excesses of a threshold | |
| N_{fail} | number of failures in reliability analysis | |
| N_i | number of stress cycles for a considered range | |
| N_{tot} | total number of load effect events | |
| P_I, P_{II}, P_{III} | bending moment from a single, double or triple axle load | kNm ($10^3 \text{ kg m}^2/\text{s}^2$) |
| P_1, P_2, P_3 | point loads from each axle in a group of three axles | kN (10^3 kg m/s^2) |
| $P1^*, P2^*, P3^*$ | bending moments caused by each axle in a group | kNm ($10^3 \text{ kg m}^2/\text{s}^2$) |
| p | number of observations until a return period | |
| P_f | probability of failure | |
| Pr | probability of occurrence | |
| R | material resistance | MPa (10^6 kg/m s^2) |
| R_p | return period | observations |
| R_t | return period | years |
| S | maximum principal stress | MPa (10^6 kg/m s^2) |
| S_{ax} | value of stress caused by passing vehicle under an axle | MPa (10^6 kg/m s^2) |
| S_D | constant amplitude fatigue limit | MPa (10^6 kg/m s^2) |
| S^{eq} | equivalent stress | MPa (10^6 kg/m s^2) |
| S_i | considered stress range | MPa (10^6 kg/m s^2) |
| S_K | detail category | MPa (10^6 kg/m s^2) |
| S_L | cut-off limit | MPa (10^6 kg/m s^2) |
| S_m | maximum stress induced by a vehicle | MPa (10^6 kg/m s^2) |
| S^{return} | return level for load effect | MPa (10^6 kg/m s^2) |
| s_R | standard deviation of the resistance | MPa (10^6 kg/m s^2) |
| s_{max} | maximum recorded stress induced by an axle or an axle group | MPa (10^6 kg/m s^2) |
| s_ζ | standard deviation of the probability of exceedance | |
| s_σ | standard deviation of the scale parameter | |
| s_ξ | standard deviation of the shape parameter | |
| T_{ref} | reference monitoring period | days |
| U | sequence of thresholds | |
| U_0 | the minimum threshold in a sequence | |
| U_p | the maximum threshold in a sequence | |
| u | threshold for a load effect | |
| V_z | random wind speed | m/s |
| W | self-weight of a structure | kN (10^3 kg m/s^2) |
| W_t | random vehicle weight | t (10^3 kg) |

| | | |
|-----------------------|--|------------------------|
| X | random variable representing a load effect x | |
| X^{max} | load effect caused by an extreme random load | |
| x_0 | starting point in fitting the Rice formula | |
| x_I, x_{II} | deterministic functions | |
| Y | threshold excesses | |
| β | reliability index | |
| β_{bm} | reliability index based on the block maximum method | |
| β_{comb} | reliability index for a structure exposed to the combination of traffic and wind actions | |
| β_{en} | reliability index based on a design model of European norms | |
| β_f, β_{f*} | reliability index for a structure exposed to fatigue | |
| β_{lcc} | reliability index based on the level cross counting method | |
| β_{pot} | reliability index based on the peaks over threshold approach | |
| β_{traf} | reliability index for a structure exposed to traffic actions | |
| β_{wind} | reliability index for a structure exposed to wind actions | |
| γ_t, γ_w | partial factors for traffic and wind actions | |
| Δ | sequence of w stress ranges defined according to the data set | |
| η | set of numbers of cycles corresponding to selected stress range | |
| ζ_u | probability of exceedance | |
| μ | mean value | |
| μ_b | location parameter of generalized extreme value distribution | |
| ν | mean rate of up-crossing for a certain level during a reference period | |
| ν_0 | mean number of up-crossings of the zero level | |
| ζ | shape parameter of generalized Pareto distribution | |
| ζ_b | shape parameter of generalized extreme value distribution | |
| ρ | air density | kg/m^3 |
| σ | scale parameter of generalized Pareto distribution | |
| σ_b | scale parameter of generalized extreme value distribution | |
| σ_x | parameter of the Rice formula | |
| τ_I, τ_{II} | given intervals for extreme load effects | |
| Φ | cumulative distribution function of the standardized Normal distribution | |
| ψ_0 | factor for combination value of accompanying actions | |
| Ω^{max} | simultaneous occurrence of extreme loads of different nature | |
| \mathcal{M} | finite element model | |

Distributions:

| | |
|---------------|---------------------------|
| \mathcal{B} | Binomial |
| \mathcal{E} | Generalized Extreme value |
| \mathcal{G} | Generalized Pareto |
| \mathcal{L} | Log-normal |
| \mathcal{N} | Normal |

Chapter 1

Introduction

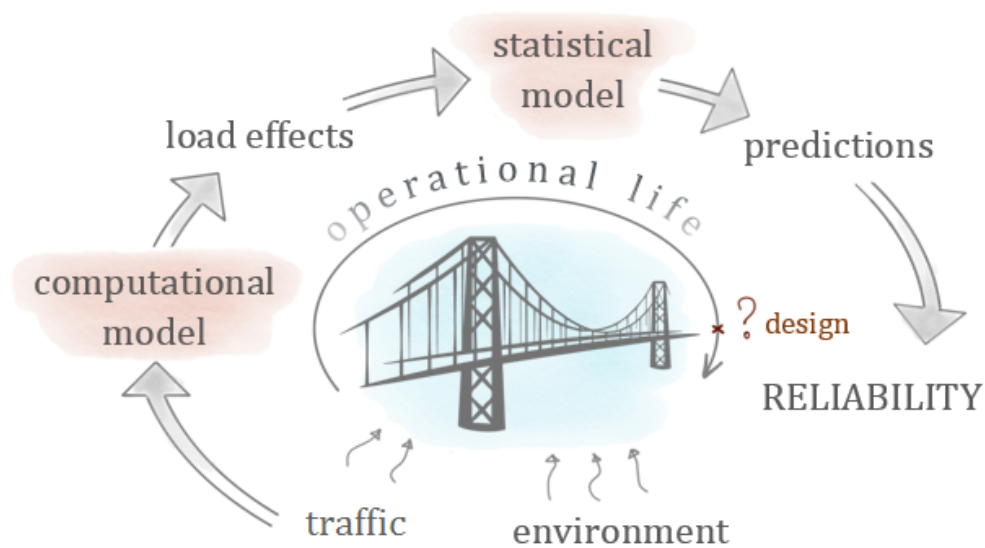


FIGURE 1.1 – From monitoring to predictions

For civil engineers, one of the most important questions is the behavior of a structure during and after its **design service life**. Each type of structure has a specific set of requirements for the design, construction, and maintenance concerning structural performance, safety, economic and environmental aspects. The ability of a structure or a structural element to fulfill such requirements is called **reliability** [10].

This Thesis is dedicated to estimating the reliability of existing bridges at different moments of the operational life based on limited data from monitoring of live and environmental actions on a structure, Figure 1.1.

This chapter is an introductory chapter. First of all, it describes the general idea of the project and the importance of the studied subject (Section 1.1). Then, research objectives are listed in Section 1.2. Section 1.3 gives an overview of the subject in recent literature, briefly describes related studies and necessary standards and guides. It is followed by Section 2 that summarizes the methodology used. Section 1.5, with listed contributions, concludes the introduction. Finally, this section shows a plan of the manuscript and provides links to different sections.

1.1 Motivation

In order to define and achieve an appropriate degree of **reliability** for a certain object, there are international and national standards and codes. Rules for the design and maintenance of structures depend usually on the location, climate, specific loads, etc. For the simplification of the design process, a lot of assumptions are used in the computational methods described in norms and standards. Such technical documents are regularly updated according to new conditions such as rapid change of climatic conditions, developing technologies, together with the expansion of human needs.

Due to the development of transport networks, more and more existing bridges are being investigated, as well as new bridges are being constructed nowadays all over the world. With the increase of traffic in quantity and weight, projects of bridges are becoming more complicated with the need to adjust to more difficult conditions. Therefore, existing norms such as **European Norms (EN)** [7, 6] do not always give sufficient results [97], and behavior, as well as reliability of bridge structures, is more difficult to predict. In addition to self-weight, bridges are affected by different types of environmental and traffic actions. Prediction of the behavior of bridges under the combination of these types of loading is desired. Such prediction is usually made by statistical analysis using the **Extreme Value Theory (EVT)** [14].

Generally, while using statistical analysis, we are mostly interested in the data that are close enough to the mean, crossing out the highest and the lowest values due to the low probability of such cases. However, the larger the design lifetime we want for a structure, the higher is the probability of appearing such extreme situations. Though, for better design, it is necessary to analyze extreme cases in order to predict the behavior and avoid possible **failure**.

Moreover, while designing any important structure with a significantly longer lifetime, it is necessary to consider all possibilities of structural **collapse** during the whole period of

use. For instance, according to international standards [10] among other reasons for the occurrence of failures, considering that the structure is designed and maintained correctly, there are the following:

- Unfavourable combination of actions on a structure within an ordinary use and circumstances;
- Exceptional environmental influences such as extreme climatic actions (wind, waves, temperature, corrosion, etc).

Therefore, the main aim of the current research is the structural resistance to extreme live and environmental actions and their combinations. There is a variety of structures exposed to such loads. This doctoral Thesis is focused on the Millau Viaduct, located in Southern France.

The goal of the current research is the estimation of reliability of a given structure within the **design service life**, taking into account extreme live and environmental actions and their combinations. According to [99], estimated reliability of a structure based on only probabilistic models may lay far from the real one, as they are mostly subjective. That is why, for this research, the estimated values are based on provided data from monitoring of traffic and wind actions on the deck of the Millau viaduct.

1.2 Research objectives

The target of the project is the reliability of the deck of the Millau viaduct during its operational life. This wide topic brings several research objectives. The first one is the **reliability assessment of critical structural details, exposed to traffic and environmental actions**, for different limit states: **ultimate limit state (ULS)**, fatigue, serviceability.

First of all, it is important to define types of critical actions that can be applied to given structures. Bridges are exposed to various environmental loads: wind, precipitation, rapid temperature shifts, corrosion of structural elements, seismic loads, etc. In cases of cable-stayed and suspension bridges, one of the most significant climatic load is the wind. Therefore, the Thesis is focused on the wind load, traffic actions as the principal live load on a bridge deck, and on their combination.

For reliability assessment, future loads during the remaining operational life of the viaduct have to be estimated. The main interest is given to the highest values of load effects as they play a crucial role in predicting the behavior of the structure. In order to perform such prediction, statistical approaches are used on monitored input data. That brings another research objective: **comparison between reliability indexes derived from statistical models with design load models** from standards.

For this comparison, traffic and static wind actions are chosen in the current work. So, the next objective is a **probabilistic model for a combination of extreme events caused by traffic and by static wind** based on monitored actions and the **EVT**.

For each case, choice of an appropriate extreme value approach is important, which is also investigated here by **comparison of reliability computed with several extreme values approaches**. Moreover, an alternative **graphical method for threshold choice** in the **Peaks Over Threshold (POT)** approach is another objective.

Direct measurements of load effects are often limited or not available, therefore, **reliability** assessment is based on recorded values of applied actions and **finite element (FE)** modeling of stresses in critical details of the deck. In addition, **influence of a duration of monitoring on confidence intervals** for return levels of traffic and wind actions is observed.

Not only extreme values are important, but also fatigue of critical details can play a crucial role in the reliability evaluation. The final objective is the use the **POT approach to predict fatigue damage** by extrapolation in time of a number of fatigue cycles in critical elements of an orthotropic deck.

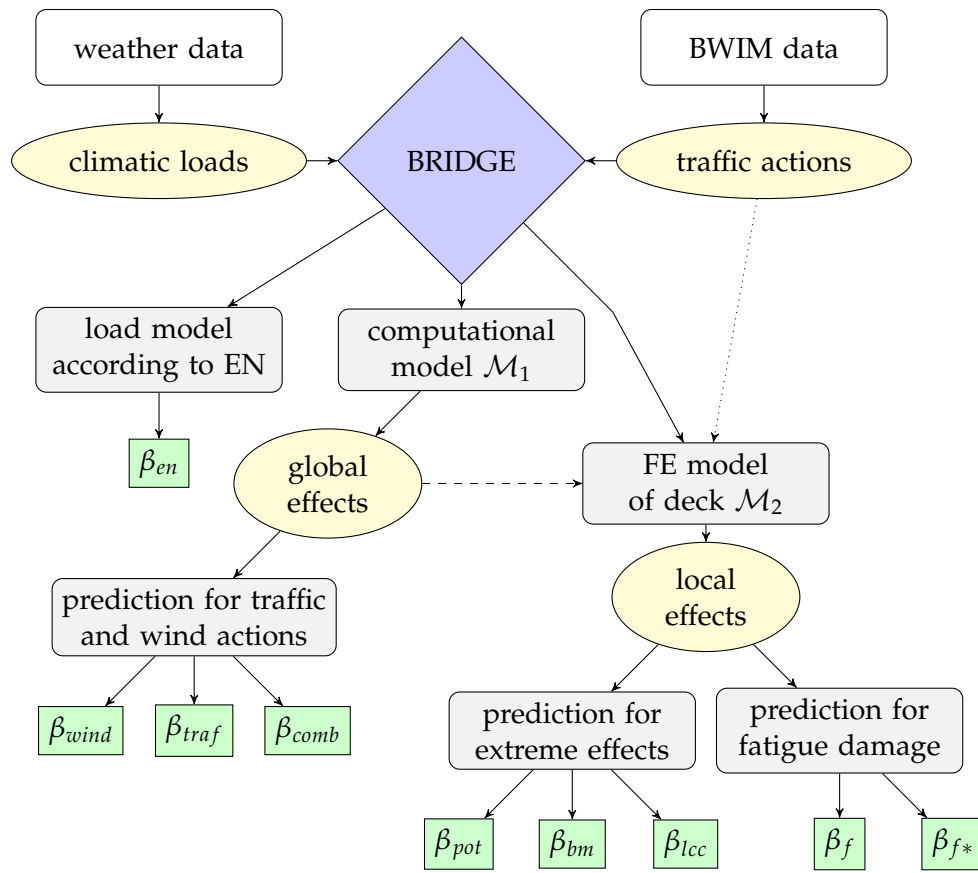


FIGURE 1.2 – General algorithm representing objectives of work

Figure 1.2 displays a flowchart that introduces the aspects covered here for the case of the Millau viaduct. Data collection from the monitoring of traffic and environmental actions is followed by computational modeling of a chosen part of the structure. The computational model \mathcal{M}_1 has to be used in order to apply both types of actions, their combination, and to obtain global load effects.

Extreme load effects from measured actions are used to perform extrapolation in time to assess reliability due to global effects from traffic β_{traf} and wind β_{wind} actions, as well as their combination β_{comb} . To compare results from statistical models based on monitored input data with design load models from EN, the reliability index β_{en} is to be assessed.

A precise 3D FE model of the part of the deck \mathcal{M}_2 is needed in order to assess local load effects in structural details of the orthotropic deck exposed to fatigue. The challenge here is the assessment of the values of load effects caused by each axle of passing vehicles taking into account the traffic configuration (dotted line in Figure 1.2), the position of the truck on the deck, vehicle type, axle distances and amplitudes of a load. Global effects from the left branch of the algorithm are also considered (dashed line in Figure 1.2) in

fatigue reliability analysis.

There are two parts of the analysis of local load effects. One branch (left) represents **ULS** by reliability indexes based on extreme values, for several **EVT** approaches, β_{pot} , β_{bm} , β_{lcc} . Another branch of the algorithm yields to a comparison of fatigue reliability β_f , linearly extrapolated in time, with the alternative method for predictions of the fatigue and calculating the reliability due to fatigue damage at any return period of interest, β_{f*} .

To summarize, the whole procedure of load effects assessment and structural reliability estimation can be divided into the following tasks.

1. Extrapolation of monitored traffic loads with three different extreme values approaches.
2. Investigation to the question of threshold choice in **POT** approach.
3. Probabilistic modeling for a combination of extreme events caused by traffic and by static wind.
4. Comparison of predicted traffic and wind actions with values obtained by design load models.
5. Influence of a duration of monitoring of traffic weights and wind speeds on confidence intervals of return levels of these loads.
6. Application of the **POT** approach for extrapolation in time of fatigue damage.
7. Reliability assessment for critical details, exposed to traffic and environmental actions.

The following section provides an overview of literature related to listed problems.

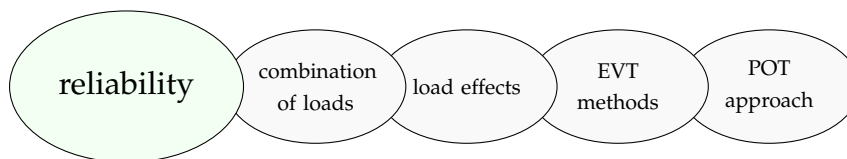
1.3 Literature review

The residual life of large complex unique bridges is an important topic for modern civil engineering work. Due to the fact that many European bridges, as well as bridges all over the world, are coming to the end of their design life, the question of the extension of their operational life is essential [40]. Moreover, some bridges were not designed to the current loading and have to be reassessed. Studying such structures allows for improving the assessment of existing structures and possibly, gaining some profit from an economic point of view by avoiding unnecessary over-design or strengthening.

The literature review covers studies on the following topics:

- reliability of existing bridges,
- combination of traffic and environmental loads in bridges,
- load effects in bridges based on monitoring of actions,
- extreme value theory for extrapolation of load effects in time,
- the use of the Peaks-Over-Threshold approach.

1.3.1 Studies on the reliability of existing bridges



A mean for estimating if a structure can operate safely after a certain period is the reliability index. There are various different methods for reliability analysis, which exist nowadays [20], each has its advantages and drawbacks. For example, the work [65] proposes a synthesis for a correct choice of the most appropriate reliability method. Its relevance depends on the studied structure, income data, initial conditions, and computational resources. In bridge engineering, the most frequently used ones are **First and Second Order Reliability Methods (FORM and SORM)**, **Monte-Carlo simulation (MCS)** (i.e. in [48]), **Importance Sampling (IS)**, all methodologies are described, for instance, by [18, 20]. Much research has been already performed for novel reliability approaches (i.e. a novel **IS**-based reliability method of steel cable-stayed bridges [85] or a probabilistic progressive collapse methodology is described for highway bridges [64]). Therefore, for the current work, the main interest is in the limit state functions definition and performing classical reliability analysis methods for predicting reliability levels at the end of design life: **FORM and SORM**.

The idea of each method is to evaluate a limit state equation accounting for all input random variables. In order to obtain the limit state function for a certain structural object, the purpose of analysis should be stated. In bridges, it can be fatigue, serviceability, and ultimate limit states EN [5]. A research [47] on the relation between the cost and reliability of steel bridges exposed to fatigue concludes that all studied cases should consider fatigue, extreme events, and serviceability. One of the conclusions shows that in reinforced concrete bridges, ULS is the leading one but it is concluded that fatigue limit state (FLS), extreme values, and serviceability have to be considered anyway.

For both ULS and FLS, monitoring data-based analysis is the most efficient in order to observe the real situations. As it was proven many times (i.e. [58]) monitoring of loads and stresses can successfully be used for fatigue reliability. In order to answer the question of which type of monitoring data is required, it is necessary to know the type of structure. Such as for bridges with steel orthotropic decks, critical structural details of a deck are exposed to fatigue and have a shorter life than other structural elements of a bridge [62].

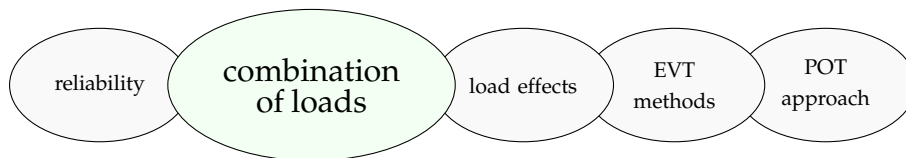
The work based on bridge Weigh-in-Motion (BWIM) data [38] yields conclusions on reliability index that stays always much higher than values required in EN [5]. The reliability analysis is done based on the probability of failure as a joint function of both, exceedance of Constant Amplitude Fatigue Limit (CAFL) (by high amplitudes of stresses using weekly block maximum approach) and fatigue damage accumulation (using Miner's rule). The use of the BWIM-based probabilistic model is suggested for simple bridge models. The verification with reliability indexes of EN [5] is made and gives conclusions on higher reliability levels depending on geometry and load cases.

The work [60] validates EN model for fatigue based on BWIM data and suggests more consistent reliability levels. It brings more attention to the welds in joints of orthotropic decks as a critical structural detail with a shorter fatigue life. Target values of reliability indexes for FLS in the welds of an orthotropic deck have to be reanalyzed. For the case of the load model based on traffic counts, [50] suggests an advanced methodology for fatigue reliability levels considering uncertainties. A comparison between a FE model and a model based on Weigh-in-Motion (WIM) data, concludes the importance of accuracy in load model in reliability analysis. In a case when direct monitoring is not available, the FE model is built to obtain stresses in critical structural details, using rules of EN to apply this load.

In addition to road traffic load, different failure modes could be assumed for the reliability check of the existing structure: floods [41], impact [87], earthquakes [53, 55], corrosion [46], and temperature [88, 61, 43]. All of the mentioned failure cases depend on each

particular situation, materials of elements, geometry, location of bridges. For example, concerning bridges with steel orthotropic decks, a study [94] combines stress ranges in steel details of a deck with the temperature effects. Derived conclusions show the 27% reduction in reliability indexes due to traffic changes and to pavement temperature levels. In certain cases, the attention should be given to wind actions [86, 57, 91] especially, in combination with traffic.

1.3.2 Traffic and wind loads in bridges, and their combination



Traffic loads on bridges is the relevant topic that is being actively studied last decade ([74, 100, 32]) due to the question of the extension of their design life. The operation life of bridges of all types can be affected by the growth of traffic in mass and volume. Some works show that an annual growth in the traffic flow of 1% significantly affects the traffic load models in European bridges (i.e. in Netherlands, [59]). The work [90] based on simulations shows a significant increase in the maximum lifetime traffic load effects with the increase of single truck weight. However, the growth of truck volume and proportion of heavy trucks causes a relatively moderate increase in load effects. The similar conclusion [100], based on monitoring data, confirms that the growth in vehicles weight (ULS) affects the reliability more than the increase of traffic volume (FLS).

Even if fatigue due to traffic loads is not a critical issue in some cases, it always has to be considered, especially, in bridges with steel orthotropic decks (i.e. if combined with seasonal temperature effects, [43]). Since the number of light-duty vehicles is quite large in most cases, they may cause fatigue of certain elements of a deck. One of the challenges of this study lays in applying the EVT to the number of fatigue cycles caused by different vehicles and axles of trucks. There were several similar studies carried out in various areas. For instance, in the area of composites, the stiffness-based model is introduced by [82] for fatigue damage and life prediction. The work [25] compares a new probabilistic fatigue assessment with a deterministic approach for railway bridges. As it has recently been proposed [34], the extreme value approaches can be used for different aspects of material fatigue. For a certain observed structure, it is important to understand which case is the most unfavorable for a bridge: high amplitude stresses caused by rare extreme events or small stresses by a high number of cycles.

| Country | Name of standards | Reference | Design load combination |
|-----------|-------------------|-----------|---|
| Europe | EN | [5] | $\mathcal{D} + 1.5\mathcal{W} + 1.35(0.4\mathcal{T}_1 + 0.75\mathcal{T}_2)$ |
| USA | ASCE 7-10 | [1] | $1.2\mathcal{D} + 1.6\mathcal{W} + \mathcal{T}$ |
| Australia | AS/NZ 1170 | [2] | $1.2\mathcal{D} + \mathcal{W} + 0.6\mathcal{T}$ |
| Canada | NBCC 2010 | [11] | $0.9\mathcal{D} + 1.4\mathcal{W} + 0.5\mathcal{T}$ |

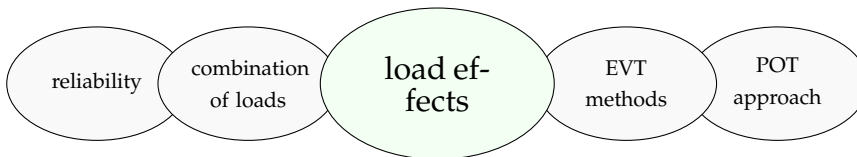
TABLE 1.1 – Examples of load combinations in standards of several countries

One of the most important and complex combinations of loads in cable-stayed or suspension bridges occurs when traffic actions combined with the wind [35]. National design standards propose combination of live, i.e. traffic (\mathcal{T}) load with wind (\mathcal{W}) and self-weight (\mathcal{D}) with different safety factors, see some examples in Table 1.1.

Variation of partial factors between several countries (Table 1.1) in design norms brings a question of alternative models for existing bridges to update the design models. The combination for an existing structure can be demonstrated in different ways. For example, in the recent work [91], it is represented by the vehicle-bridge-wind dynamic system that simulates interactions between both types of loads with a bridge at each time step. In their work, authors propose to consider a vehicle on the bridge as a point event and compare the response of the bridge to the wind with or without a heavy truck. The main conclusions of their work are about the wind speed velocity: higher wind speed actions do not necessarily cause shorter fatigue life; however, it is important to consider both extreme effects, from the traffic and the wind, as their combination induces large stresses in the structure. Another work of the bridge dynamic structural response to wind and traffic at the moment of monitoring [86] concludes that both loads play a similar role in scenarios with strong winds.

Depending on the observed load effects, availability of **structural health monitoring (SHM)** data, the geometry of bridges, the wind can be applied as a static load [39], which simplifies calculations, or dynamic load, which requires a thorough investigation in every particular case [75].

1.3.3 From measurements to predictions



In general, to control the amount of traffic passing on the highways, the **WIM** system [4] was used worldwide for a couple of decades. The idea of measurements is in receiving

signals from sensors affected by passing vehicles, which allows evaluating the speed and the weight of each truck. For highways, usually, the **WIM** sensors are installed inside the pavement on a special beam placed in the direction transverse to the road.

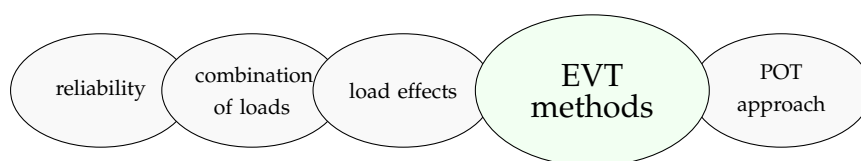
For bridges, a special type of the same system exists – **BWIM**. The principle of the system was firstly proposed by Fred Moses [66] and then widely used in the practical application and research [84, 51, 78]. The best place to install the **BWIM** equipment is the middle of a bridge span since it provides information about traffic action for obtaining the maximum bending moment and the maximum displacement of deck spans.

Modern **BWIM** equipment and software, such as SiWIM [102], provide a good tool to get a bridge response for traffic even in a case of multi-presence – a situation when more than one truck passes sensors at the same moment. There are also some disadvantages [51] such as initial error of the sensor, a time-demanding process for obtaining precise results of vehicle weights, the need in temperature correlation. However, **BWIM** system is the best way to measure traffic actions on bridges, therefore data provided by such equipment are used in the current work.

Even knowing all weights of heavy vehicles, obtaining load effects caused by them is still a complex task. It is important to carefully estimate bridge responses to extrapolate them in time and predict the bridge behavior, especially, when working with a large amount of data. There are different computational tools designed exactly for this purpose. The oldest works in France were presented in the second part of the 20th century: TRAFMUL [49] and later CASTOR [42]. They show the main steps to evaluate load effects (internal forces, equivalent stresses) from the initial data provided. Recent works [100] are adapted to the modern amount of traffic and allow easier data processing.

In the current work, the load effects are obtained using **FE** models made with the Workbench [101, 19] of Ansys software that was created by Swanson [105]. These **FE** models are combined with computational models written in Matlab [104] with the Statistics Toolbox [103] and the UQLab extension.

1.3.4 Extreme value theory for extrapolation of load effects



Research on extreme values began between 1920 and 1940 when the extreme value theory was developed by Fisher, Tippet and von Mises, and Gnedenko in 1943. These mathematical developments were followed by works of Gumbel [17], who started applying theory to problems in engineering. In the 1970s, Pickands [76], de Haan and Balkema [27] have introduced a theorem in extreme value theory, giving a better basis for statistical models. Since the 1980s, methods for the application of Extreme Value Theory have become widespread in different areas.

For the evaluation of extreme traffic loads on bridges, first of all, it is necessary to choose a method of extreme load effects assessment. To make predictions for the load model LM1 of European standards EN [7], background works give certain rules [98, 22]. ULS methods have been derived based on extreme values of axle lorry loads [96] using:

- half-normal curve fitted to the histogram tail,
- Gumbel distribution fitted to the histogram tail,
- asymptotic method based on the use of the Rice formula.

Apart from those, there are different other approaches that might be applied depending on the amount of initial data provided for the bridge and their quality, as it is reviewed in [73, 92].

Usually, these approaches are based on the extrapolation in time of known load effects. Based on the provided measurements, the estimation of the future effects is desired. Two main groups of methods [93] in the literature are the following:

1. tail distribution methods, which first find the underlying distribution of load effect (LE) and then raise it to a certain power to fit a maximum value distribution [14]: the Normal distribution, the Gumbel distribution, the Weibull distribution, the Rice formula based on the Level Crossing Counting (LCC) method, and the generalized Pareto distribution (GPD). An illustration is shown in Figure 1.3.
2. Periodic maximum methods that choose samples of observations over a certain time period and fit a series of its local maximum to standard extreme value distributions: the Weibull distribution, the Gumbel distribution or generalized extreme value (GEV) distribution. An illustration is shown in Figure 1.4.

Table 1.2 summarizes the most common approaches with their advantages and drawbacks. The most used tail fitting approaches are POT, Block Maximum (BM), and LCC. The literature review on the POT approach is done in the following subsection.

The idea of the BM method is to find the maximum value in every chosen block of measurements and fit the data-set composed of these maximums to generalized extreme

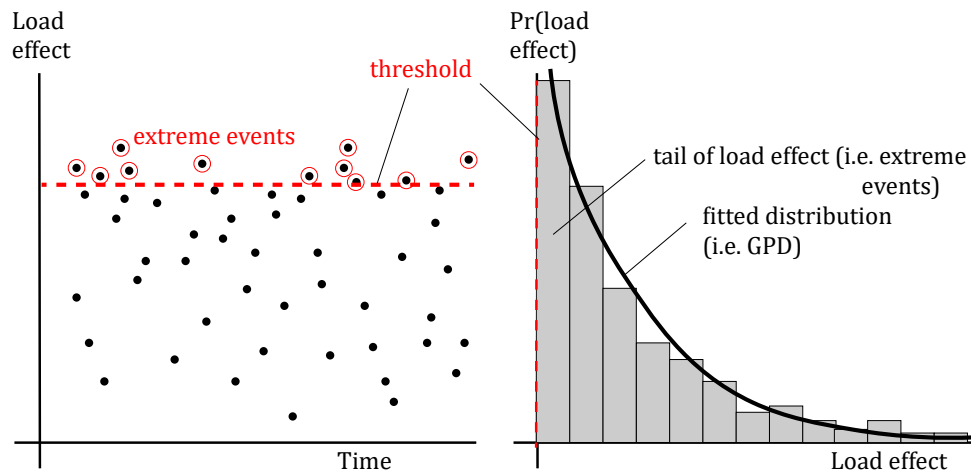


FIGURE 1.3 – Illustration of a tail distribution method

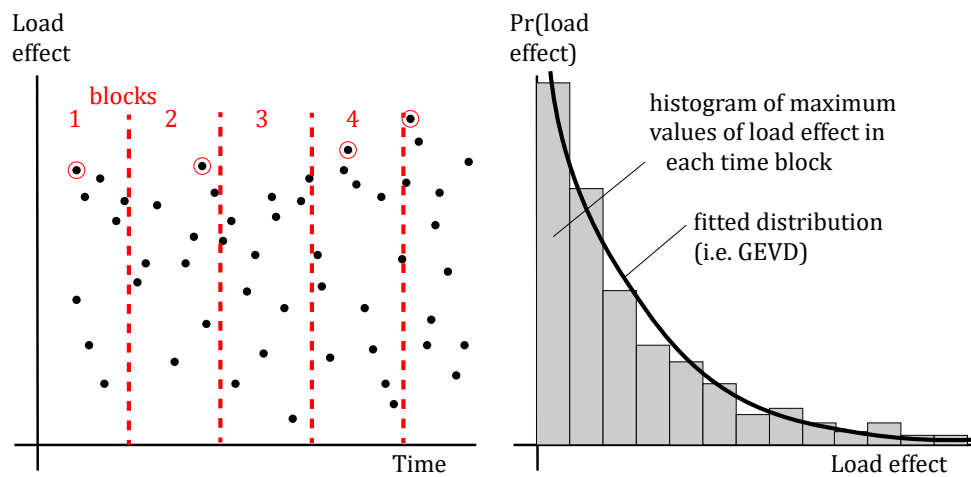


FIGURE 1.4 – Illustration of a periodic maximum method

| Method | Objective | Difficulties | Advantages | Comments |
|-----------------------|---|--|---|---|
| POT | Load effects that exceed a certain threshold are fitted to GPD | Choice of the threshold and estimation of parameters | Good for complex examples and mathematically simple | see 2.2.1 |
| BM | Maximum load effects of each chosen block of data are fitted to GEV distribution | Fit to three different distributions to make a correct choice, does not allow for uncertainties | Good for structural behavior predictions as blocks are equal periods of time | Possible fitting to Normal distribution |
| LCC | The Rice formula is fitted to a normalized level crossing histogram | Up-crossing frequencies are fitted to the formula rather than to the data, a starting interval choice | Possible to estimate both maximum and minimum extreme values, applicable to any area | suggested by EN [7] |
| Box-Cox | The model with a chosen threshold converges to GEV or to GPD | Extreme data are strictly positive, finding parameter estimates, correct specification of the limit distribution for minimum and maximum | Allows for different loading event types, predictions are quite stable for thresholds below mean value | i.e. [30] |
| Bayesian updating | Based on measured data, updating of the initial probability distribution applied to the BM | Different ranges of accuracy for different load effects, take into account all the data, not only a tail | Gives efficient updating and quite precise results in certain cases | i.e. [89] |
| Predictive likelihood | Determination of the maximized joint likelihood of a predict and (identified for a required probability level) and observations | Take into account all the data, not only the tail, poor results for a mixture distribution, strict definitions of acceptable safety levels is required | It presents the increase in the information that can be gained from a sample, which gives more reliable results | Various extensions of this method exist, [31] |

TABLE 1.2 – Advantages and drawbacks of several extreme value approaches

value distribution (GEVD). The common problem here is the case of non-homogeneous datasets. In order to handle them, a few methods are proposed in the literature, aiming at obtaining approximately idealized conditions of independent and identically distributed observations. One such approach [33] proposes a composite distribution model that describes bridge load effects from a mixture of different loading event types, representing a different number of trucks on the bridge contributing to a maximum value of the **LE**. Such a model accounts for the actual physical nature of the bridge loading process, and hence allows for higher accuracy in extreme value estimates, as also shown in a recent work [72].

Rice formula [77, 24] represents the mean value of up- or down-crossings for given levels during a reference period of time. A histogram of **LCC** might be obtained [36] from applied loads via influence surfaces: moments of time when an upper or a lower level is crossed. The histogram is normalized so that each class interval is an approximated mean value of a level crossing.

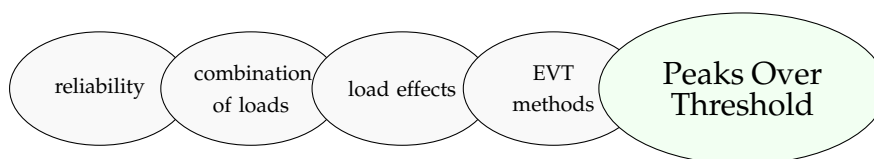
Box-Cox approach [28] used by [30] for bridges. This approach is valuable in specific cases as it removes the disadvantages of **POT** and **BM**. The model of strictly positive values of **LE** that cross a rather low threshold converges to either **GPD** or **GEV** distribution which gives quite stable predictions.

The Bayesian approach was used in the work [89] for the proposed decorrelated tail model and it was found to give quite precise results in certain cases. However, a recent work [73] proves that the updating by the Bayesian approach does not give good results for all desired load effects.

As well as the Bayesian approach, the Predictive Likelihood method also requires all load effects for a probability distribution; and [73] mentions the significant influence of the set of data and this work does not give good results in bridges applications.

One of the most efficient approaches to be used is the **POT** method [14], which was not used during the mentioned background works for **EN**, but which has proven to work well in diverse fields.

1.3.5 The use of the Peaks-Over-Threshold approach



A favorable difference with the **BM** method: **POT** considers all the peaks of a certain load effect above a specified threshold and fits them to the **GPD** while **BM** only counts one maximum load effect in a given block of time with the following fitting of these extremes to the **GEV** distribution. It uses data efficiently without considering unimportant data when values are low and without losing extremes as the **BM** method.

The main principle of the **POT** approach is based on the method described by [76] and applied later by [93] - for traffic loads. The **POT** approach has its difficulties such as selecting an optimized threshold [93]. On one hand, it should be reasonably high, so, that extreme event types are not mixed, in order to assure their convergence. On the other hand, the threshold must be low enough to provide a necessary amount of peaks for obtaining reliable results. Different techniques were developed for choosing a threshold, for instance, in the field of finance [16] and risk management [21], but the choice always stays difficult. A graphical technique used here [68] is described in Section 2.2. Choice of parameter estimators for the **GPD** is also a drawback of the approach. The main idea is given by [14]. In this Thesis, a choice of estimators is done with respect to the comparison proposed in [100].

As it was proven by [100] and reviewed in [73], the **POT** method is efficient for the estimation of traffic effects. In addition, it does not need the data to be Gaussian. Moreover, the **POT** approach is used in wind engineering [26], precipitation predictions with non-stationary data [79], electricity demand estimation with a time-varying threshold [83], and other fields. Therefore, **POT** method, see Appendix 2.2.1, is chosen in the current research not only for the traffic loads but also for the wind.

1.4 Methodology

This Thesis is focused on a bridge structure – the Millau viaduct that represents a complex bridge with a steel orthotropic deck exposed to traffic and environmental actions. The question of the remaining operational life is studied based on values of a reliability index and the probability of failure. Among all possible failure modes, the steel orthotropic deck is considered here due to the fact that its structural details are subjected to fatigue. The following questions are covered in this work:

- transformation of local and global loads into values of the load effects,
- combination of the static wind load and global traffic actions based on data from monitoring,
- comparison of results based on predictions of extreme actions by several statistical methods,
- fatigue reliability based on **POT**,
- comparison of reliability indexes obtained for **ULS** and **FLS** using monitored data with those derived from design load models of European standards [6, 8, 7].

Figure 1.2 of Section 1.2 shows the main algorithm used to give answers to the listed questions. For each studied case, the applied methodology yields a formulation of the **limit state function (LSF)** to be used to assess reliability.

1.5 Scientific contributions

This Thesis on reliability of structures exposed to traffic loads and environmental loading reflects several important issues for advanced analyses in bridge engineering:

- reliability of critical structural details of the Millau viaduct (complex bridge structure),
- extrapolating in time traffic loads applied to the bridge based on monitoring data and methods of the **EVT** for ultimate and fatigue limit states,
- combination of traffic and wind actions for the deck analysis of the Millau viaduct,
- comparison between monitoring based models with design **EN** models.

Predicting actions and load effects in engineering structures is an important issue nowadays. When considered for bridges, there are two aspects: the safety of the structure and the extension of its operational life.

On the example of the unique and strategic structure of the Millau viaduct, we show the importance of the monitoring of actions. Moreover, we propose algorithms for estimating the reliability of the viaduct based on limited monitoring data. In the Thesis, the influence of the duration of monitoring of actions applied to the structure is analyzed for confidence intervals of predictions. It permits to make conclusions on how the quality of monitoring affects the estimation of the reliability at the end of the expected operational life.

While computing the reliability of the structure, a **LSF** must be defined correctly. In order to take into account the extrapolation in time of load effects, the **LSF** can be based on different methods of the **EVT**. The comparison between reliability indexes based on several approaches (**POT**, **BM**, **LCC**) is suggested as a part of this work and was presented in [71].

The other contribution of the Thesis is the study of the combination of traffic and environmental actions (represented here by the static wind) based on monitored actions with the design load combination according to European standards. The first analysis was proposed in 2017 [69], and further published in [68]. It is expanded for solving the reliability problem of the combination of traffic and wind actions and presented in 2019 [67]. For details, see Section 3.4 of Chapter 3 of the manuscript.

Moreover, the study of fatigue of critical structural details is presented, based on Palmgren-Miner's rule. The methodology, based on European standards and short-time monitoring, was studied in [80] (academic secondment). This methodology is compared with the one developed and presented in [70], based on the estimation of the fatigue damage with the use of the **EVT** for numbers of stress cycles.

1.6 Plan of manuscript

The manuscript is composed of two principal chapters.

Chapter 2 presents the methodology. It starts with the reliability method that is applied for extrapolated load effects, Section 2.1. Section 2.2 gives details on the use of the POT approach and on the updated methodology for a threshold choice. Methodology used in the Thesis to combine traffic and environmental actions is explained in 2.3. The following Section 2.4 describes other EVT methods used to compare with the POT approach. Finally, Section 2.5 gives a methodology for the application of the POT approach to extrapolate in time numbers of fatigue cycles.

The main work, that is focused on the Millau viaduct, is described in Chapter 3. The chapter begins by introducing the viaduct (Section 3.2), its geometry, the location and the description of monitoring of applied actions. Analysis of the recorded traffic flow and the main approach for predicting traffic actions are given in Section 3.3. As a part of the global loading on the deck of the viaduct, a probabilistic analysis of the combination of traffic queues with the static wind is proposed in Section 3.4. Section 3.6 describes computing local effects from passing vehicles on critical structural details of the deck, which are exposed to fatigue by using rules of European standards and extrapolating number of fatigue cycles in time by applying the POT approach. In order to finalize the study of the Millau viaduct and to compare the results obtained, a summary of the reliability of critical structural details is given in Section 3.7 for every case studied in this chapter.

The final chapter of the Thesis lists the final conclusions of every section of Chapter 3 and summarizes the scientific contributions. Ideas for further research are also provided in this chapter.

Chapter 4 is followed by the list of reference literature: normative documents, textbooks, journal articles, and other scientific sources. Appendix A gives the necessary excerpts from standards.

Chapter 2

Methodology

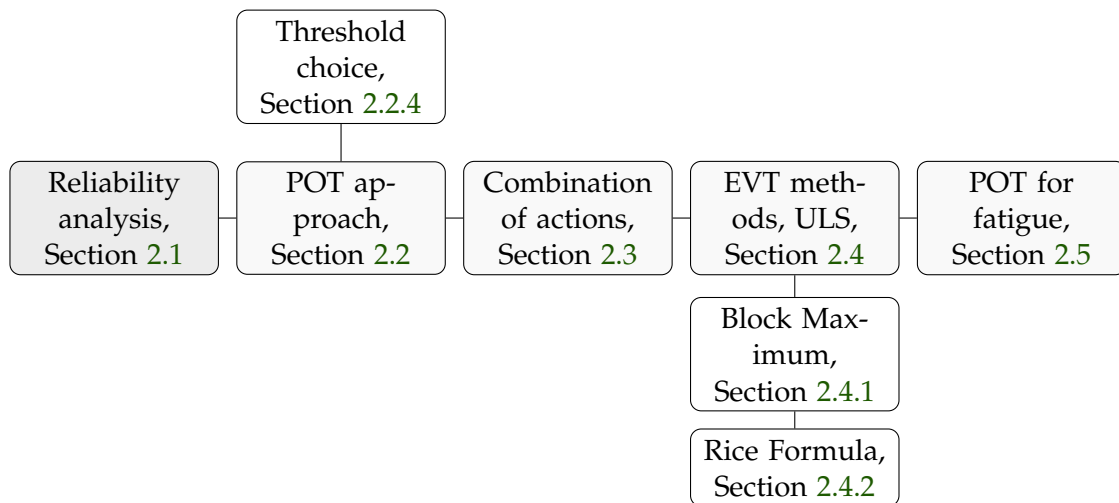


FIGURE 2.1 – Plan of methodology

First of all, this chapter introduces the reliability method that is applied for the extrapolated load effects (Section 2.1), Figure 2.1. It is followed by Section 2.2, which gives details on the **Peaks Over Threshold (POT)** approach and proposes an updated algorithm for choosing a threshold in Section 2.2.4. The **POT** method is used for a combination of the applied wind and traffic actions, which is presented in Section 2.3. Two other extreme-value approaches are used to compare with the **POT**: (i) **Block Maximum (BM)** with different block sizes and (ii) **Level Crossing Counting (LCC)**. The methodologies are described in Section 2.4. For the **fatigue limit state (FLS)**, Section 2.5 proposes the methodology to predict fatigue damage by using **Extreme Value Theory (EVT)** and, in particular, the **POT** approach.

2.1 Applied reliability method for extrapolated load effects

To assess the reliability of structural details, first of all, a **limit state function (LSF)** is needed.

Let $R \sim \mathcal{L}(\mu_R; s_R)$ be a real-valued random variable representing the initial resistance of material with a mean value μ_R and a standard deviation s_R , which is assumed to follow a Log-normal distribution \mathcal{L} . Let $S(x)$ be the real-valued random variable representing a load effect, depending on the nature of load x . A basic **LSF**, $G(x) = 0$ with:

$$G(x) = R - S(x), \quad (2.1)$$

is defined by comparison of R and $S(x)$. The values of reliability index β and the probability of failure P_f are found using **First Order Reliability Method (FORM)**. For each case of load effect, modeled by the real-valued random variable X , the reliability index β is found for the corresponding probability of failure P_f :

$$\beta = -\Phi^{-1}(P_f) = -\Phi^{-1} \left(\int_{G(x) \leq 0} q(x) dx \right), \quad (2.2)$$

where $q(x)$ is the probability density function of the load effect X and $\Phi(a)$ is the **cumulative distribution function (CDF)** of the normalized Gaussian distribution:

$$\Phi(a) = \frac{1}{\sqrt{2\pi}} \int_{-\infty}^a e^{-y^2/2} dy. \quad (2.3)$$

In order to perform the reliability analysis, the **LSF** are defined for all studied cases to obtain reliability indexes with the **FORM** method [18], based on values of load effects described in Chapter 3.

For the case of **ultimate limit state (ULS)**, when the interest is brought to extreme values of load effects, several different methodologies exist. In order to assess the reliability at the end of the design life, **EVT** approaches are used to define **LSF**. The most relevant ones (according to Section 1.3) are applied to compare the results.

2.2 POT approach with the updated methodology for a threshold choice

2.2.1 Peaks Over Threshold approach

The **POT** approach has been recently proved to be a good solution for predictions of extreme traffic actions [100, 93]. As time-series, the peak values of **load effect (LE)**, which lay above a certain threshold, are fitted to the **generalized Pareto distribution (GPD)**.

The peak values of **LE** that lay above a certain threshold u are fitted to the **GPD**. The conditional cumulative distribution function of Y given $X > u$, denoted by $F_u(y)$, can be expressed as:

$$F_u(y) = P[Y \leq y | X > u] = \frac{F(y+u) - F(u)}{1 - F(u)}, \quad (2.4)$$

in which $Y = X - u$, and where the threshold excesses are denoted by Y_i so that $Y_i = X_i - u$, and where $F(u)$ is the cumulative distribution function of random variable X .

The main principle of the POT approach was described a few decades ago [76] and is based on the following expression: $F_u(y)$ tends to the upper tail of a **GPD** with shape and scale parameters (σ and ξ). Under the following hypothesis, i) $y = x - u \geq 0$, ii) $x > u$ for $\xi \geq 0$, and $u \leq y \leq u - \sigma/\xi$ for $\xi < 0$, iii) $\sigma > 0$, we have,

$$G(x; \xi; \sigma; u) = \begin{cases} (1 - [1 + \xi(\frac{x-u}{\sigma})]^{-1/\xi}), & \xi \neq 0 \\ 1 - \exp(-\frac{x-u}{\sigma}), & \xi = 0 \end{cases} \quad (2.5)$$

The following assumptions have to be made for the application of the **EVT** :

- identical probability distribution of random variables X_i ,
- random variables X_i are independent,
- threshold u is sufficiently high.

For a long period, the observations can be based on the cumulative distribution function of extreme values over a shorter period [37]. Provided, for instance, in [14], for the probability $P[Y \leq y | X > u]$ with the probability of exceedance $\zeta_u = P\{X > u\}$, the return level is written as:

$$S_{pot}^{return}(p) = \begin{cases} (u + \frac{\sigma}{\xi}[(p\zeta_u)^\xi - 1]), & \xi \neq 0 \\ u + \sigma \log(p\zeta_u), & \xi = 0 \end{cases} \quad (2.6)$$

where $S_{pot}^{return}(p)$ is p -observation return level – a **quantile** that exceeds once every p observations with large enough p to provide $S_{pot}^{return}(p) > u$. The POT approach has also its drawbacks, such as selecting of an optimized threshold [73]. On one side, it should be reasonably high, so, that extreme event types are not mixed, in order to obtain their convergence. On the other side, the threshold must be low enough to provide a necessary number of peaks for obtaining reliable results. The correct choice of parameter estimators σ, ξ for the **GPD** is also a drawback of the approach [100].

2.2.2 Confidence Intervals

In this work, the means of comparison between several load cases is the value of the statistical uncertainty represented by values of **confidence interval (I)** for a **return level (RL)**. Here, 95% - **I** is used for return levels and it depends on the value of variance:

$$I = \pm 1.96 \sqrt{\text{Var}(S_{pot}^{return}(p))} \quad (2.7)$$

The value of variance for **RL** depends on variance of **GPD** parameters ξ, σ and on probability of exceedance ξ_u . All three parameters have maximum likelihood estimates: $\hat{\xi}, \hat{\sigma}$ and $\hat{\xi}_u$ [14], as the number of exceedances over threshold follow the Binominal distribution with $(N_{tot}, \hat{\xi}_u)$ and its natural estimator can be expressed as:

$$\hat{\xi}_u = \frac{N_e}{N_{tot}} \quad (2.8)$$

If $v_{i,j}$ represents values of variance-covariance matrix of **GPD** parameters ξ and σ , the complete variance-covariance matrix for all parameters is found as:

$$V = \begin{bmatrix} \hat{\xi}_u(1 - \hat{\xi}_u)/N_{tot} & 0 & 0 \\ 0 & v_{1,1} & v_{1,2} \\ 0 & v_{2,1} & v_{2,2} \end{bmatrix} \quad (2.9)$$

For a p -observations **RL**, $\nabla(S_{pot}^{return}(p))$, evaluated with parameters estimates $(\hat{\xi}, \hat{\sigma}, \hat{\xi}_u)$.

$$\nabla S_{pot}^{return}(p) = \begin{bmatrix} \partial(S_{pot}^{return}(p))/\partial\zeta_u \\ \partial(S_{pot}^{return}(p))/\partial\sigma \\ \partial(S_{pot}^{return}(p))/\partial\zeta \end{bmatrix} = \begin{bmatrix} \sigma p^\zeta \zeta_u^{\zeta-1} \\ \zeta^{-1} \{(p\zeta_u)^\zeta - 1\} \\ -\sigma \zeta^{-2} \{(p\zeta_u)^\zeta - 1\} + \sigma \zeta^{-1} (p\zeta_u)^\zeta \log(p\zeta_u) \end{bmatrix} \quad (2.10)$$

Then, the variance is assessed based on the delta method [52] and given by:

$$Var(S_{pot}^{return}(p)) = \nabla(S_{pot}^{return}(p))^T V \nabla S_{pot}^{return}(p). \quad (2.11)$$

It was recently concluded [81] that the efficiency of the described method is high enough under the assumption of normal distribution of return levels estimators. Therefore, it is used further in the current research.

2.2.3 POT for the reliability analysis

For a fixed period p , the LSF (2.1) based on the value of return level $S_{pot}^{return}(p)$ (2.6) takes the following form:

$$G_{pot} = R - S_{pot}^{return}(p; u, \sigma, \zeta, \zeta_u) = R - \begin{cases} u + \frac{\sigma}{\zeta} [(p\zeta)^\zeta - 1], & \zeta \neq 0 \\ u + \sigma \log(p\zeta), & \zeta = 0 \end{cases} \quad (2.12)$$

where $\zeta_u \sim \mathcal{B}(\mu_{\zeta_u}; s_{\zeta_u})$ is the amount of load effects, that exceed the threshold, over a total amount of monitored events, $\sigma \sim \mathcal{L}(\mu_\sigma, s_\sigma)$ and $\zeta \sim \mathcal{N}(\mu_\zeta; s_\zeta)$ are parameters of a fitted GPD (2.5), \mathcal{B} is Binomial distribution.

2.2.4 Threshold choice

The main drawback of the POT approach is the choice of a threshold, therefore, an updated algorithm is provided based on previous works in other fields [16], [21].

One of the most used ways to estimate the threshold is the mean residual life plot. The idea is to choose a sufficiently high limit so that the values exceeding it are well fitted to the GPD with corresponding shape and scale parameters. To reach that, the threshold is usually taken at the tail of the mean residual life plot (MRLP) when the function of the mean value excesses begins to be less curvy and has a tendency to be linear. Basically, the

MRLP is given by the set ζ of the "locus of points" (2.13) such that for an element x_i of the load effect, which exceeds a threshold u , with $i = 1, \dots, N_e$ and N_e the total number of excesses,

$$\zeta = \left\{ \left(u, \frac{1}{N_e} \sum_{i=1}^{N_e} (x_i - u) \right) : u < x_{max} \right\} \quad (2.13)$$

Another solution used is checking several different thresholds by evaluating of confidence intervals for return levels.

Let $U = U_0, \dots, U_k, \dots, U_p$ be the sequence of thresholds with U_0 corresponding to the value of 90%-quantile (as it was concluded to be the most appropriate choice, for instance, in the recent study for temperatures [95]) and U_p corresponding to the value of maximum threshold so that there are at least 30 events above it (as higher values of threshold would lead to an insufficient number of excesses $N_{e,k}$ to fit I, [99]). By substituting U into Eq. (2.7) of Section 2.2.2, we obtain a sequence of confidence intervals $I(U)$ and for each U_k , the probability of exceedance is written as

$$\zeta_{u,k} = \frac{N_{e,k}}{N_{tot}}, \quad (2.14)$$

in which N_{tot} is the total number of events.

Then, both $I(U)$ and $\zeta_u(U)$ are plotted in the one graph in order to choose the threshold that gives the smallest value of confident intervals. In the current section, the methodology according to the **EVT** is described. However, the motivation for the choice of a threshold level comes also from the design and serviceability purposes.

2.3 Combination of load effects caused by live and environmental actions

Let $X_I^{max} = x_I(L_I^{max})$ and $X_{II}^{max} = x_{II}(L_{II}^{max})$ be the independent random variables that model load effects in the same detail of a structure induced by the extreme values L_I^{max} of the first random load and the extreme values L_{II}^{max} of the second random load. The probability distributions of the extreme values L_I^{max} and L_{II}^{max} correspond to the same period of measurements. Both deterministic functions x_I and x_{II} are increasing functions (for positive values of a load effect). These two functions are associated with a computational model. Let Ω^{max} be the event defined by:

$$\Omega^{max} = \{X_I^{max} \in \tau_I\} \cap \{X_{II}^{max} \in \tau_{II}\}, \quad (2.15)$$

in which τ_I and τ_{II} are any given intervals. Since L_I^{max} and L_{II}^{max} are assumed to be independent random variables, we have:

$$Pr\{\Omega^{max}\} = Pr\{X_I^{max} \in \tau_I\} \times Pr\{X_{II}^{max} \in \tau_{II}\} \quad (2.16)$$

Considering **POT** as an approach for the computation of return levels for both traffic and wind actions, Eq. (2.12) is used for each load the way it was described in Section 2.2. The solution by **First and Second Order Reliability Methods (FORM and SORM)** gives β_{traf} and β_{wind} , see Eq. (2.2). The **LSF** G_{comb} for the combination of loads for the case when $\xi_t \neq 0$ and $\xi_w \neq 0$:

$$G_{comb} = R - S_G - (u_t + \frac{\sigma_t}{\xi_t}[(p\xi_t)^{\xi_t} - 1] + u_w + \frac{\sigma_w}{\xi_w}[(p\xi_w)^{\xi_w} - 1]) \quad (2.17)$$

where S_G is the stress induced by the self weight of the structure, u_t is a threshold for maximum values of stress from each passing vehicle, $\xi_t \sim \mathcal{B}(\mu_{\xi_t}; s_{\xi_t})$ is the amount of load effects, that exceed the threshold, over a total amount of monitored trucks, $\sigma_t \sim \mathcal{L}(\mu_{\sigma_t}, s_{\sigma_t})$ and $\xi_t \sim \mathcal{N}(\mu_{\xi_t}; s_{\xi_t})$ are parameters of a fitted to traffic load effects **GPD** (2.5), u_w is a threshold for stresses calculated from hourly wind velocities, $\xi_w \sim \mathcal{B}(\mu_{\xi_w}; s_{\xi_w})$ is the amount of extreme events (velocities that exceed the threshold) over a total amount of hours, $\sigma_w \sim \mathcal{L}(\mu_{\sigma_w}, s_{\sigma_w})$ and $\xi_w \sim \mathcal{N}(\mu_{\xi_w}; s_{\xi_w})$ are parameters of the **GPD** fitted to wind load effects.

The monitoring-based predictions for the combination of loads, Figure 2.2 provides β_{traf} , β_{wind} , and β_{comb} . They have to be compared with design models of European standards. The index β_{en} is computed with the respect to the load models of **European Norms (EN)** [7, 6]. The references are provided in Annex A.2 for traffic actions and in Annex A.1 for the wind.

In order to combine both types of loads and to compare them with European standards, calculations of design traffic actions F_t are made according to the load model LM1 of **EN** [7]. According to **EN** [5], the design value of an action can be crossed in 10% of cases every 100 years in case of traffic on bridges. The design model for wind actions F_w is based on the procedure explained in **EN** [6], Annex A.1, for the case of wind loads on bridges. According to **EN** [5], the design value of an action can be crossed in 2% of cases every year for the wind (as a climatic action).

The design combination of both loads is computed for **ULS** and **serviceability limit state (SLS)** respecting formulations proposed in European standards, see Table 1.1, Section 1.3.2. Considering W to be the value of self-weight of the structure, the wind to be a leading action $(F_w)_{lead}$, and traffic to be the accompanying action $(F_t)_{accomp}$, for a design combinations, the **LSF** (see Eq. (2.1)) can be written as follows:

$$G_{en} = R - S(W, \gamma_w, (F_w)_{lead}, \gamma_t, \psi_0, (F_t)_{accomp}), \quad (2.18)$$

where ψ_0 is a factor for combination value of accompanying variable traffic actions, γ_w and γ_t are partial factors for the wind and traffic.

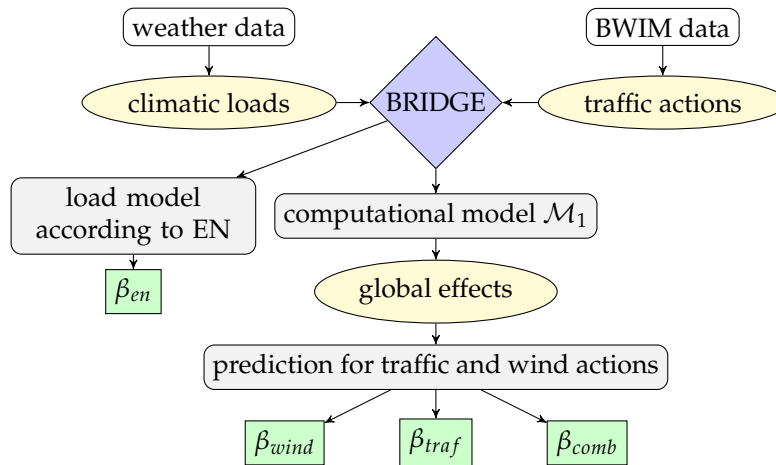


FIGURE 2.2 – General algorithm, case of combination of actions

2.4 Comparison between different approaches for load extrapolation

The main method for extrapolation of load effects in time, used in this work, is **POT** that has been described in Section 2.2. In addition, a comparison of this method with two more approaches (**BM** and **LCC**, see Table 1.2, Section 1.3.4) is made, Figure 2.3. The figure shows a branch of the algorithm that is meant to compare reliability indexes β_{pot} , β_{bm} and β_{lcc} obtained with mentioned three methods. The **LSF** for β_{pot} has been described in Section 2.2, Eq. (2.12).

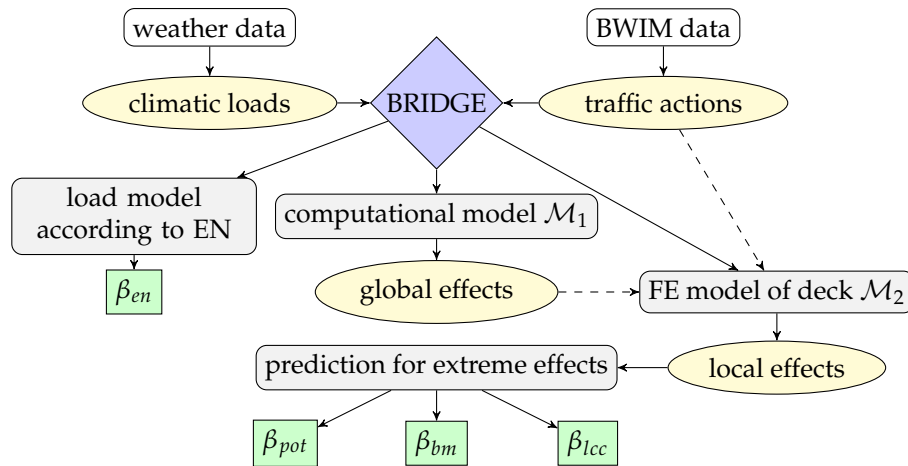


FIGURE 2.3 – General algorithm, case of local load effects, comparison of approaches

2.4.1 Block maximum method

The **BM** method is based on a limit theorem stating that the **generalized extreme value distribution (GEVD)** is an approximation for describing sample maximum for large sample sizes. This holds for the condition of the **BM** being (approximately) independent observations with identical distributions [14]. A **BM** series is generated by separating the time history for a load effect X into q intervals of a chosen size d_x and determining the maximum $x_{max} = \max(X \in d_x)$ in each interval. A definition of a return value for the load effect gives the basis for a **LSF** (with a reference block size d_{ref} and return period d_{return}):

$$G_{bm} = R - S_{bm}^{return}(\mu_b, \sigma_b, \xi_b) = R - \begin{cases} \mu_b - \frac{\sigma_b}{\xi_b} [1 - (d_{ref}/d_{return})^{-\xi_b}], & \xi_b \neq 0 \\ \mu_b - \sigma_b \log(d_{ref}/d_{return}), & \xi_b = 0 \end{cases} \quad (2.19)$$

where $\mu_b \sim \mathcal{N}(\mu_{\mu_b}; s_{\mu_b})$, $\sigma_b \sim \mathcal{N}(\mu_{\sigma_b}; s_{\sigma_b})$, $\xi_b \sim \mathcal{N}(\mu_{\xi_b}; s_{\xi_b})$ are location, scale, and shape parameters of the fitted **GEVD**, and where \mathcal{N} is the Normal distribution.

2.4.2 Rice formula

The Rice's formula [77] describes the mean rate ν of up-crossing for a certain level ν during reference period d_{ref} , and is fitted to the significant tail regions to the **up-crossing rate histogram (URH)** [36]. The starting point x_0 for the fit with Rice's formula is chosen as low as possible. It should be as low as possible, to ensure a sufficient amount of data for statistical extrapolation, but not too low to still provide a reasonable approximation of the significant tail region. In this study, optimal starting points are identified with evaluating the goodness of fit by means of a modified Kolmogorov test [36]. The **LSF** based on the **LCC** takes the following form:

$$G_{lcc} = R - S_{lcc}^{return}(d_{return}, \sigma_x, m_x, \nu_0) = R - (m_x + \sigma_x \sqrt{2 \ln(\nu_0 d_{return})}) \quad (2.20)$$

where d_{return} is the time reference that depends on a return period and the reference period d_{ref} , σ_x and m_x are estimated parameters of the fitted Rice's formula to the upper tail of **URH**, respectively, standard variation and the mean, ν_0 is a mean number of up-crossings by the zero level.

2.5 POT approach for numbers of fatigue cycles

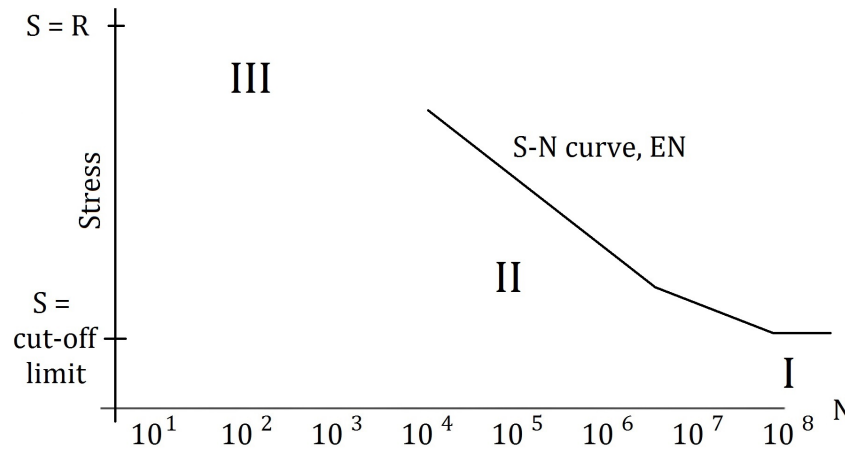


FIGURE 2.4 – Relation between stress and number of cycles: (I) - no any damage, (II) - fatigue damage, (III) - extreme load effects

A simple graph can represent the two cases of possible damage in a bridge structure, see Figure 2.4. Values of stress cycles of low and medium amplitudes (Figure 2.4, zones I and II) that are repeated millions of times can cause material fatigue in a structural detail. While the stress of a very high amplitude takes place quite rare, it is close to the critical value (Figure 2.4, zone III) and it affects highly the reliability of the detail. Either of them can cause damage in the future, therefore, predictions for both cases have to be made.

Usually, the EVT is used to estimate return levels for load effects of high amplitude, so, this question is covered in Section 2.2. In order to assess fatigue in an existing structure, EN [8] provides S-N curves for diverse structural details or elements, A.3. The LSF based on two-slopes S-N curve can be written as:

$$G_f = D_{cr} - R_p \left(\frac{1}{A} \sum_i dS_i^m N_i + \frac{1}{B} \sum_j dS_j^n N_j \right) \quad (2.21)$$

where $A = 2 \times 10^6 K^m$ and $B = 5 \times 10^6 (0.74K)^n$, m and n are slopes of the S-N curve, K is the detail category according to EN [8], $R_p = 365.25Y/d_m$ is the extrapolation in time reference for the number of years Y and monitored days d_m , D_{cr} is the critical damage accumulation, S_i is a considered stress range, such that $S_i \geq 0.74K$ with the corresponding number of cycles N_i , S_j is a considered stress range, such that $0.74K > S_j \geq 0.4K$ with the corresponding number of cycles N_j .

That gives a value of reliability index β_f , Figure 2.5, based on the model suggested in EN. Another methodology is used to assess the alternative value of a reliability index

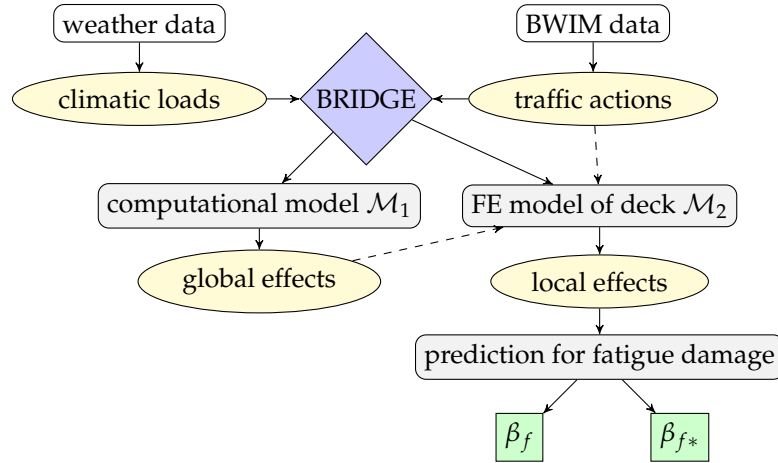


FIGURE 2.5 – General algorithm, case of fatigue

β_{f*} , Figure 2.5. As it has been proposed in Section 1.2, the use of the GPD with its shape and scale parameters makes it possible to assess values of return levels for the number of fatigue cycles at different levels of loading.

Let $\Delta = \{\Delta^{(1)}, \dots, \Delta^{(i)}, \dots, \Delta^{(r)}\}$ be the sequence of r stress ranges defined according to the dataset. Let $C^{(i)} = \{c_1, \dots, c_j, \dots, c_z\}$ be a daily number of cycles that is counted for each stress range $\Delta^{(i)}$, where z is the number of available days of monitoring (in a case of traffic loads, weekdays is separately counted from weekends and national holidays). Then, the probability distribution of each $C^{(i)}$ is exposed to the application of the POT approach (Section 2.2, 2.2.1 and 2.2.2). The resulting value of P -years return level $C_r^{(i)}$ for each $\Delta^{(i)}$ is an updated value of number of stress cycles for the P -years return period. Finally, fatigue damage is computed according to EN [8], see Annex A.3 using updated values of $C_r^{(i)}$ for $i = 1, \dots, r$, see Figure 2.6, that is written for given k and j .

$$G_{f*} = D_{cr} - \left(\frac{1}{A} \sum_i dS_k^m C_r^{(i)} + \frac{1}{B} \sum_i wdS_j^n C_r^{(i)} \right) \quad (2.22)$$

$$G_{f*} = D_{cr} - \frac{1}{A} \sum_{i=1}^b dS_k^m \left[u_i + \frac{\sigma_i}{\xi_i} ((p\xi_i)^{\xi_i} - 1) \right] - \frac{1}{B} \sum_{i=b}^w dS_j^n \left[u_i + \frac{\sigma_i}{\xi_i} ((p\xi_i)^{\xi_i} - 1) \right] \quad (2.23)$$

where $A = 2 \times 10^6 K^m$ and $B = 5 \times 10^6 (0.74K)^n$, m and n are slopes of the S-N curve, K is the detail category according to EN [8], D_{cr} is the critical damage accumulation, S_k is a considered stress range, such that $S_k \geq 0.74K$ with the corresponding number of cycles N_k , S_j is a considered stress range, such that $0.74K > S_j \geq 0.4K$ with the corresponding number of cycles N_j . The algorithm is detailed in Section 2.5.

The application of all the proposed methodologies is demonstrated in Chapter 3 for the case of the deck of the Millau viaduct.

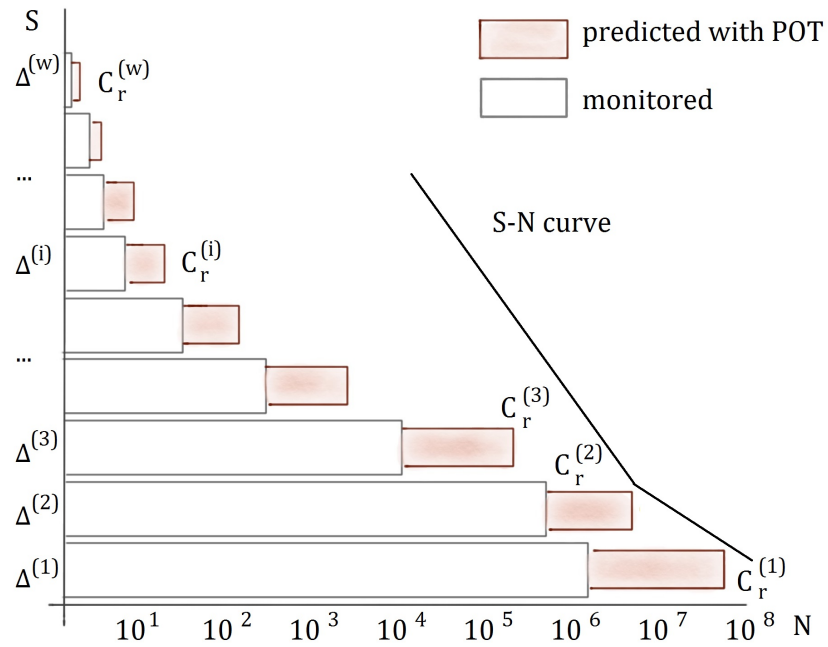


FIGURE 2.6 – Extrapolation of number of fatigue cycles, schematic graph

Chapter 3

Millau viaduct



FIGURE 3.1 – Perspective view of the Millau Viaduct

"Millau viaduct is a magnificent example, in the long and great French tradition, of audacious works of art, a tradition begun at the turn of the nineteenth and twentieth centuries by the great Gustave Eiffel."

(Jacques Chirac, former President of France)

3.1 Overview

Currently, in **European Norms (EN)**, information on evaluation of existing structures is quite limited for bridges (see Section 1.3). Due to the absence of a single valid set of rules or a standard procedure, every object has to be studied individually. At any moment of the **design service life** of an existing bridge, updating of its computational model can be done based on results from real-time monitoring. That leads to a better estimation of the **reliability** of structural elements and allows take necessary measures in time.

The object of study is the Millau viaduct, Figure 3.1. Among all other critical structural elements (such as steel cables exposed to the temperature actions, soil-foundation and thermal interaction under 250 meters high pile, dynamic influence of the wind on cables, etc), the deck is investigated in the current work. The attention is drawn to the effects in the deck of the viaduct under the extreme traffic load, fatigue, and combination of static wind actions and queues of lorries. More specifically, the focus is on welded connections between stiffeners to the plate of the **orthotropic** deck that are exposed to **fatigue** loading from heavy traffic.

Following the description of the viaduct (Section 3.2), the traffic actions are analyzed and extrapolated in time in Section 3.3. The literature review (Section 1.3) has shown the lack of probabilistic studies based on monitoring data for the combination of traffic and wind actions. Therefore, the chosen structure is a contribution into existing research in the field of combination of wind and traffic actions on bridges for both **serviceability limit state (SLS)** and **ultimate limit state (ULS)**, Section 3.4. Moreover, the comparison with design models proposed in **EN** is needed to observe whether European design load models are close to reality.

The interest to the case of **fatigue limit state (FLS)** was brought by conservative methods for predicting the fatigue life of steel elements in existing standards. In the current work, another approach is used based on application of **Extreme Value Theory (EVT)** to a given number of stress cycles, see Section 2.5. Details on the proposed method and results of its application to the deck of Millau viaduct are given in Section 3.6.

It is important to mention that monitoring data described in Section 3.2, are limited in quantity, which brings an additional challenge to the current work.

3.2 Object description

3.2.1 Location of the viaduct



FIGURE 3.2 – Location of the Millau viaduct in France, 

The Millau Viaduct is located in the South France, Aveyron region, in the communes of Millau and Creissels, see Figure 3.2. The bridge crosses the Tarn valley above its deepest point, making a link between two limestone plateaus. According to the history of the area, before the viaduct was constructed, traffic had to descend into the valley that caused heavy congestion.

The Millau bridge is a part of the A75 highway connecting two cities Clermont-Ferrand and Béziers, and more globally a high-speed road from Paris to Southern France and to Spain that significantly reduces the time of travel.

3.2.2 Geometry of the viaduct

Millau viaduct, Figure 3.3, is a cable-stayed bridge that consists of 8 spans with the total length of 2460 m. It is supported by reinforced concrete piles of various heights, from 77 to 245 m, each with a 90 m high steel pylon. The stiff orthotropic steel deck is suspended by 11 steel cables at each span. The expansion joints at the abutments permit openings

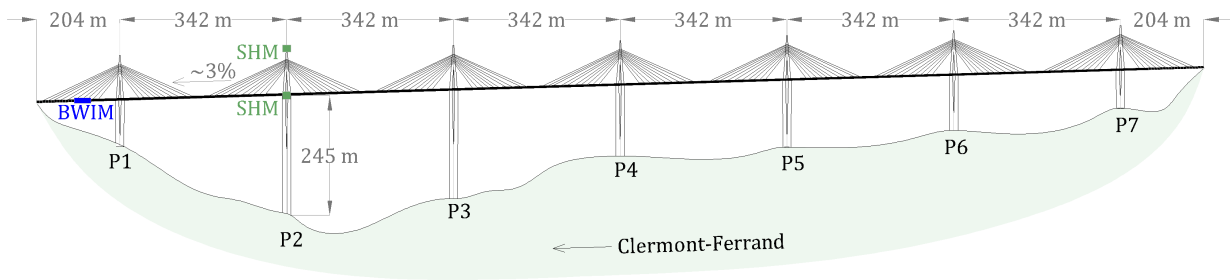


FIGURE 3.3 – Scheme of the Millau Viaduct

up to 80 cm in the longitudinal direction. Each span of 342 m is composed of four or six meters long elements separated by transversal stiffeners.

The cross-section of the deck, Figure 3.4, shows that the viaduct has two traffic lanes in each direction:

- slow lane, where traffic is mainly composed by heavy vehicles,
- fast lane, that is used by lorries only to overtake.

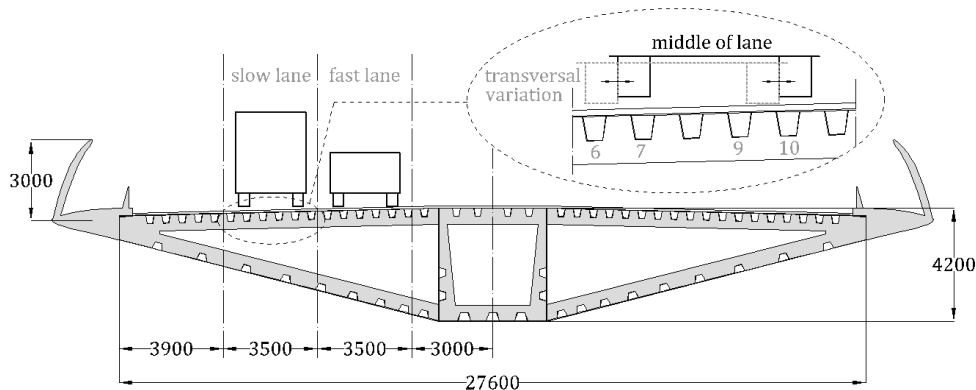


FIGURE 3.4 – Cross section of the deck of the Millau Viaduct

The orthotropic deck has a width of 27.6 m including the four meters wide box in the middle. Each side of the deck has 18 longitudinal stiffeners with trapezoidal cross-section shape and 7 mm thickness of the web. The width of both lanes is 3.5 m that brings attention mostly to 6th, 7th, 10th and 11th stiffeners, see Figure 3.4, that appear to be directly under wheels of passing heavy trucks. The steel plate of the thickness 14 mm (designed with the respect of EN [9]), is connected to stiffeners by welding, which is the critical detail of interest in a fatigue study. The deck is covered with the 60 mm thick layer of bitumen asphalt that contributes into wheel loading distribution on the plate of the deck. The deck has three meters high wind barriers on both sides that prevent trucks from losing stability due to the wind.

3.2.3 Monitoring of traffic

For the purposes of the current work, the results of the monitoring with the **bridge Weigh-in-Motion (BWIM)** system were provided.

It includes the following traffic data:

- total **gross vehicle weight (GVW)**, [$\text{kg} \times 10^3$] and axle weights, [kN],
- total and axle distances, [m],
- vehicle speed, [m/s],
- vehicle axles configuration.

Recordings were made between October 2016 and June 2017 with a few interruptions. At first, data for 44 days (43 days and the day of the calibration) were provided in the year 2016, then it was updated with a set of three more periods of monitoring results in 2017. In total, 180 days of data for traffic recorded on the Millau viaduct are used in this Thesis, Figure 3.5.

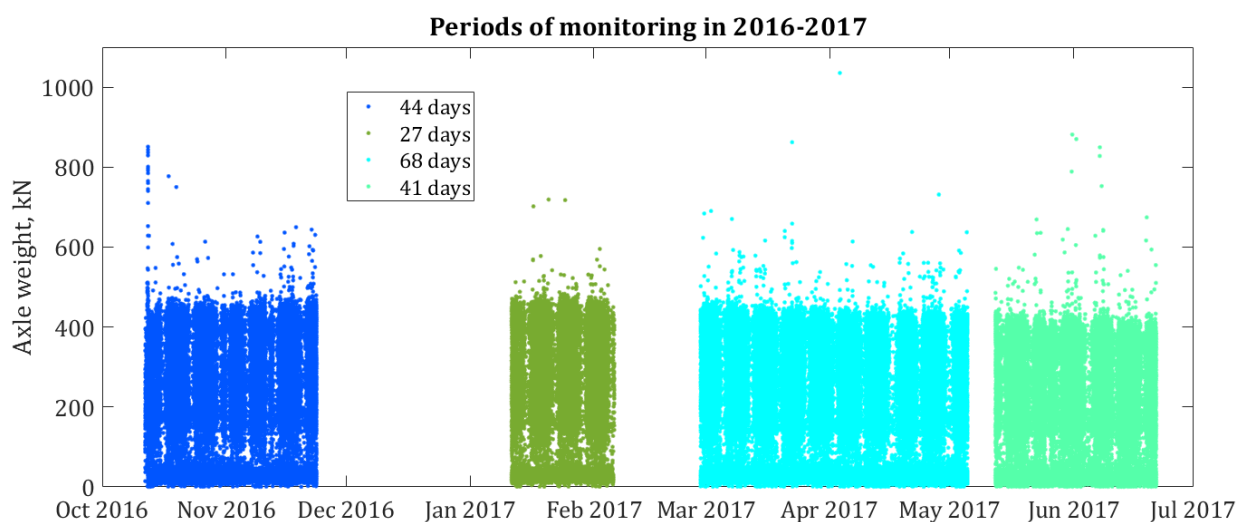


FIGURE 3.5 – GVW recorded with BWIM system, four periods of monitoring

The **BWIM** system was located in the middle of the first span of the viaduct, see Figure 3.3, and recorded all trucks passing the bridge.

The system itself, Figure 3.6, is composed of strain gauges, amplifiers, antialiasing filters, fast signal converters, and a computer. To weigh vehicles in motion, the strains were measured on the main longitudinal members inside of the bridge deck. Provided records describe the behavior of the deck elements under the moving load from traffic. Each strain transducer is introduced by four strain gauges in a full Wheatstone configuration. The measured strains are elongation and compression δL detected between two anchors

placed at a distance about $L = 200$ mm. The anchors are glued onto the inside surface of the bridge deck plate.

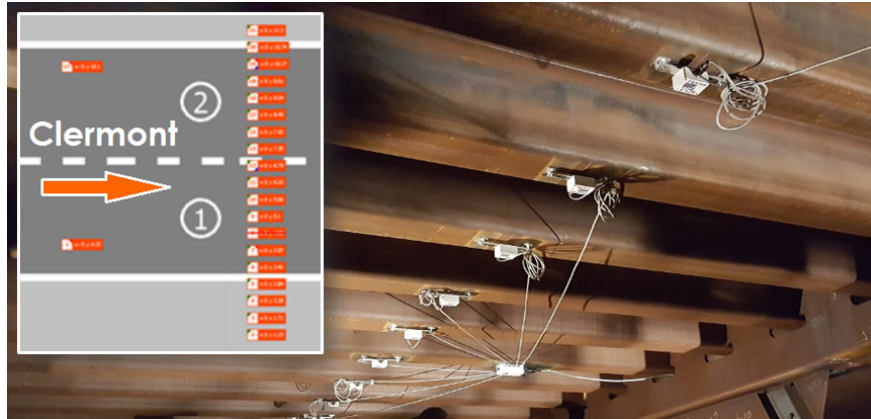


FIGURE 3.6 – BWIM system, scheme and photo inside the deck of the viaduct

The geometry of the bridge, especially the deck, is carefully taken into account while the system installation. Before being used, the system was calibrated with several trucks of known speeds and axles weights passing over it. The accuracy of monitoring results are reached by the classical theory of estimation with confidence intervals [54]. It is done under the COST-323 [4] specified test plans in order to achieve the 95-% confidence level. The calibration ensures that the static weight of trucks provided by BWIM system software is close enough to the reference weights, which had been measured just before entering the bridge. Moreover, the effects from site conditions (the pavement temperature) and the vehicles speeds are also implemented into the BWIM system software thanks to the calibration procedure.

Monitoring was done only in a more loaded direction, which does not allow a precise evaluation of effects on the viaduct. However, it permits to use recorded data for the study of one side of the deck, and to estimate reliability of the most critical structural details in the deck, but not of reliability of the bridge as a complex system.

Table 3.1 gives data for most common categories of vehicles recorded on the bridge during 180 days of monitoring. An example of data collection is given in Table 3.2 for a few trucks.

3.2.4 Data collection for wind

In order to observe the influence of some climatic conditions (here, the wind), the global effects on the entire structure are considered. The wind profile is formed according to the wind data at four different heights of the pile P2 and its pylon collected by the bridge








| Axle type | Image | % | Allowed GVW, ($\times 10^3$ kg) | I - 43 days | | II - 176 day | |
|-----------|---|----|----------------------------------|----------------|--------------------|----------------|--------------------|
| | | | | Total recorded | GVW over limit (%) | Total recorded | GVW over limit (%) |
| "113" |  | 47 | 44 | 17611 | 12.1 | 76754 | 7.0 |
| "11" |  | 35 | 19 | 12781 | 1.1 | 57442 | 0.7 |
| "112" |  | 9 | 38 | 3489 | 1.2 | 14658 | 1.0 |
| "111" |  | 2 | 26 | 878 | 2.9 | 3827 | 3.0 |
| "12" |  | 2 | 26 | 589 | 11.4 | 2908 | 8.7 |
| "1111" |  | 1 | 32 | 518 | 7.9 | 2211 | 8.8 |
| "1211" |  | 1 | 44 | 264 | 3.4 | 1084 | 3.3 |

TABLE 3.1 – Monitored data for different types of trucks

| Type (axles) | Distance between axles (m) | | | | Axle group | Weight of each axle (kN) | | | | |
|--------------|----------------------------|-------|-------|-------|------------|--------------------------|-----|-----|----|----|
| | 1 - 2 | 2 - 3 | 3 - 4 | 4 - 5 | | 1 | 2 | 3 | 4 | 5 |
| 113 (5) | 3.64 | 5.50 | 1.27 | 1.23 | 113 | 15 | 22 | 17 | 17 | 17 |
| 40 (2) | 5.27 | - | - | - | 11 | 41 | 119 | | | |
| 61 (4) | 3.69 | 6.73 | 1.31 | - | 112 | 32 | 139 | 34 | 34 | - |
| 100 (3) | 8.7 | 3.61 | 5.1 | - | 111 | 46 | 65 | 5 | - | - |
| 56 (3) | 6.8 | 1.46 | - | - | 12 | 78 | 142 | 142 | - | - |

TABLE 3.2 – Example of vehicles types

management system (BMS) and a Creissels national weather station located nearby (see Figure 3.2).

First of all, data from the structural health monitoring (SHM) system installed in the structure is used. It includes measurements of wind speeds and directions at the level of the deck and at the top of the pylon of the highest pile P2. The SHM system is operating only if the wind speed up-crosses the value of 25 m/s [45], which is not sufficient for the statistical analysis and for making predictions. For research purposes, during one week (16-20 May 2017) the SHM system was turned on during working hours to observe the values of the wind near the bridge structure (a sample of recorded signal is shown in Figure 3.7) and compare these values with those of the weather station. The following conclusions can be made based on provided results.

- The values of hourly mean or maximum of wind speeds are used in the further predictions: according to experience [24], these values are considered as independent observations of the wind speed.
- One of the most frequent directions is perpendicular to the longitudinal direction of the bridge deck (winds from North-West, Figure 3.8), what brings attention to

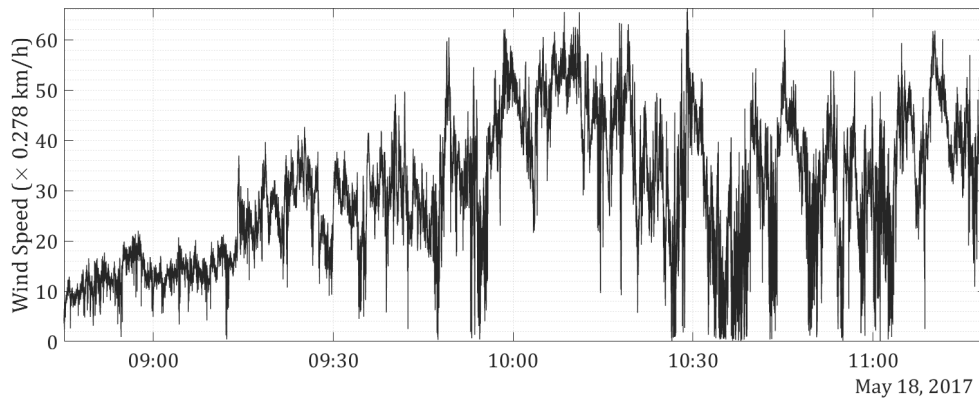


FIGURE 3.7 – Recorded wind speeds at the top of P2 of the Millau viaduct

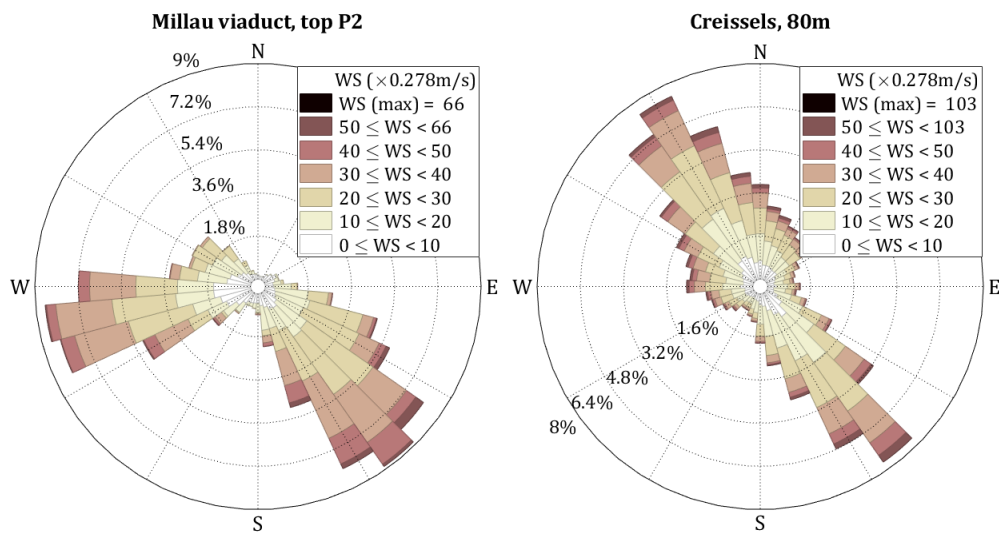


FIGURE 3.8 – Wind roses for the top of the pylon P2 and for the weather station

both **ULS** and **SLS** of the deck of the viaduct including possible torsion in the deck (see Section 3.4, Figure 3.28).

- The wind speed at the top of the tower is about 20% higher than at the level of the deck (Figure 3.9), which makes it necessary to take this difference into account in calculations.

Secondly, weather data for wind velocities in the area are coming from the climatic station located nearby, in Creissels, and comprise values of wind speeds and directions for each hour at the height of 80 m above the ground. To obtain values of the wind speed at the level of the deck (249 m height) and at the top of P2 (339 m height) of the viaduct, a simplified calibration has been done depending on the mean values of differences between wind velocities at several heights. Monitored wind velocities for certain hours

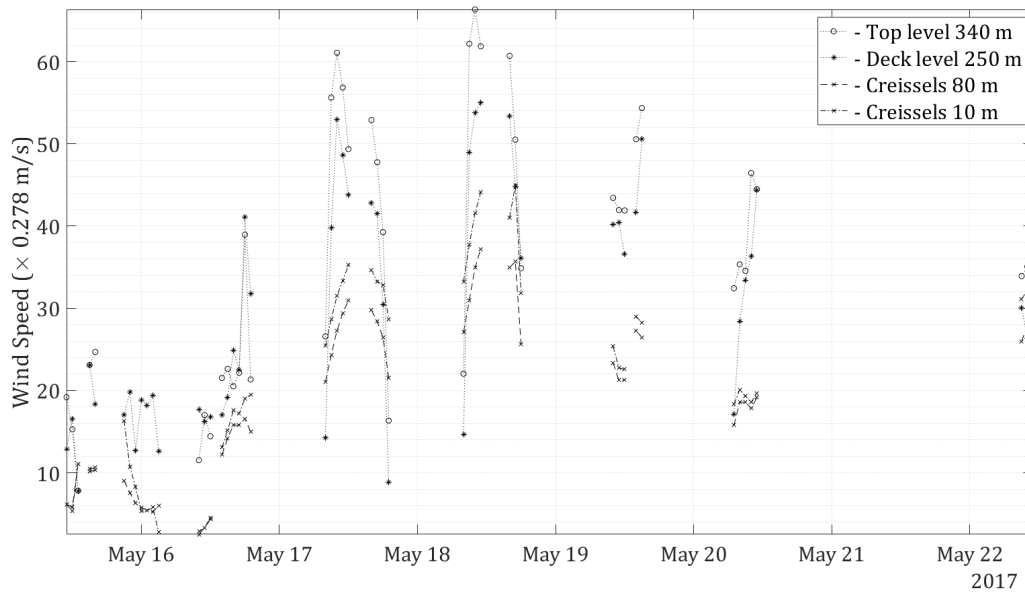


FIGURE 3.9 – Wind speeds at different levels based on different recorded data for Millau viaduct

between 16th and 20th of May, 2017 (Figure 3.9) are compared with wind velocities from the Creissels weather station.

Figure 3.9 shows that the "peaks" of velocities arrive approximately at the same time. The random variables represent the differences of wind speeds between several heights (the Creissels weather station, the deck and the top of the pylon P2 of the Millau viaduct). From the measurements, the statistical estimation of their probability distribution functions show that these random variables follow Normal distribution. Only velocities of more than 30 km/h are considered.

The period of weather data is chosen to be the same as for the monitoring of traffic: (11/10/2016 – 21/06/2017). The obtained histograms of wind speeds at four different levels of the pile and pylon are shown in Figure 3.10. In the considered direction, the maximum wind speed recorded during this period is 55 km/h (15.2 m/s). The 95%-estimate of the confidence interval of wind speed is 74.6 ± 10.4 km/h (20.7 ± 2.9 m/s) at the top of the considered pylon P2 and 68.6 ± 8.4 km/h (19.0 ± 2.3 m/s) at the deck level. The values of the wind force as a function of the wind speed are evaluated according to the methodology given in Appendix A.1. The summary is given in Table 3.3 for different bridge elements of the considered span, Figure 3.11. The geometry corresponds to the real geometry of the viaduct but only a part of the viaduct is considered including the highest pile and its pylon, cables and a 342 m part of the deck from the middle of the

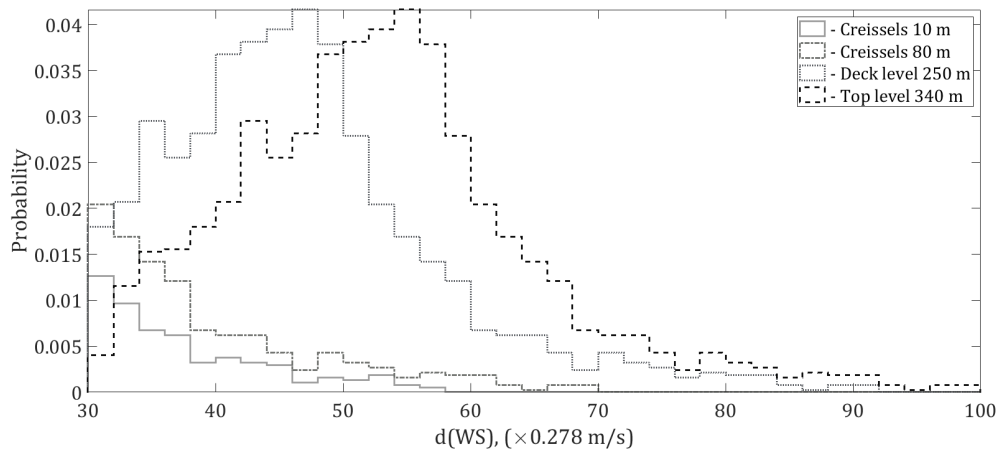


FIGURE 3.10 – Histogram of the wind speeds at different levels for the period Oct 2016 – June 2017

second span till the middle of the third span.

| element | Speed (m/s) | Pressure (Pa) | Area (m^2) | Load (kN/m) | Comment |
|-----------------|----------------|------------------|-------------------|----------------|------------------------|
| Pier, bottom | 28.6 | 528.8 | 2635 | 9.0 | |
| Pier, top | 31.7 | 647.8 | 1530 | 11.0 | |
| Deck | 34.7 | 778.8 | 2394 | 266.4 | wind barrier 3m height |
| Pylon, bottom | 34.7 | 778.8 | 360 | 7.8 | |
| Pylon, middle | 35.8 | 829.5 | 295.2 | 6.8 | |
| Pylon, top | 36.9 | 881.7 | 43.5 | 2.6 | |
| Cables to pylon | 35.8 | 829.5 | 665 | 27.6 | as distributed load |
| Cables to deck | 34.7 | 778.5 | 665 | 518 kN | as concentrated load |

TABLE 3.3 – Wind load as a function of wind speed

In addition, due to the availability of data and for statistical calculations, these data were extended twice: one with the period of bridge operation (16/12/2004 – 01/03/2018) and one with the entire period of available climatic data at the Creissels weather station (01/01/1985 – 01/03/2018) in order to observe the influence of monitored duration on results. The results are discussed in Section 3.4.

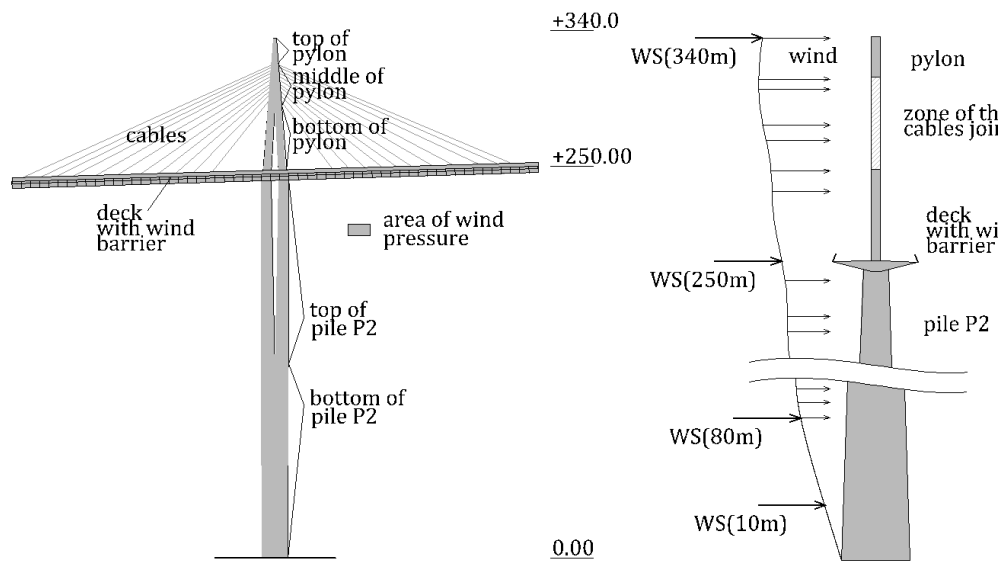


FIGURE 3.11 – Wind load collection from wind speed at four different levels of considered part of the viaduct

3.3 Analysis of monitored traffic actions on the deck of the viaduct

This Section presents a detailed analysis of recorded traffic by **BWIM** system in order to prepare the data obtained from monitoring and to perform the extrapolation of traffic loads in time.

3.3.1 Amount and stationarity of traffic

The data from **BWIM** monitoring on the deck of the Millau viaduct include axles configuration of passing vehicles, as well as axle weights and distances, the speed and the time of passages. These data are used to build a statistical model for extrapolating in time loads and load effects using the **EVT**. One of the requirements for application of **EVT** is that the input data is stationary in time.

The graph in Figure 3.5 has shown **GVW** in time for all available periods of measurements. It was observed that traffic is rather stationary every week – more traffic is passing in weekdays and there are hours with fewer trucks on weekends. Four constant periods of monitoring give a bar-chart, Figure 3.12, with probabilities of occurrence of vehicles depending on the day of week for each of four periods, where $Pr = 1.0$ is equal to the total amount of trucks recorded during the period. Further in work, the assumption of

continuity of monitoring is made by ignoring the "gaps" in time where data were missing, so a period of 180 days is studied.

The bar-chart in Figure 3.12 shows the peak in volume on Wednesdays, less trucks are observed on Saturdays, and the least amount on Sundays. However, for the summer period, the number of vehicles is very high on Sundays what raises a question to weekly stationarity. Though, if too look closer to data, only the number of light vehicles increases in summer but not of lorries. It means that weights of trucks cannot be treated all together but the different types of vehicles must be separated, and brings attention to different axle configurations, Figure 3.13.

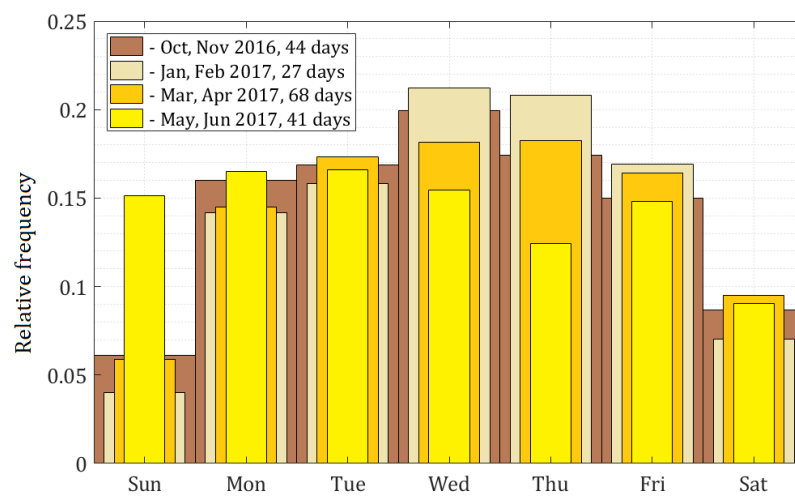


FIGURE 3.12 – Relative frequency of occurrence of vehicles per day of week, four periods of monitoring

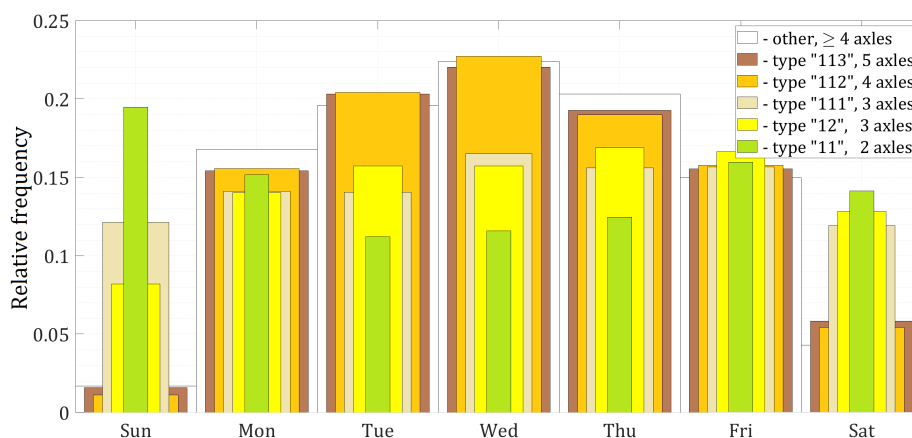


FIGURE 3.13 – Relative frequency of types of recorded vehicles per day of week

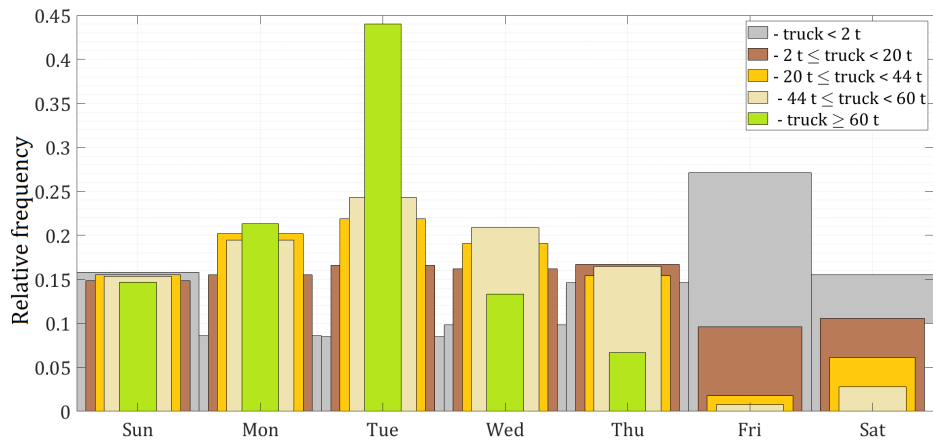


FIGURE 3.14 – Relative frequency of masses of recorded vehicles per day of week

The bar-chart in Figure 3.13 divides the volume of vehicles (for the entire 180 days of monitoring) into a few different types: two-axes trucks "11", 3-axes "111" and "12", then, "112" as a common four-axes truck and "113" for five-axes one, according to Table 3.1. The relative frequency per day of week shows the larger vehicles with four and more axes and has almost the same distribution (with the most amount on weekdays), while the lighter vehicles with three axes or less do not change much in number from day to day. It means that predictions for trucks have to be separately made for each type, more details are given in Section 3.3.2.

Second important issue is the stationarity of traffic in weight, Figure 3.14. The third bar-chart shows that light vehicles (under two tons) cross the viaduct mostly from Friday to Sunday, while the largest amount of overweighted (more than 44 tons) and highly overweighted (more than 60 tons) trucks can be mostly seen during the middle of the week. Section 3.3.3 gives more details on the issue. The amplitude of load plays the most important role, when the ULS is considered, while the amount of traffic is more important for the question of fatigue in structural details.

To conclude the topic of weekly stationarity of traffic actions, Figure 3.15 shows an extract of the recorded "113" vehicles. It can be clearly seen that the outline of distribution of vehicles over time repeats itself from week to week. Red color shows recorded overweighted trucks. So, weekly stationarity of traffic actions depending on vehicles type is assumed further in the work.

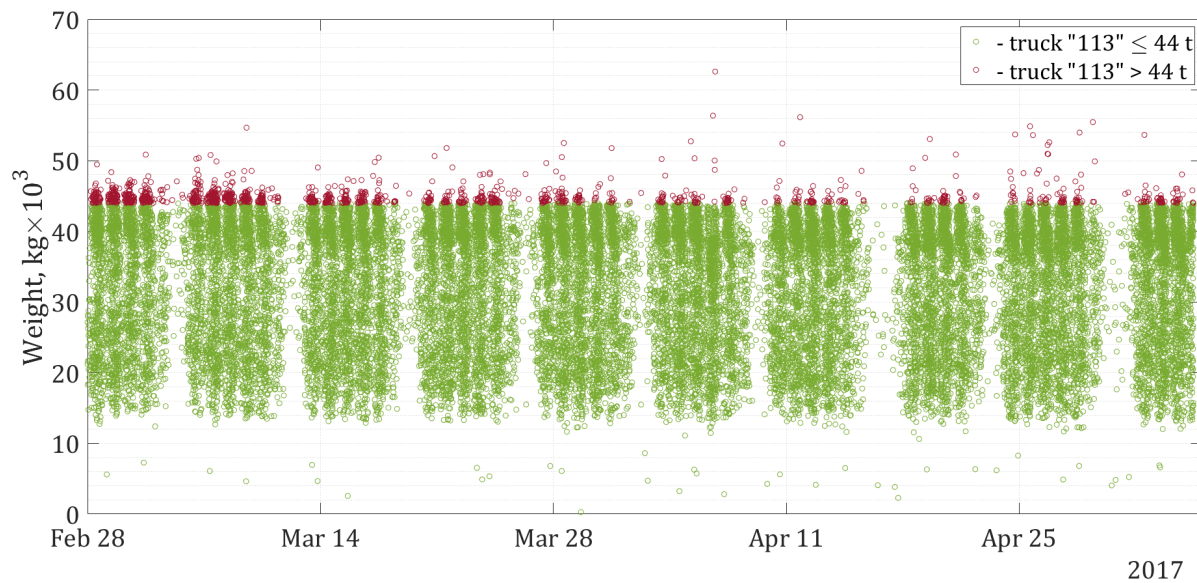


FIGURE 3.15 – Evidence of weekly stationarity, vehicle type "113"

3.3.2 Vehicles types

The distribution of the most common vehicle types is shown in the Figure 3.16, as we can see, it is mostly composed of two-, three-, four- and five-axes vehicles. If the two-axes type is represented only by type "11", for all other axle numbers there are a few different types of axes combinations. They are shown on pie-charts of Figure 3.17.

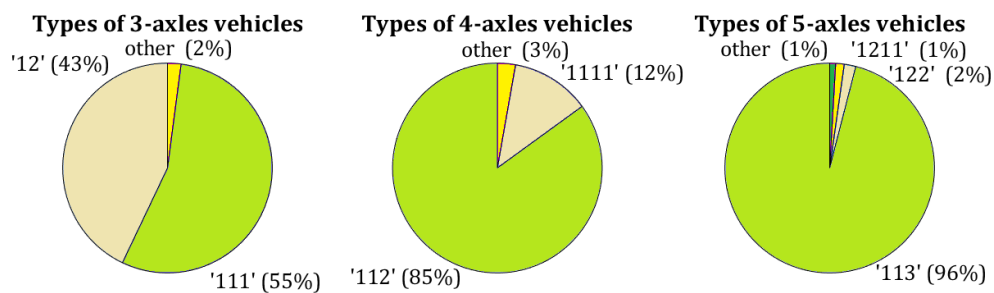


FIGURE 3.17 – Common numbers of axes for different types of vehicles

It is clearly seen that the type "113" represents a half of all heavy transport going through the viaduct and 96% of all vehicles in the five-axes category are given by this type. Type "113" (see example in Figure 3.18) is the most common truck in France, therefore, a special attention is given to this type in the current work. As well, other categories mentioned in pie-charts, are considered, see Table 3.4.

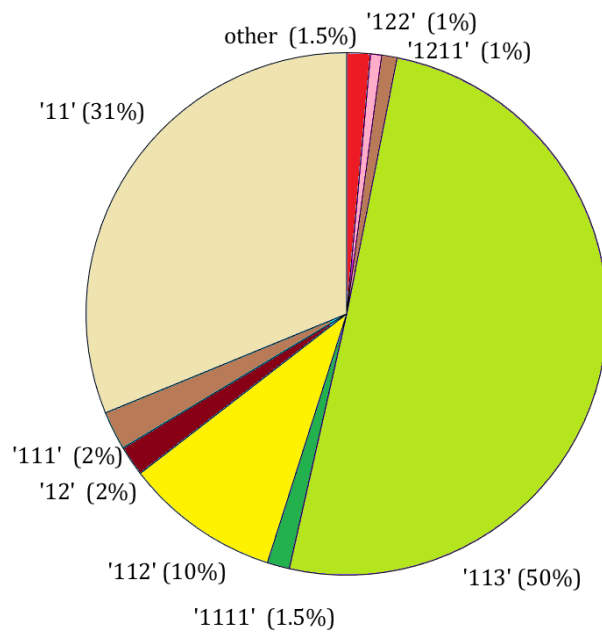


FIGURE 3.16 – Axles configuration types of vehicles on the Millau viaduct

| Axles types, T | Number of axles | $Pr(T)$, % |
|------------------|-----------------|-------------|
| '11' | 2 | 31 |
| '111' | 3 | 2 |
| '12' | 3 | 2 |
| '112' | 4 | 10 |
| '1111' | 4 | 1.5 |
| '113' | 5 | 50 |
| '122' | 5 | 1 |
| '1211' | 5 | 1 |
| other | ≥ 3 | 1.5 |

TABLE 3.4 – Proportion of number of axles of each axles type

Further in the work, predictions are made for the following types: "11", "12", "111", "112", "113", "1111", "1211". Other types are neglected as they occur so rare that during 180 days of monitoring that their amount is not enough to apply the extreme value analysis. Also, predictions for all vehicle together are made to observe the contribution from each type into the total "extreme" loads distribution.

Another important point here is a grouping of axles into two (type "12", "112", "1211") or three ("113"). If not the total mass of the vehicle is considered but a mass of each axle, then, for extreme value analysis the biggest amplitude of the group has to be considered and for fatigue analysis - values of stress caused by the group shall be calculated and not from each axle separately. This topics are covered in Sections 3.3.5 and 3.5 for extreme value analysis and 3.6 for fatigue. A few more details are given in the following Section 3.3.3.

3.3.3 Amplitude of load effects

In previous sections, it has been explained that trucks of different types should not be treated together. So, a set of histograms, Figure 3.19, shows amplitudes of loads for each vehicle type obtained from the monitored data by BWIM system on the deck of the Millau viaduct. Number of occurrences N is plotted for values of GVW [kN] of every considered type of trucks. The bin width is taken equal to 10 kN. Histograms have complex shape



FIGURE 3.18 – The most common type "113" of heavy vehicles in France

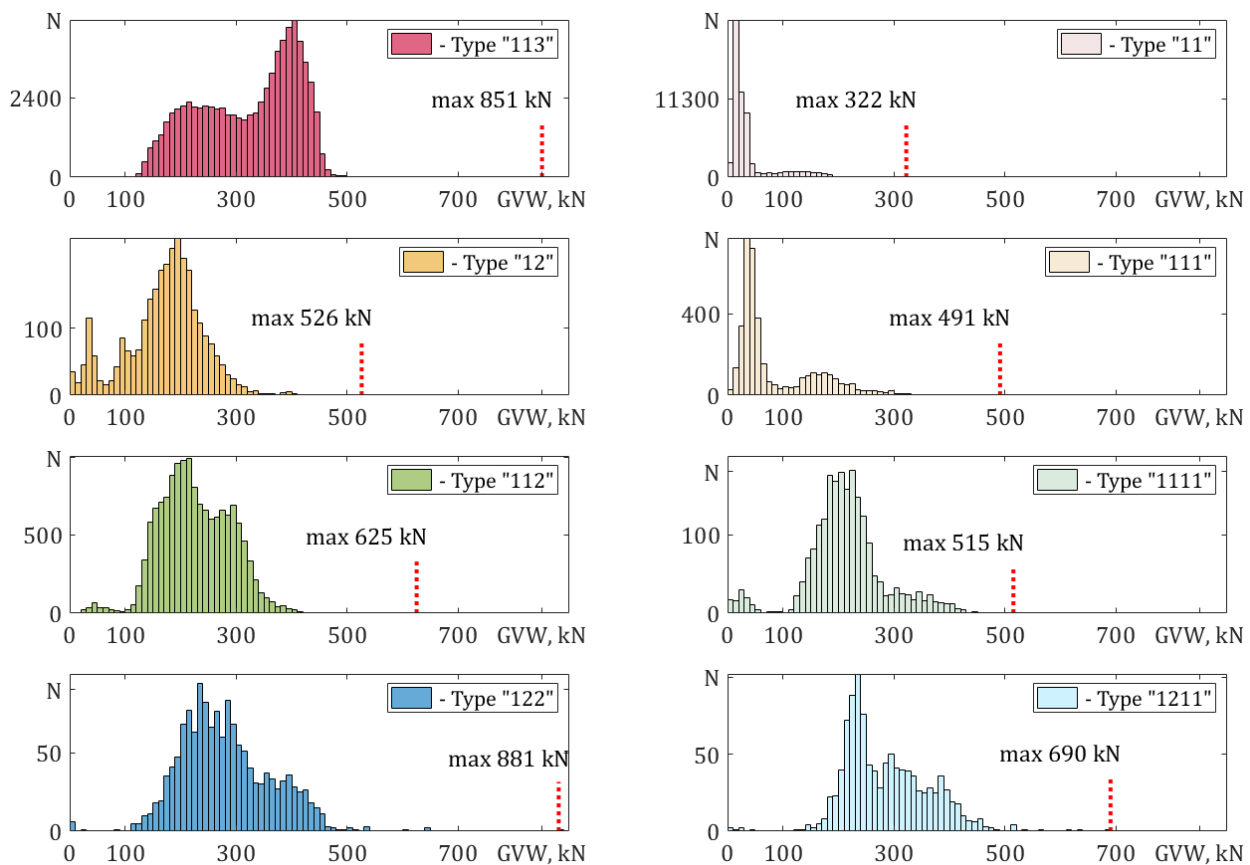


FIGURE 3.19 – Histograms of total vehicles mass per vehicle type

and cannot easily be fitted to a parametric distribution. However, the main goal here is to make extrapolation in time based on **EVT** methods, which requires only a tail of these histograms to be fitted.

For each considered type of vehicles, the value of **GVW** differs depending on number of axles and a level of charging of a vehicle. In France there are certain regulations for

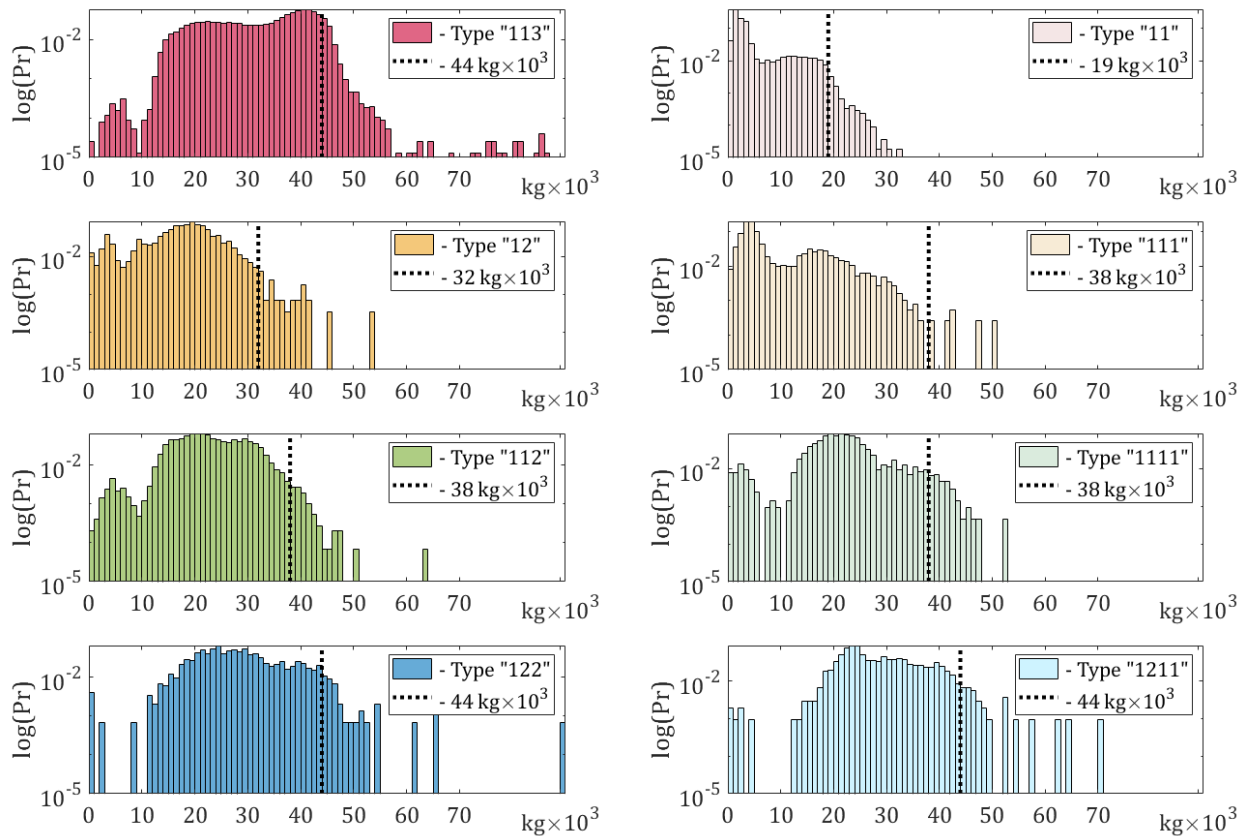


FIGURE 3.20 – PDFs of total vehicle mass and allowed mass per vehicle type

maximum values of the **GVW** for each type, as well as for axle loads [13]. Permitted masses Values of permitted in France masses of vehicles for axle distances d [m] are reflected in Table 3.5. The heaviest five-axles vehicle should have no more than 44 t with the maximum axle group mass of 19 t.

| axles type | permitted GVW , t | max single axle mass, t | group of axles mass, t | | |
|---------------|-----------------------------|----------------------------|------------------------|----------------------|------------------|
| | | | $(d < 1m)$ | $(1 \leq d < 1.35m)$ | $(d \geq 1.35m)$ |
| 11 (truck) | 19 | 13.0 | - | - | - |
| 11 (bus) | 32 | 12.0 | - | - | - |
| 111 | 38 | 12.0 | - | - | - |
| 12 | 32 | 13.5 | 13.5 | 16.0 | 19.0 |
| 112 | 38 | 13.0 | 13.5 | 16.0 | 19.0 |
| 1111 | 38 | 13.0 | - | - | - |
| 113 | 44 | 13.0 | 27.0 | 27.0 | 27.0 |
| 122 | 44 | 13.0 | 13.5 | 16.0 | 19.0 |
| 1211 | 44 | 13.0 | 13.5 | 16.0 | 19.0 |

TABLE 3.5 – Permitted in France masses of vehicles for axle distances d [m]

Figure 3.20 shows a set of histograms for the same vehicle types. Each PDF is related to

the occurrence of the mass of vehicles [kg] with the bin width of 1000 kg. The permitted total vehicles masses are shown (black dotted line) to highlight a few trucks that overpass a limit. The logarithmic scale allows better observation of histograms tails.

3.3.4 Invalid input data and assumptions made in the current work

Before beginning the extrapolation of traffic loads in time, it is important to mention invalid input data. First of all, out of all 180 days of data received from BWIM system, $\approx 2\%$ of data carried a measurement error, such as missing record of time, negative values of the weight, impossible values of vehicle lengths (less than a meter or superior 18.75 m [12]), see Table 3.6.

| error source | initial number of data | number of error data | % | reduced number of data |
|-----------------------|------------------------|----------------------|--------|------------------------|
| Invalid date and time | 165 906 | 3 | 0.0002 | 165 903 |
| Invalid truck length | 165 903 | 1 364 | 0.8 | 164 539 |
| Negative truck weight | 164 539 | 1 984 | 1.2 | 162 555 |

TABLE 3.6 – Errors from BWIM measurements

Moreover, $\approx 0.1\%$ of all recorded vehicles had an error in axles types definition. To find out this error it is necessary to separate vehicles passing on slow traffic lane 1 and on high-speed lane 2. After removing invalid data, it was obtained 151 025 vehicles for the slow lane that is 92.9% of total amount. So, the rest 7.1% or 11 530 vehicles were passing the fast lane. Table 3.7 gives the number of invalid data per vehicle type (considered in Section 3.3.1) for each of two lanes. The last row shows the exact amount of vehicles of other types of axles configurations.

Vehicles passing on the fast lane are much fewer in volume and in weight compare to the slow lane. Figure 3.21 shows distributions of vehicles on fast (black histogram) and slow (color histogram) lanes. Further in the work, most of results are shown for the slow lane as more charged with heavier vehicles. As well, more data are available that leads to better fit the statistical distributions. The error of the computation of GVW provided by BWIM system (www.cestel.eu) is 3%.

The main assumptions introduced in the current work are:

1. statistical independence of events of a vehicle passage over the bridge,
2. identical distribution of vehicles in time, considering that every week day there are more vehicles than during weekend,

| considered vehicle type | lane 1 151025 vehicles | | | | lane 2 11530 vehicles | | | |
|-------------------------------|---------------------------|---------------------|------|-------|--------------------------|---------------------|------|------|
| | number | invalid distance | axle | % | number | invalid distance | axle | % |
| "11" | 47 058 | 38 | | 0.08 | 10 356 | 0 | | 0 |
| "111" | 3 545 | 79 | | 2.23 | 198 | 2 | | 1.01 |
| "12" | 4 094 | 6 | | 0.15 | 85 | 1 | | 1.17 |
| "112" | 4 095 | 9 | | 0.22 | 84 | 0 | | 0 |
| "1111" | 2 073 | 17 | | 0.82 | 42 | 10 | | 4.2 |
| "113" | 76 180 | 2 | | 0.003 | 599 | 0 | | 0 |
| "122" | 1 421 | 2 | | 0.14 | 25 | 0 | | 0 |
| "1211" | 1 052 | 0 | | 0 | 8 | 0 | | 0 |
| | invalid: | 213 | | 3.56 | | 13 | | 6.38 |
| other | 2 200 | | | 1.46 | 79 | | | 0.68 |

TABLE 3.7 – Errors in axles types definition in input BWIM data

3. continuous records by **BWIM** systems, gaps in time (between four periods of measurements, see Figure 3.5) are ignored,
4. vehicles are passing in the middle of the lane.

3.3.5 Extrapolating of monitored traffic actions in time with the POT approach

Two installations of **BWIM** system in the deck of the bridge give two available periods of traffic measurements allow for comparing predictions made by using short time (43 days) BWIM-I monitoring with results based on a longer period BWIM-II (180 days). These measurements provide sets of values of vehicle masses (**GVW**), which are used in the **EVT**, based on the threshold models [14]. Extreme effects (**GVW** that crosses a **threshold** (**TH**)) are fitted to **generalized Pareto distribution** (**GPD**), see Appendix 2.2.1 with the following computation of return levels.

Figure 3.22 represents the different steps of the procedure that are used for each type of vehicles. The methodology for the application of **Peaks Over Threshold** (**POT**) (Figure 3.23) to recorded values of **GVW** and for the calculation of the return levels is given in Appendix 2.2.1.

The return levels are estimated for the guaranteed lifetime of the bridge of 120 years [15]. The evaluation of confidence intervals is detailed in Appendix 2.2.2. The confidence intervals of return levels of **GVW** for BWIM-I and BWIM-II are compared in order to observe the influence of monitoring duration on the results. The distribution of single vehicles is made for each axles type (Figure 3.21) separately and for all vehicles together.

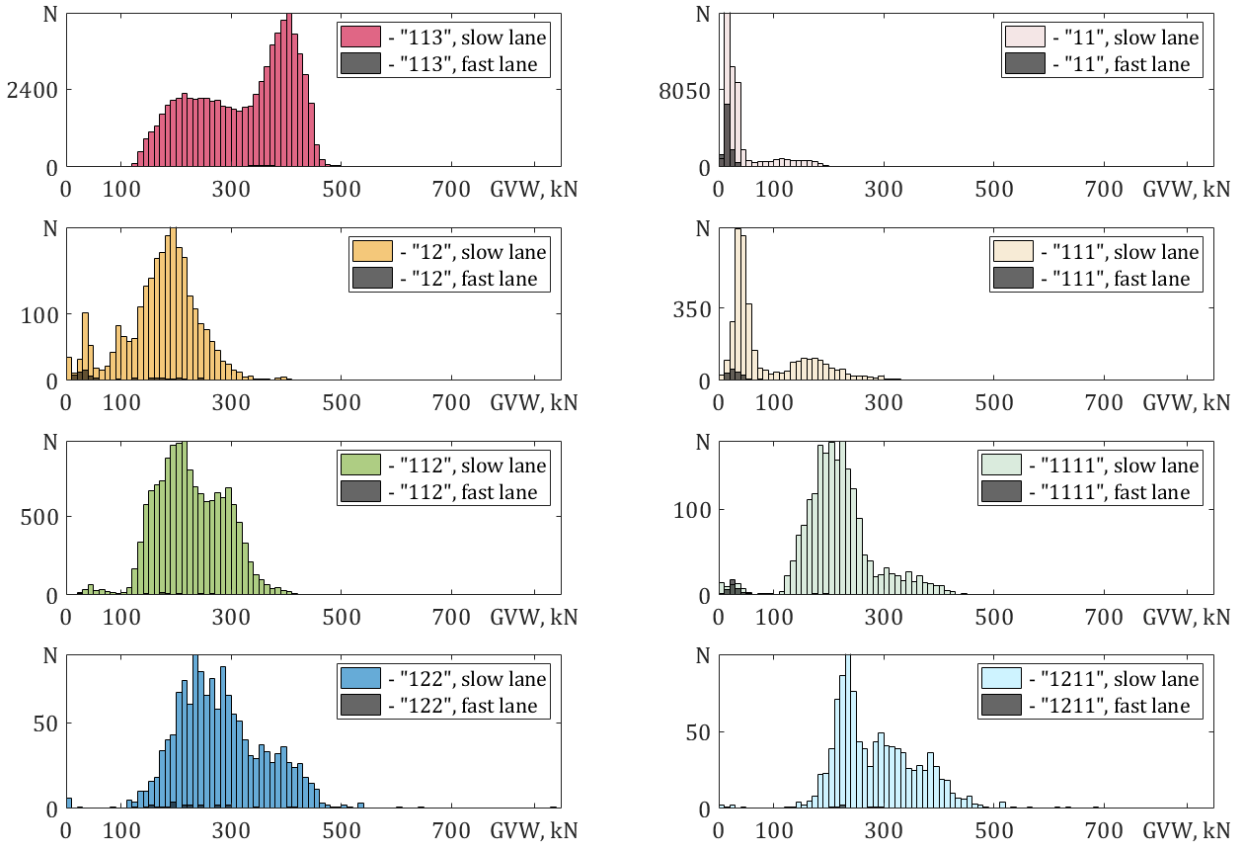


FIGURE 3.21 – Histograms of vehicles on slow and fast lanes

1. The first difficulty of the POT approach is finding a correct threshold. The most common methods proposed in EVT [14] are the following:
 - (a) observing the **mean residual life plot (MRLP)**, see Eq. (2.13) in Section 2.2,
 - (b) observing the stability of shape and scale parameters of **GPD** depending on the threshold.

An example for both methods is given in Figure 3.24 for axle type '1111'. The threshold is supposed to be chosen at the part where the mean residual life curve becomes linear. As for stability of shape and scale parameters of **GPD**, in this particular example, there is no any part, where either of them would be stable, so, the threshold choice becomes unclear. However, for the given example, the area of such linearity is too large with possible threshold between 29 and 39, so, the methods become quite inaccurate.

Another graphical method is proposed here - the updated algorithm for a threshold choice. It consists in checking several different thresholds with corresponding model checking and evaluating the confidence intervals for return levels, as it is

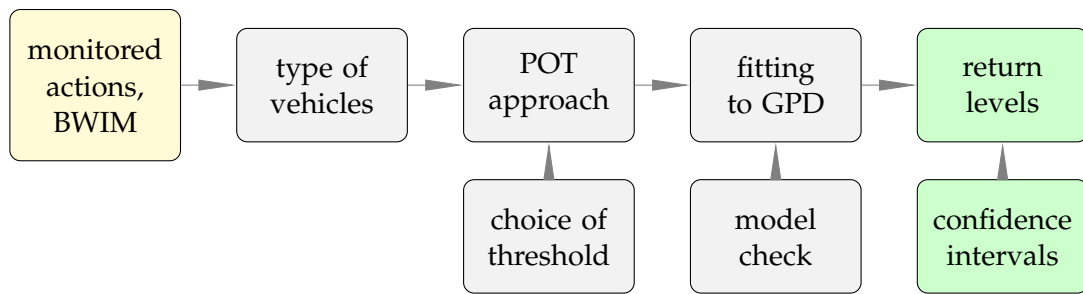


FIGURE 3.22 – Steps to be taken from monitoring to predictions of traffic actions and load effects

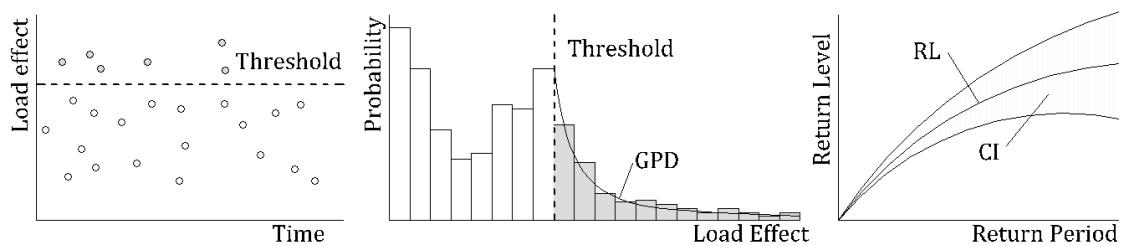


FIGURE 3.23 – Representation of the POT approach

explained in Section 2. The algorithm has been written in MATLAB and an example for the same axle type '1111' is presented in Figure 3.25. This figure shows three curves: return level, confidence intervals, and **probability of exceedance (PE)** as a function of a TH (threshold). The best value of a TH is such that:

- the confidence interval has a minimum value,
- the probability of exceedance stays inside an accepted range [90, 99.9]%,
- there are at least 30 data points above the threshold ¹

In the given example, TH=34 with the **confidence interval (I)**=63 and PE = 6.5%.

2. At the next step, the **GPD** defined by Eq. (2.5) in Appendix 2.2.1, is estimated as to the distribution of "extreme" load effects – effects that lay over the chosen TH – with the corresponding (fitted) parameters. The parameters are fitted by the maximum likelihood method.
3. The analysis of the quality of the estimation is done by probability plots (e.g. Figure 3.26). Empirical points (cross symbols in Figure 3.26) are sorted and they should tend to be linear following the theoretical curve (dashed line in Figure 3.26). This is followed by KS-tests [63] based on the differences between the empirical and theoretical distributions. This test returns a "true" or "false" decision if one distribution follows another distribution with an accepted significance level. In the

1. there has to be at least 30 values left in order to fit the distribution, [99]

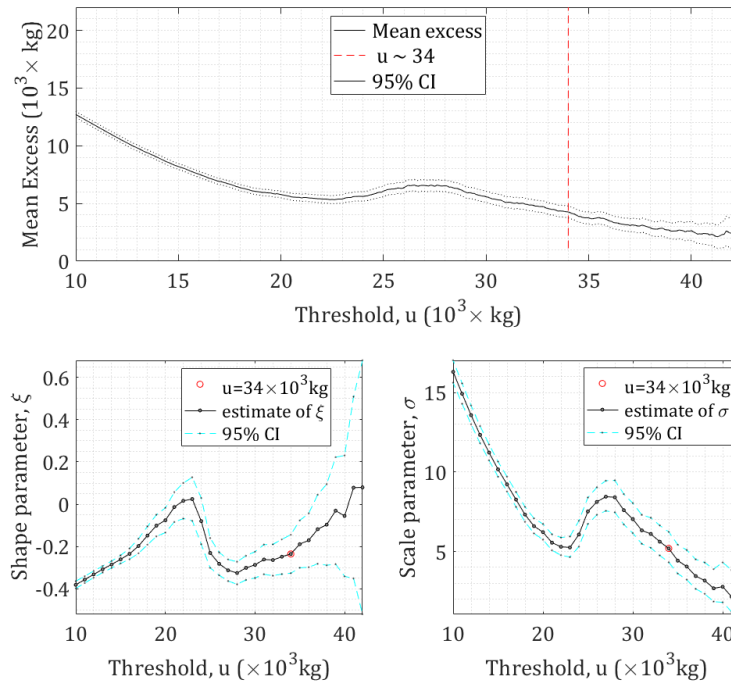


FIGURE 3.24 – Threshold choice (a) by MRLP for the mass of traffic

current work, only the result "true" was found for all cases with the significance level of 5%.

4. Return levels are assessed according to Eq. (2.6) in Appendix 2.2.1 for the return period equal to the design life of the bridge using estimated GPD shape and scale parameters.
5. The last step is the calculation of 95% confidence intervals for the computed return level (e.g. Fig. 3.26, dashed lines) according to Eqs. (2.7) to (2.10) in Appendix 2.2.2.

For the first part of the study BWIM-I, only 43 days of data were available. The calculations have been done according to the presented algorithm and the results are summarized in Table 3.8.

For each type of vehicles, allowed weight and maximum recorded are provided, as well as the number of monitored trucks per day. Table 3.8 also includes TH chosen by proposed alternative method for each axle type and the percentage of vehicles weights over this TH. Moreover, the return levels and the confidence intervals are presented for the return period of 120 years - the guaranteed lifetime of Millau viaduct - as it was mentioned in Section 3.2. It is more difficult to fit the distribution when there is not much data available as, for example, "1211" with only 6 trucks per day. Therefore, the confidence intervals are too large to rely on values of the return levels. Comparing the column "113" with "ALL", it

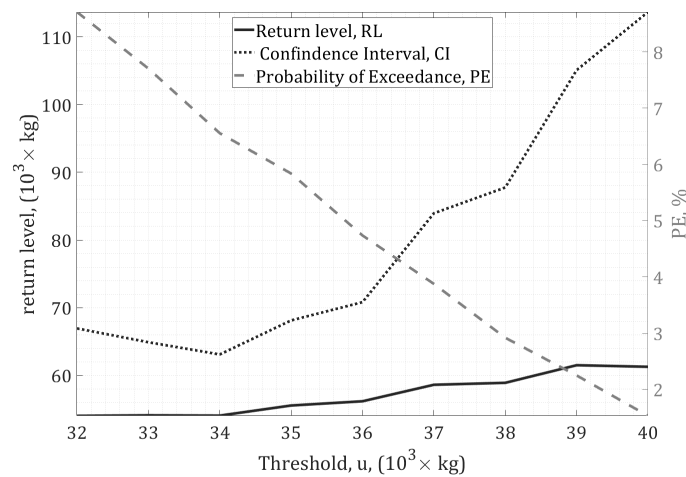


FIGURE 3.25 – Threshold choice (b) depending on confidence intervals and the probability of exceedance

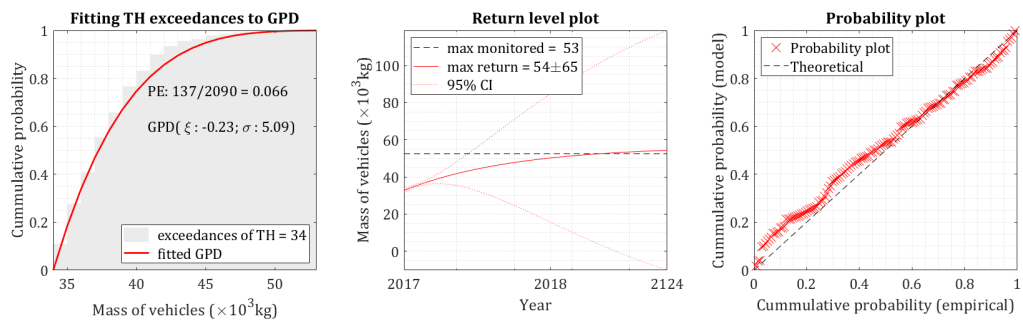


FIGURE 3.26 – Analysis of the quality of the estimation, example, vehicle type "1111"

| Axle Type | | "11" | "12" | "111" | "112" | "113" | "1111" | "1211" | ALL |
|---------------------------|----------|------|------|-------|-------|-------|--------|--------|------|
| Allowed | GVW | 19 | 26 | 26 | 38 | 44 | 32 | 44 | 44 |
| ($\times 10^3$ kg) | | | | | | | | | |
| Max | recorded | 32.8 | 41.2 | 35.7 | 47.8 | 86.7 | 45.3 | 62.5 | 86.7 |
| ($\times 10^3$ kg) | | | | | | | | | |
| Trucks per day | | 297 | 14 | 20 | 81 | 410 | 12 | 6 | 841 |
| Threshold | | 17 | 29 | 26 | 35 | 44 | 34 | 41 | 44 |
| Pr($X > TH$) | | 3% | 4% | 3% | 3% | 12% | 6% | 9% | 6% |
| RL, 120 | years | 39 | 47 | 37 | 54 | 169 | 55 | 162 | 169 |
| ($\times 10^3$ kg) | | | | | | | | | |
| CI ($\times 10^3$ kg) | | 36 | 222 | 56 | 59 | 78 | 65 | 1119 | 78 |
| RL+CI ($\times 10^3$ kg) | | 75 | 269 | 93 | 112 | 246 | 120 | 1281 | 248 |

TABLE 3.8 – Return levels with confident intervals based on BWIM of 43 days

is obvious that the heaviest and most frequent type of trucks is contributing the most into the entire picture, since the value of both the return levels and the confidence intervals is

approximately the same for both cases.

The second part of the work, BWIM-II, includes all data available after the second installation, in total, 180 days, Table 3.9. The same procedure is applied in order to obtain the return levels and the confidence intervals for values of **GVW** of all types of trucks. Results allow for updating the value of the confidence intervals. Table 3.9 shows the comparison of return levels and confident intervals based on 43 and 180 days of monitoring. With the same threshold of 44 t and around 6% difference in a number of tracks per day, the **PE** of the threshold is two times higher for the three times longer period of monitoring. We can observe that adding more data (longer period of measurements) permits to decrease the values of the return levels with the corresponding confidence intervals if the recorded maximum stays the same.

| Period | Trucks per day | TH ($\times 10^3$ kg) | PE | RL ($\times 10^3$ kg) | CI ($\times 10^3$ kg) | RL+CI ($\times 10^3$ kg) |
|----------|-------------------|---------------------------|-----------|---------------------------|---------------------------|------------------------------|
| 43 days | 841 | 44 | 6% | 169 | 78 | 248 |
| 176 days | 903 | 44 | 3% | 113 | 28 | 141 |

TABLE 3.9 – Updated return level with confidence interval based on BWIM-II of 180 days with same thresholds

Moreover, Figure 3.27 shows fitting **GPD** to the "extreme" traffic actions, the probability plots, and the return level plots for all types of vehicles given in Table 3.9. These results are used further in Section 3.4 to combine the traffic and wind actions.

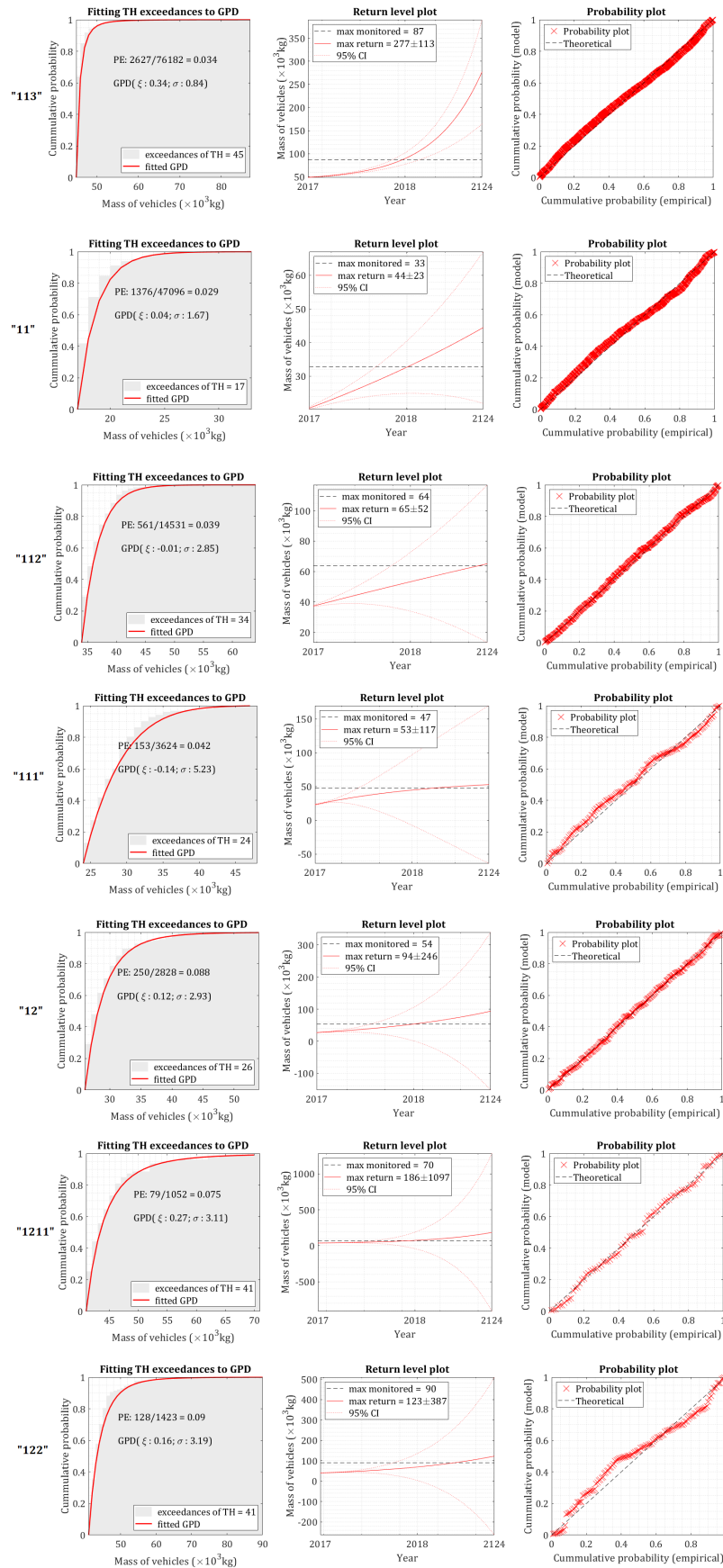


FIGURE 3.27 – Analysis of the quality of the estimation for all the vehicles types

3.4 Combination of traffic and wind actions

Usually, if the wind is too strong, important bridges on highways are closed to transport or the access to large vehicles is restricted, so, the combination of extreme wind action together with the extreme traffic action cannot take place. The idea of this part of work is to obtain the response of the structure in the situation when the wind is close to the critical value, but still, the bridge is continuing to operate.

3.4.1 Computational model for global load effects

In order to transform wind and traffic actions into the load effects in the deck, the bending moments at the level of the deck are found for both types of actions, as well as for their combination. Figure 3.28 displays a schematic view of one of the possible deformations for the highest pile of the bridge.

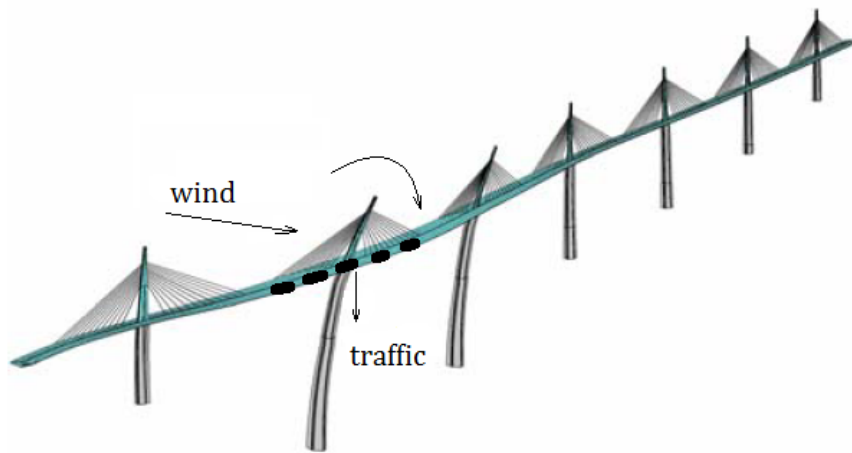


FIGURE 3.28 – Schematic view of one of the deformation modes of the deck for the considered part of the bridge, [29]

To obtain the response of the part of the bridge (see Figure 3.29, left), a static linear 2D beam finite element model \mathcal{M}_1 of pile P2 with its pylon has been developed using MATLAB, [104] (see Figure 3.29, middle). The traffic forces are directly obtained from known weights coming from BWIM data. The wind forces are calculated from the values of monitored wind speeds, see Section 3.2.4, according to the general algorithm proposed in EN [6], see Annex A.1. Both monitored maximum actions and predicted actions at the end of the lifetime are applied to this part of the structure.

Figure 3.29 (right) shows how the wind load is transferred from the real 3D model to the 2D computational model.

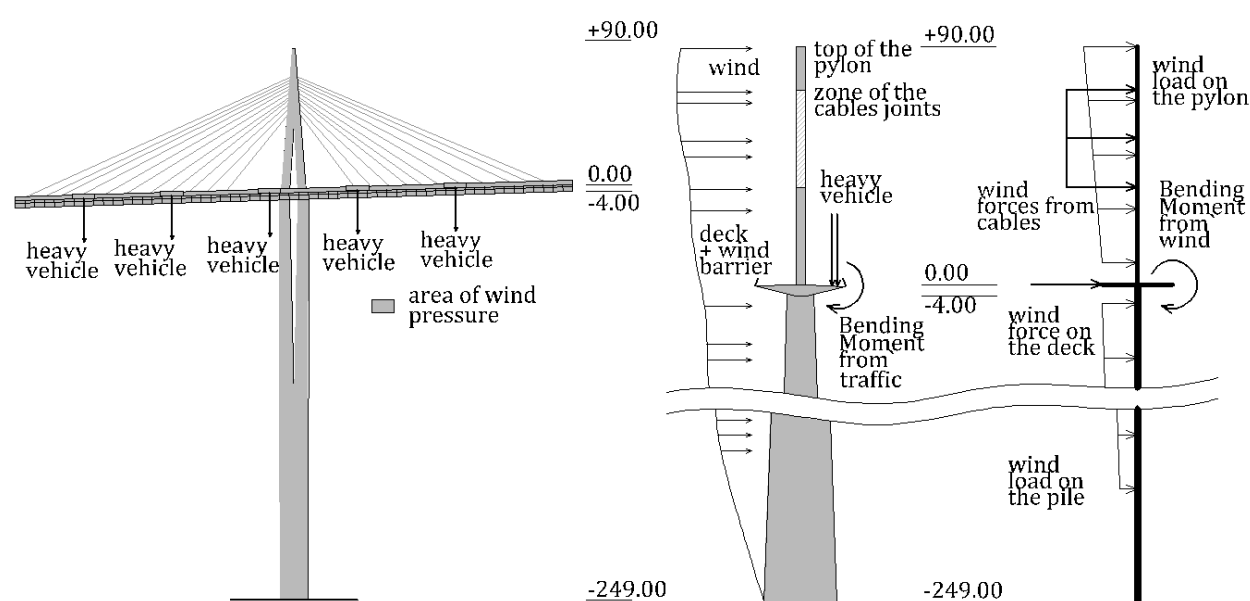


FIGURE 3.29 – Part of the bridge considered for the 2D computational model (left), scheme of the pile with its pylon P2 (middle), 2D computational model (right)

The result wind forces for all the elements of the considered part of the bridge (pylon, pile, deck, and cables) have been shown in Table 3.3. The wind pressure used in calculations is obtained from the measurements for the known wind velocities at different levels. As described in Section 3.2, the wind speeds have been measured in two elevations: one at the level of the deck and one at the top of the pylon of the highest pile, P2. The reference areas used in calculations correspond to actual dimensions of the studied Millau viaduct. Table 3.10 shows the values of the bending moments at the deck level of the bridge that are caused by the wind forces applied to the 2D computational model \mathcal{M}_1 for various wind speeds.

It is necessary to take into account that five-axles vehicles are often transporting goods in groups of two, three or four trucks. Analyzing time-series data available from the BWIM monitoring and recorded speeds of vehicles, situations with the presence of several heavy vehicles on one span at the same time have been detected. This allows for assessing the probabilities of occurrence (Table 3.11) of such situation that can lead to larger values of overall load effects.

All calculations for traffic (Section 3.3) are shown for a passage of a single truck. As for queues of lorries, for predictions of return levels, the mean value of the vehicle mass is used in each case according to Table 3.11. Knowing the speed and the time difference between vehicles in line, we can easily assess the distance between them and find how

| | Weekly max | | Max recorded | |
|-------------------------------|---------------------|---------------|---------------------|---------------|
| | Wind speed (m/s) | Force (kN) | Wind speed (m/s) | Force (kN) |
| Pile, bottom | 9.8 | 161.8 | 19.2 | 625.3 |
| Pile, top | 12.8 | 162.1 | 22.2 | 488.1 |
| Deck | 15.9 | 389.1 | 25.3 | 988.2 |
| Pylon, bottom | 15.9 | 58.5 | 25.3 | 148.6 |
| Pylon, middle | 17.0 | 54.9 | 26.4 | 132.8 |
| Pylon, top | 18.1 | 9.2 | 27.5 | 21.3 |
| Cables | 17.0 | 123.7 | 26.4 | 299.2 |
| Bending moment, deck (kNm) | 13411 | | 32524 | |

TABLE 3.10 – Wind speed, associated wind force applied to the 2D computational model, and computed bending moments

| 5-axes trucks in a queue | Number / 180 days | each week | Mean mass of a vehicle ($\times 10^3$ kg) | Mass of a queue ($\times 10^3$ kg) | % of occurrences |
|--------------------------------|-------------------------|--------------|--|---|---------------------|
| 1 | 70412 | 2708 | 32.6 | 32.6 | 90.460% |
| 2 | 7024 | 270 | 33.0 | 66.0 | 9.024% |
| 3 | 389 | 15 | 32.7 | 98.1 | 0.500% |
| 4 | 11 | 0.5 | 29.2 | 116.8 | 0.014% |
| 5 | 2 | 0.08 | 29.9 | 149.5 | 0.002% |

TABLE 3.11 – Occurrence of five-axes trucks

many trucks are present on a lane at the same time. Table 3.11 gives the numbers of occurrence of single five-axes vehicles, groups of two, three, four, and five five-axes vehicles, as well as the mean and total mass for each case. The expected **GVW** in 120 years, caused bending moment and the corresponding probability are computed.

3.4.2 Probabilistic model

Let $M_t^{max} = m_t(W_t^{max})$ and $M_w^{max} = m_w(V_w^{max})$ be the random variables that model the bending moments in the same section at the level of the deck induced by the extreme values W_t^{max} of the random vehicle weight and the extreme values V_w^{max} of the random wind speed. The probability distributions of the extreme values W_t^{max} and V_w^{max} correspond to the same period of measurements. The deterministic function m_t is linear that is an increasing function (for positive moment) and the function m_w is also an increasing function (for positive moment). These two functions are associated with the 2D computational model \mathcal{M}_1 . Then, Ω^{max} , see Eq. (2.15) takes the following form:

$$\Omega^{max} = \{M_t^{max} \in C_t\} \cap \{M_w^{max} \in C_w\}, \quad (3.1)$$

in which C_t and C_w are any given intervals. Since W_t^{max} and V_w^{max} are assumed to be independent random variables, we can also rewrite Eq. (2.16):

$$Pr\{\Omega^{max}\} = Pr\{M_t^{max} \in C_t\} \times Pr\{M_w^{max} \in C_w\} \quad (3.2)$$

3.4.3 Return levels for wind and traffic actions and load effects

Prediction of traffic weights and wind velocities has been done by using the POT approach, described in Section 2.2 and Appendixes 2.2.1 and 2.2.2.

For traffic actions, the predictions have been made for different types of trucks, Table 3.12. In order to make a combination with the wind actions, the bending moments are computed based on the values obtained with POT.

| case | GVW ($\times 10^3$ kg) | Load (kN) | BM (kN \times m) | Occurrence every |
|------------------------|----------------------------|-----------|-----------------------|-----------------------|
| Maximum "113" | 86.7 | 850.5 | 7017 | 26 weeks |
| Weekly maximum | 59.5 | 583.7 | 4815 | 1 week |
| 2 \times "113" | 66.0 | 647.5 | 5341 | 40 min |
| 3 \times "113" | 98.1 | 962.4 | 7939 | 12 hours |
| 4 \times "113" | 116.8 | 1145.8 | 9453 | 2 weeks |
| 5 \times "113" | 149.5 | 1466.6 | 12099 | 13 weeks |
| RL+CI 1 \times "113" | 113+27 | 1383.2 | 11411 | 120 years |
| RL+CI 5 \times "113" | 565+56 | 6092.0 | 50260 | 10 ⁷ years |

TABLE 3.12 – Bending moments (BM) for the traffic actions and their occurrence

The values of the bending moment provided for traffic, Table 3.12, contribute to the resulting bending moment three times less than the wind. As well, the combination, which brings very high values of the bending moment, is probably extremely rare.

The algorithm for fitting GPD to the extreme load effects with the following estimation of return levels explained in Section 3.3, is also applied to the wind loading. The choice of threshold is done by the proposed graphical method (Section 2.2). Table 3.13 gives the values of wind forces [kN] and the resulting bending moment [kNm] for the return wind speeds that have been found with the POT approach for the return period of 120 years.

| RL, 120 years | Wind speed (m/s) | Force (kN) |
|-----------------|------------------|------------|
| Pile, bottom | 52.5 | 4691 |
| Pile, top | 55.6 | 3051 |
| Deck | 58.6 | 5313 |
| Pylon, bottom | 58.6 | 799 |
| Pylon, middle | 59.7 | 680 |
| Pylon, top | 60.8 | 104 |
| Cables | 59.7 | 1532 |
| BM, deck (kN×m) | 167140 | |

TABLE 3.13 – Wind force associated with the predicted wind speed in 120 years and computed bending moments

Table 3.14 shows the return levels with the confidence intervals for the wind based on three observation periods for the wind speed: i) 1985-2018, 12113 days, ii) 2004-2018, 4824 days, iii) 2016-2017, 254 days. The probability of occurrence of the wind NW direction, considering only four possible directions, is given in the second column of Table 3.14.

| Based on data at 80m height | Pr(NW) | Wind speed ($\times 0.278\text{m/s}$) | | | | Over TH (%) |
|-----------------------------|--------|---|----|-----|-----|-------------|
| | | Max | TH | RL | CI | |
| 1985-2018, 12113 days | 0.378 | 119 | 55 | 134 | 219 | 1 |
| 2004-2018, 4824 days | 0.387 | 103 | 55 | 110 | 203 | 0.4 |
| 2016-2017, 254 days | 0.305 | 69 | 55 | 70 | 119 | 0.6 |

TABLE 3.14 – Results for the return levels and confidence interval for the wind data collected at Creissels, Pr(NW) is the probability of occurrence of the wind NW direction, for 4 possible directions

Even if the measured values are not so high, it is possible to combine strong winds occurring in the perpendicular direction to the deck with heavy trucks passing in lane I (slow lane, Figure 3.4), which is closer to the edge of the deck. Therefore, the next step is the combination of effects caused by both loads together.

3.4.4 Combination of actions and comparison with load models from European standards

Real-time live and climatic loads recorded directly on the Millau viaduct allow to compare the monitored traffic and wind actions on the deck with the design actions computed with European standards. The combination of bending moments is done without application of any partial factors and their probabilistic combination according to Section 3.4.2.

There are several load models proposed in EN [7] for traffic actions on bridges. The load model LM1 is used here for calculations of design traffic actions F_t . Results for bending

| Case | Traffic only | | Wind only | | Combination | | |
|---------------|--------------------------|-------------------------------|--------------------------|-------------------------------|---------------------------------|---------------------------------|-----------------------------------|
| | $\mu_t^{max},$ (kN×m) | $Pr(M_t^{max} > \mu_t^{max})$ | $\mu_w^{max},$ (kN×m) | $Pr(M_w^{max} > \mu_w^{max})$ | $\omega_{SLS}^{max},$ (kN×m) | $\omega_{ULS}^{max},$ (kN×m) | $Pr(\Omega^{max} > \omega^{max})$ |
| 1×"113" | 8 661 | 8.3×10^{-2} | 13 411 | 5.9×10^{-3} | 22 072 | 31 809 | 4.8×10^{-4} |
| 5×"113" | 12 099 | 8×10^{-2} | 32 524 | 3.5×10^{-4} | 44 624 | 65 120 | 2.8×10^{-5} |
| RL, 120 years | 12 450 | 9.5×10^{-7} | 167 140 | 9.5×10^{-7} | 179 590 | 267 518 | 9.1×10^{-13} |
| Design [5] | 154 830 | 0.1 per 100 years | 276 410 | 0.02 per 1 year | 340 740 | 494 520 | - |

TABLE 3.15 – Combination of extreme wind action with extreme traffic action, and probability to their simultaneous occurrence

moments computed according LM1 are shown in the last row of Table 3.15. The load consists of two parts: a tandem system from two concentrated axle loads in the middle of a span F_{TS} and the uniformly distributed on the surface of a lane load F_{UDL} . The deck of Millau viaduct has two lanes, therefore, values of F_{TS} and F_{UDL} are:

$$\text{lane I } F_{TS} = 300\text{kN}; F_{UDL} = 9\text{kN/m}^2$$

$$\text{lane II } F_{TS} = 200\text{kN}; F_{UDL} = 2.5\text{kN/m}^2$$

The design model for wind actions F_w is based on the procedure given in EN [6] for the case of wind loads on bridges. Methodology is shortly explained in Annex A.1, and the values obtained for the bending moment based on wind speeds computed with design load model are shown in the last row of Table 3.15.

The design combination of both loads is computed for ULS and SLS respecting formulations proposed in EN [5]. Considering W to be the value of self-weight of the structure and the wind to be a leading action, the design combinations E_d can be written as follows:

$$ULS : E_d = W + \gamma_w(F_w)_{lead} + \gamma_t(\psi_0 F_t)_{accomp}, \quad (3.3)$$

$$SLS : E_d = W + F_{w,lead} + (\psi_0 F_t)_{accomp}, \quad (3.4)$$

where ψ_0 is the factor for the combination value of accompanying variable traffic actions, $\psi_{0,TS} = 0.75$ – for the concentrated axle load (LM1, EN [7]), and $\psi_{0,UDL} = 0.4$ – for the uniformly distributed load (LM1, EN [7]). Considering values of partial factors for the wind ($\gamma_w = 1.5$) and traffic ($\gamma_t = 1.35$), Eq. (3.3) and Eq. (3.4) take the following form:

$$ULS : E_d = W + 1.5F_w + 1.35(0.75F_{TS} + 0.4F_{UDL}), \quad (3.5)$$

$$SLS : E_d = W + F_w + 0.75F_{TS} + 0.4F_{UDL}. \quad (3.6)$$

The results for combination of the extreme wind and extreme traffic actions and the probability of their simultaneous occurrence are represented in Table 3.15. For weekly duration, for 120 years return level, and for 13 weeks duration, Table 3.15 displays the probabilities of the extreme wind actions, the extreme traffic actions, and the combination of the simultaneous occurrence of these two extreme actions.

Table 3.15 shows both, **ULS** and **SLS** for each case. In the case of monitored traffic actions, the combination coefficient is taken as $\psi_0 = 1$. It can be observed from Table 3.15 that the design values of actions, even using reduction coefficients, are much higher than values predicted on the base of monitoring. This confirms that the structure has reliability margins even in the worst case, which can probably arrive during the design operational life.

The results obtained in this section are used further in Section 3.7.2 to estimate the reliability of the studied part due to the combination of traffic and wind actions.

3.5 Extrapolation in time of the load effects in the deck

The predictions, not only for traffic actions but also for load effects caused by them, are in a range of interest. The values of load effects that occur in a structural element of the bridge depend on several factors:

- list of all the charges on the considered part of the bridge at the moment, Section 3.4.
- amount of traffic and its stationarity in time, Section 3.3.1,
- type of the passing vehicle (composition of axles and axles groups), Section 3.3.2,
- amplitude of loading from each axle, Section 3.3.3,
- location of the critical element, Section 3.5.1.

3.5.1 Finite Element Model

The "cleaned" data from BWIM system provide a weight of every passing axle, but not the stress induced by it in the deck. In order to obtain the distribution of stresses over a cross section of the deck caused by every passing axle, the finite element model (FEM) \mathcal{M}_2 is built, see Figure 3.30.

The following issues have to be taken into account, when finding a stress value:

- self-weight of the structure and weight of the surfacing asphalt layer,
- composite action of the steel deck plate and covering bitumen based material [44],
- distribution of loading from each wheel on surface of the steel plate EN [7],
- the amplitude of load from a passing axle,
- contribution from every other axle of the same truck into the stress value,
- global loading of the deck.

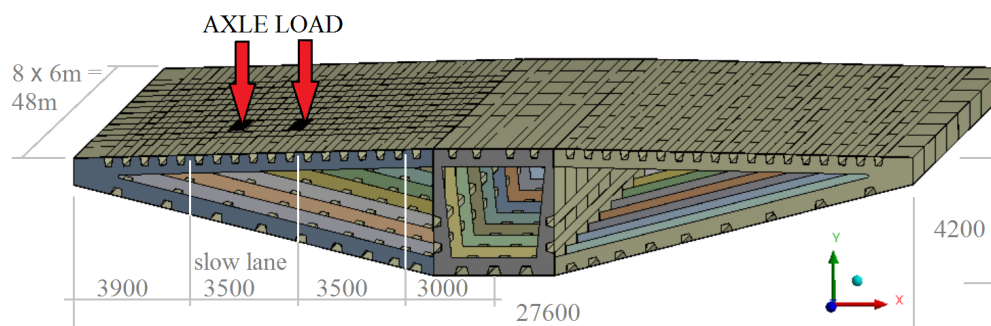


FIGURE 3.30 – Geometry for the FE model analyzed with ANSYS software, [67]

to obtain stresses for all the monitored data during 180 days, a computational model is build using MATLAB, [104], in addition to FEM \mathcal{M}_2 .

Let ax be the number of an axle for a given vehicle $j = 1, \dots, n$. Let M_{ax} be the value of the bending moment under axle ax of vehicle j and $M_j = \sum_{ax} M_{ax,j}$ - the bending moment caused by the entire vehicle under the axle j . Let $S_{ax,j}$ be the value of the stress caused by passing a n -axles vehicle under the considered axle and defined by:

$$S_j^{(vehicle)} = \sum_1^n S_{ax,j}^{(vehicle)} = \sum_1^n \left(\frac{y M_{ax,j}}{I^4} \right)^{(vehicle)}, \quad (3.7)$$

where $S_{ax,j}^{(i)}$ is the value of the stress caused by i -axle of the vehicle, for fixed geometry, I is a moment of inertia of the cross section and y is a distance from the center of mass. An example is given in Figure 3.33 for the type "113".

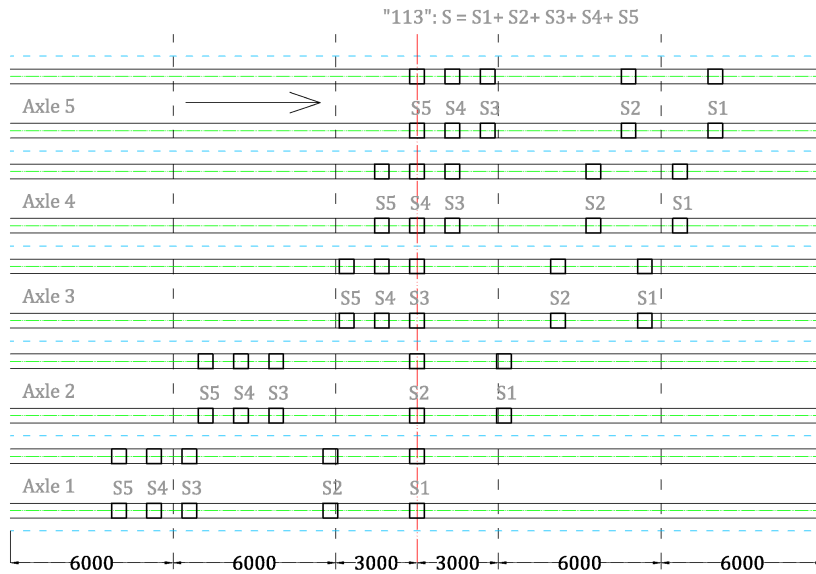


FIGURE 3.33 – Axle position on the slow lane of FEM \mathcal{M}_1 for "113"

The errors related to the finite element method itself should not be considered as uncertainties [23], although they have to be possibly reduced. Here, four different mesh sizes are compared in terms of computational time and chosen to be optimal in order to assess stresses in the deck. An example is given in Table 3.16 for a smaller model and a location that corresponds stiffener "w7", Figure 3.4. The model uncertainty induced by the error of the finite element model \mathcal{M}_2 is found using recorded signals from the BWIM system. For

the day of the load-proof test to calibrate the newly installed **BWIM** system in the deck of the bridge, recorded signals are provided. They include influence lines in the bottom of longitudinal stiffeners of the orthotropic deck at the distance of approximately one meter from a transversal beam. Recording of strains were not provided but only shapes of signals from different sensors. From all signals, cases when a vehicle is moving in the middle of the lane were chosen due to the absence of exact transversal position of vehicle for the entire period of measurements. When the truck is passing in the middle of the lane, signals from sensors "w7" and "w10" have approximately same shapes. Stresses in locations corresponding to positions of sensors "w7" and "w10" were taken from finite element model. The ratio δ between recorded signals and obtained from **FEM** \mathcal{M}_2 stresses is computed for several cases and given in Table 3.17.

| | | | | | | |
|-------------------------------------|------|------|-----|------|------|------------|
| mesh | 0.4 | 0.2 | 0.1 | 0.05 | 0.04 | 0.2&0.04 |
| computational time, s | 16 | 20 | 67 | 243 | 559 | 11 790 |
| simplified model, stress, MPa, "w7" | 13.3 | 10.4 | 31 | 16.6 | 16.9 | main model |

TABLE 3.16 – Computational time and example of stress values for different mesh sizes of a simplified FEM and chosen mesh for the main FEM

| sensor | N of samples | mean value μ_δ | standard deviation s_δ | CoV |
|--------|--------------|-------------------------|-------------------------------|-----|
| "w7" | 10 | 0.135 | 0.190 | 14% |
| "w10" | 10 | 0.140 | 0.021 | 15% |

TABLE 3.17 – Validation of the finite element model

3.5.2 Return levels for local and global load effects based on several EVT approaches

As well as for predictions of loads, recorded values for a certain period of time are required for predictions of load effects in an existing structure. In a case of bridges, not always monitored strains or accelerations are available. In the deck of the Millau viaduct, only the **BWIM** system was installed (Section 3.2.3), which provides data for traffic actions but not for the load effects caused by them. Therefore, in the current work, two types of extrapolation in time are made:

- extrapolation of traffic actions for different types of vehicles, Section 3.3.5,
- extrapolation of stresses obtained from the **FEM** \mathcal{M}_2 that was based on monitored traffic actions, Section 3.5.1.

The algorithm, Figure 3.34, shows the steps to be taken in the case of extrapolation of stresses.

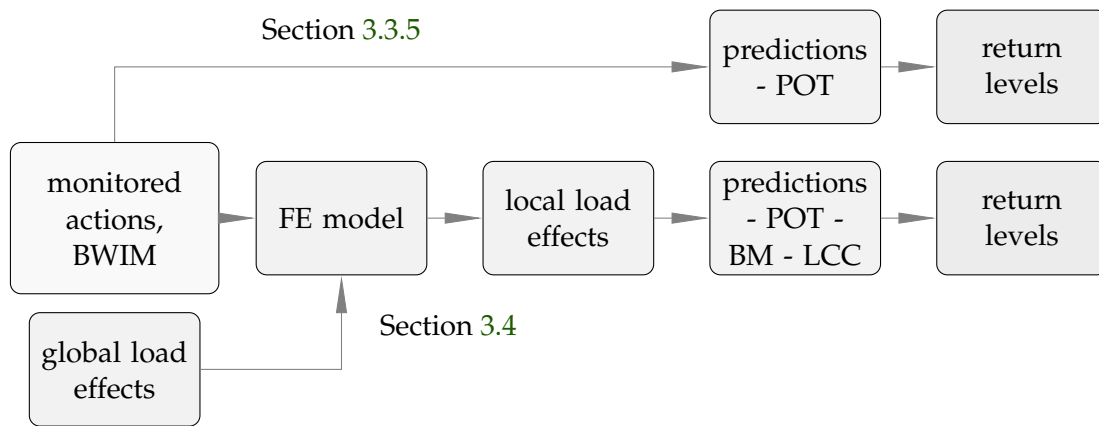


FIGURE 3.34 – Steps to be taken from monitoring to predictions of traffic actions and load effects

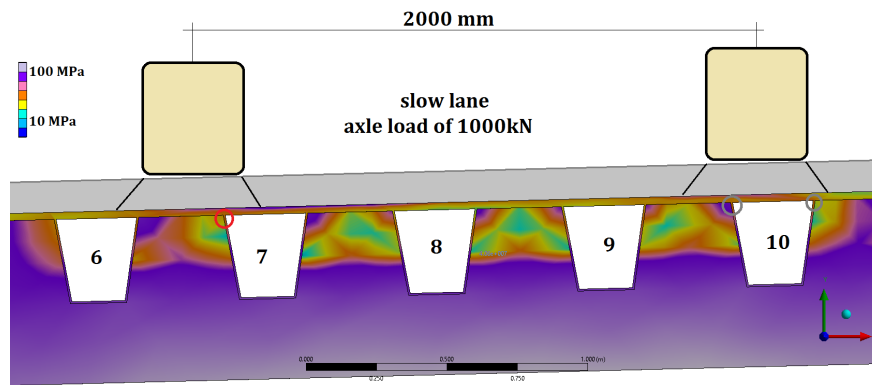


FIGURE 3.35 – Studied detail, deck of Millau viaduct

The literature review, see Section 1.3, has shown that the most common EVT methods are POT and Block Maximum (BM). Therefore, both methods are compared in this section. In addition, they are compared with one of the methods used in background works for Eurocodes - Level Crossing Counting (LCC) approach with the fit of the Rice formula.

In order to compare the three methods and to obtain the results for the reliability analysis, the extrapolation is done not for recorded traffic actions but for stresses caused by them in structural detail under a left wheel on the slow lane, see Figure 3.35. The stresses are obtained with the FE model \mathcal{M}_2 , see Section 3.5.1, taking into account local load effects from each axle of passing vehicles and global load effects from queues of lorries and, in some cases, the static wind, see Section 3.4. Figure 3.36 shows the histogram of stresses from all recorded vehicles. In order to assure statistical independence of random variables in EVT, only maximum stress S_m , values induced by every vehicle, are considered:

$$S_m = \max_j (S_j^{(vehicle)}), \quad (3.8)$$

where $S_j^{(vehicle)}$ is the stress induced by each axle or axle group, see Section 3.5.1.

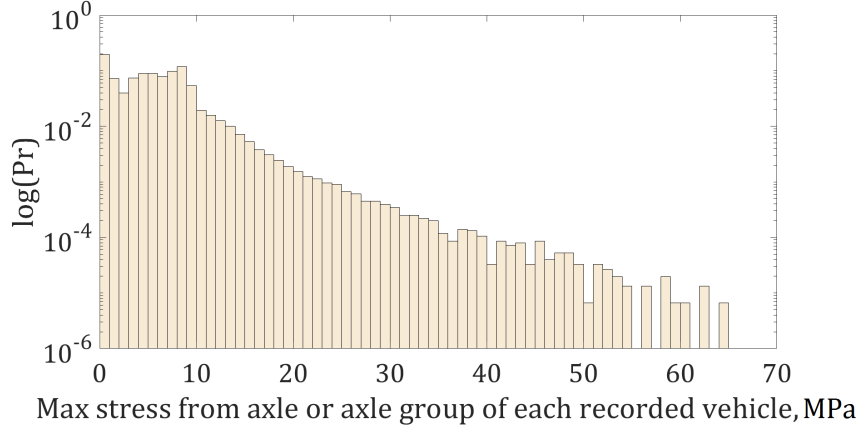


FIGURE 3.36 – PDF in log-scale of the stresses, MPa, in the studied detail

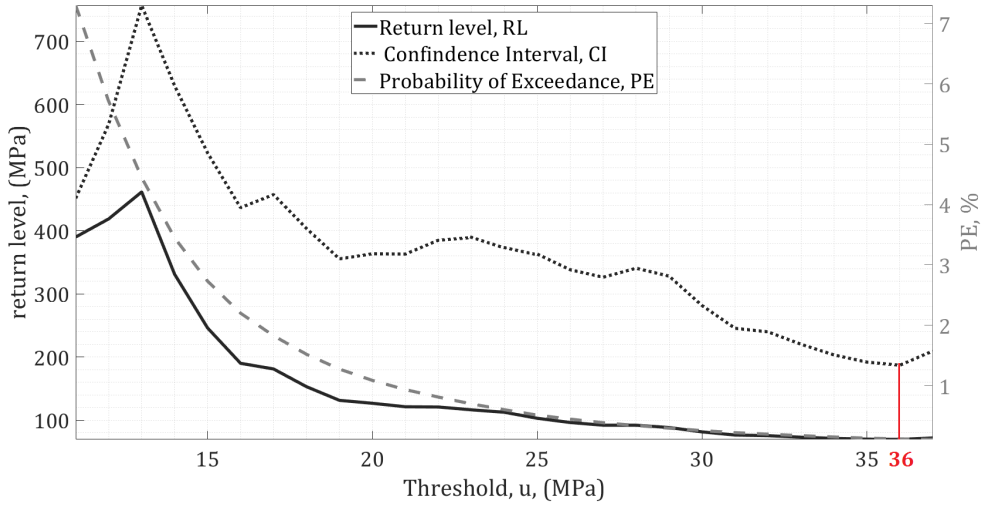


FIGURE 3.37 – Threshold choice for stresses in the studied detail

POT approach applied for stresses

The POT approach has been presented before, so, this section provides only results of its application to stresses in a critical structural detail of the deck. Here, the stresses $S_{pot} = S_m - u, S_m > u$ are used as extreme events to fit GPD, Eq. (2.5), Appendix 2.2.1.

First, only local traffic actions are considered. Load effects from one single vehicle at time are obtained through the numerical model \mathcal{M}_2 . Figure 3.36 gives the probability

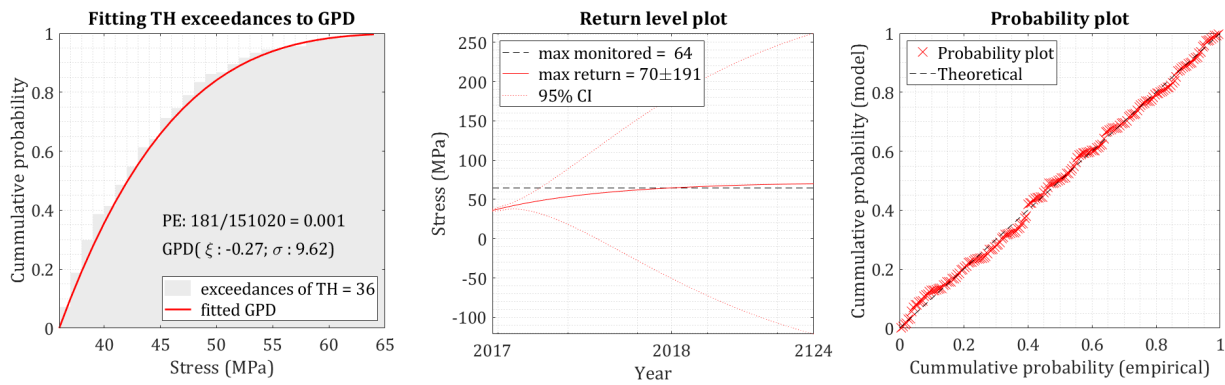


FIGURE 3.38 – POT approach for stresses in the studied detail

distribution function (PDF) of the stresses obtained only from traffic actions that depend on the amplitude of axle load and axle configuration of single vehicles. Figure 3.37 gives the choice of threshold u and Figure 3.38 – results for fitting stress values given by return levels S_{pot}^{return} , Eq. (2.6), Appendix 2.2.1. However, the presence of several vehicles on both lanes of the deck has to be considered. So, the influence of global effects caused by queues of lorries on the slow lane and traffic on the fast lane are added to the evaluation of stresses. Therefore, values of stresses obtained from FE analysis, see Section 3.5.1, are reassessed by adding global effects into the model.

A new PDF with higher values of stresses is given in Figure 3.39. As well, new results for the application of POT approach are provided, see Figures 3.40 and 3.41. Figure 3.40 allows the threshold u to be chosen and Figure 3.41 – results for fitting stress values given by return levels S_{pot}^{return} , Eq. (2.6), Appendix 2.2.1. Parameters of the chosen distribution are used further in the reliability analysis. Updated stresses are used by both other methods and in reliability analysis in Section 3.7.1.

Block maximum approach for daily and weekly stresses

As it was explained in Section 2, BM method separates the time history for load effects into intervals of a chosen size and determines the maximum in each interval. The method is based on a limit theorem stating that the **generalized extreme value (GEV)** distribution is an approximation for describing sample maximum for large sample sizes. This holds for the condition of the method being approximately independent observations with identical distributions [14]. For the given structural detail of the deck, two cases are compared:

- time block of a week is chosen due to the assumption that traffic is stationary every week, Figure 3.42, top,

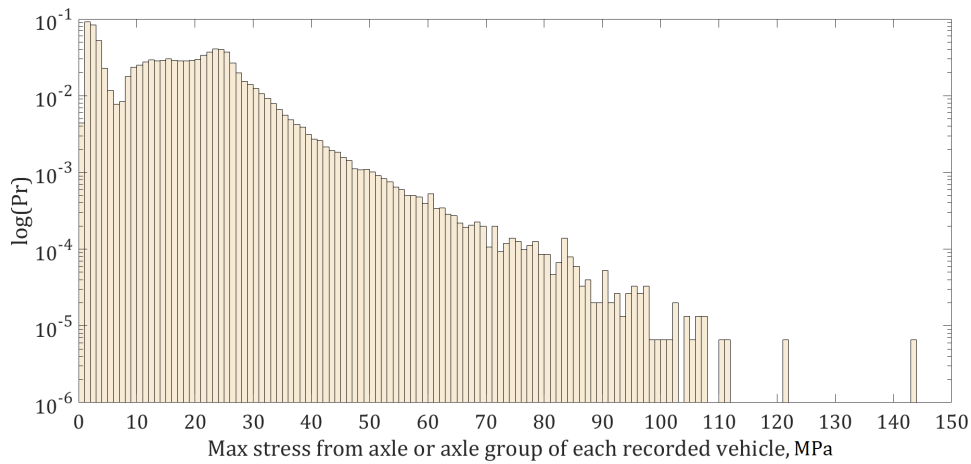


FIGURE 3.39 – PDF in log-scale of stresses, MPa, considering global load effects (traffic on both lanes)

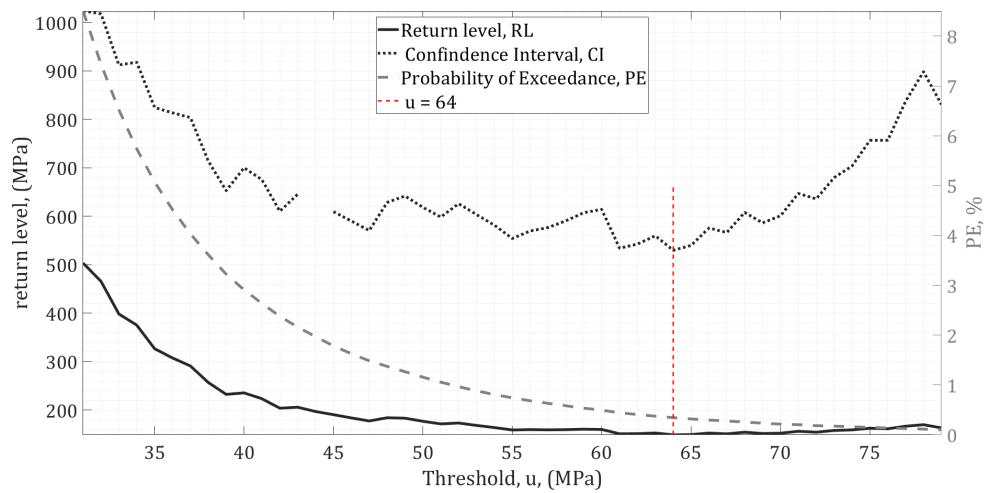


FIGURE 3.40 – Threshold choice for updated stresses in the structural detail

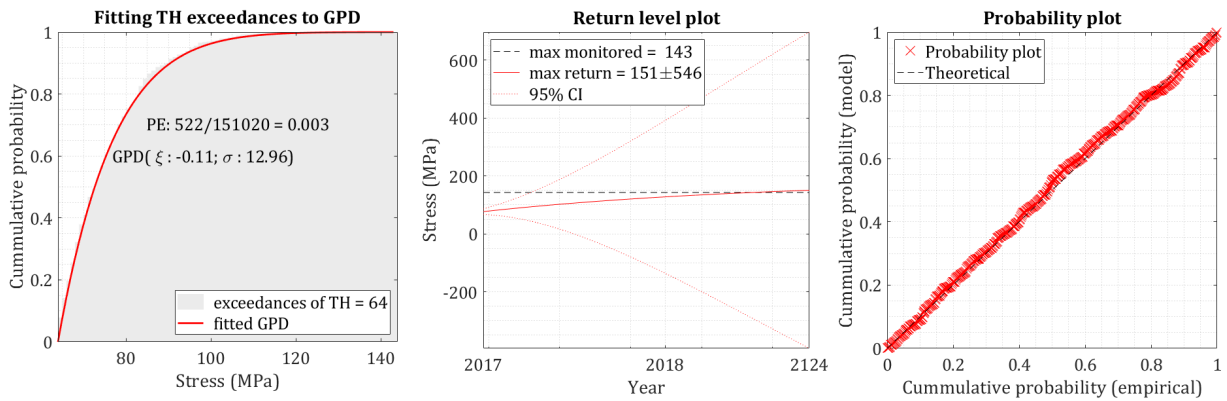


FIGURE 3.41 – POT approach for updated stresses in the structural detail

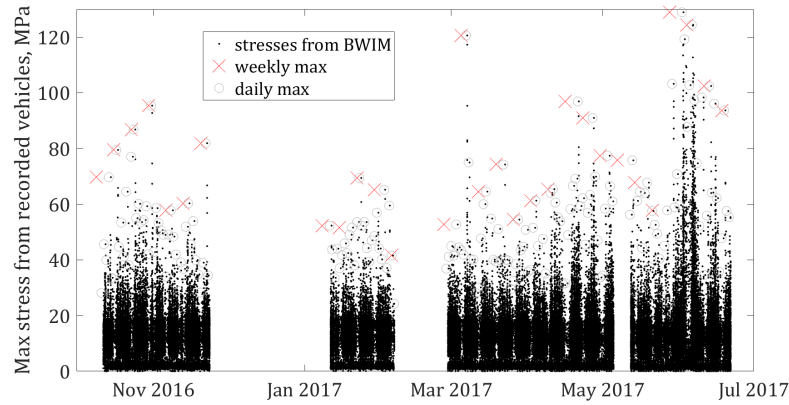


FIGURE 3.42 – BM approach for stresses in the structural detail

- time block of a day, only for weekdays is considered to observe how a choice of a block influences results, Figure 3.42, bottom.

Let S_{bm} be a random variable that consists of maximum weekly stresses x in a critical structural detail during the monitoring period T_{ref} of 180 days. In order to get valid results, the number of blocks should be sufficient enough to fit extreme load effects S_{bm} to the **GEV** $E(S_{bm}) \sim \mathcal{E}(\mu_b, \xi_b, \sigma_b)$ distribution with its location, shape and scale parameters:

$$E(x, \mu_b, \xi_b, \sigma_b) = \exp\left(-\left(1 + \xi_b\left(\frac{x - \mu_b}{\sigma_b}\right)^{-1/\xi_b}\right)\right) \quad (3.9)$$

The solution of the function gives return values for stresses at given return period d_{return} :

$$S_{bm}^{return}(\mu_b, \sigma_b, \xi_b) = \mu_b - \frac{\sigma_b}{\xi_b} \left[1 - (1/d_{return})^{-\xi_b} \right], \quad (3.10)$$

Maximum weekly stresses are obtained and fitted to the **generalized extreme value distribution (GEVD)**. Figure 3.43 provides results of the fitting that are used in the further reliability analysis.

Fitting Rice formula using the number of up-crossings

The **LCC** approach is similar to the **POT** but it is used for the case when data can take both negative and positive extremes. Here, the Rice formula [56] is fitted to the upper tail of an **up-crossing rate histogram (URH)**. It is based on the assumption of a stationary Gaussian process describing the time variations of load effects on bridges [36]. The number of times is counted at which positive values are crossed upwardly in a given time history. By normalizing the resulting level crossing histogram with respect to the time history

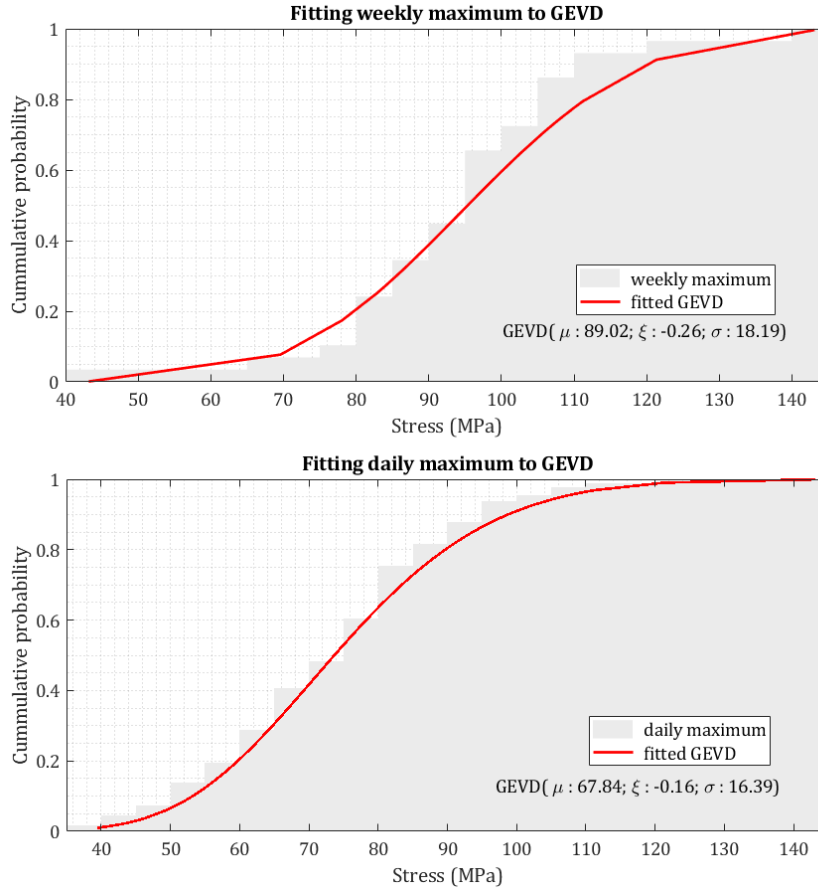


FIGURE 3.43 – Fitting the GEV distribution to maximum stresses: top - block = 1 week, bottom - block = 1 weekday

length, the **URH** is obtained, representing for each level the mean rate of its crossing during a reference period of monitoring (180 days). The Rice formula (3.11) with its model parameters (m, σ, ν_0) describes the mean rate $\nu(x)$ of up-crossing for a certain level during d_{ref} of 180 days, and is fitted to the significant tail regions to the **URH**,

$$\nu(x) = \nu_0 \exp\left(-\frac{(x - m_x)^2}{2\sigma^2}\right) \quad (3.11)$$

For $x = S_{lcc}^{return}$, Eq. 3.11 yields,

$$S_{lcc}^{return} = m_x \pm \sigma \sqrt{2 \ln(\nu_0 d_{return})} = -\frac{a_1}{2a_2} + \sqrt{-\frac{a_0}{a_2} + \left(\frac{a_1}{2a_2}\right)^2 - \frac{\ln(d_{return})}{a_2}}, \quad (3.12)$$

where $d_{return} = R_p/d_{ref}$ is the time reference that depends on a return period R_p and the reference period d_{ref} , $a_0 = \ln(\nu_0) - m_x^2/2\sigma_x^2$, $a_1 = m_x/\sigma_x^2$, $a_2 = -1/2\sigma_x^2$ are parameters of a second order polynomial function $\ln \nu(x) = a_0 + a_1x + a_2x^2$ used in order to fit the

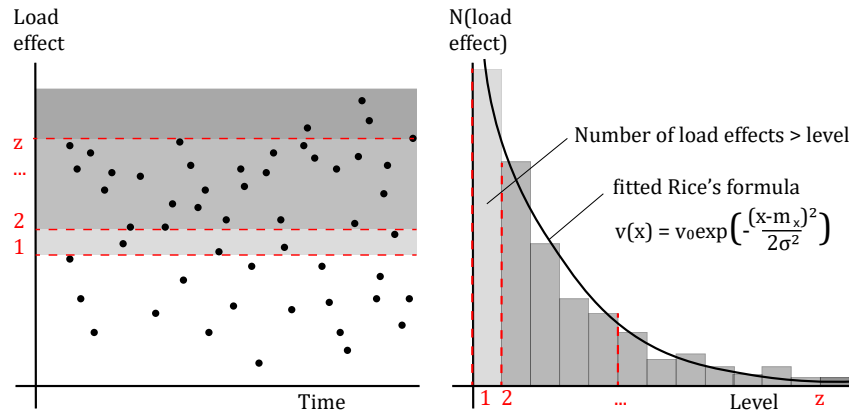


FIGURE 3.44 – Example of fitting Rice formula using the number of levels out-crossings

Rice formula to level up-crossings, σ_x and m_x are estimated parameters of the fitted Rice formula to the upper tail of URH, respectively, standard variation and the mean, ν_0 is a mean number of up-crossings of the zero level.

In this study, optimal starting point x_0 is identified with evaluating the goodness of fit by means of a KS-test [63] as it was mentioned in Section 3.3.5.

For $T_{ref} = 180$ days of monitoring and $R_t = 120$ years from the opening of the viaduct for traffic, parameters are given in Table 3.18 to be used further in the reliability analysis.

| parameter | value |
|------------------------------------|------------------------|
| $a_0 = \ln(\nu_0) - m^2/2\sigma^2$ | 8.23 |
| $a_1 = m/\sigma^2$ | -1.03×10^{-2} |
| $a_2 = -1/2\sigma^2$ | -8.06×10^{-4} |

TABLE 3.18 – Parameters found from URH for the fitted Rice formula

3.6 Generalized Pareto Distribution for fatigue life estimation

3.6.1 Cycles counting based on BWIM data

First, speaking about fatigue of a bridge, stresses and number of cycles for each stress range are needed. Therefore, critical elements subjected to fatigue loading have to be chosen. In the case of the Millau bridge, values of stresses in the deck are not measured directly. Therefore, it is not possible to observe the presence of dynamic effects. However, the estimation of fatigue is still achievable by using the results of **BWIM** measurements. The system provides not only total weights of each vehicle but also the weight of each axle and distances between them, see Section 3.2.3.

For the evaluation of fatigue, the use of long-term **BWIM** data is possible even though it does not directly give stress cycles. The system provides forces from each axle of passing heavy trucks, which gives stress cycles in elements of the deck. At the same time, the absence of data for light vehicles does not cause a problem here, as such vehicles do not cause much stress in a stiff orthotropic deck, and do not contribute to the fatigue damage accumulation. Knowing the exact action applied to the bridge, stress in the whole cross-section might be evaluated, as it is done in Section 3.5.1. However, fatigue cycles are equal to absolute values of stress, a difference between the maximum and minimum values of stress that occur in the same detail. Usually "rainflow" counting [3] is done in order to compute number of cycles of each stress range. In the current work, only stresses from axles group of passing vehicle are needed, and they are directly obtained from the **FEM** \mathcal{M}_2 . Therefore, in a case of a group of axles, instead of counting separately stress cycles from each axle load in a group, the maximum value produced by the group is considered, see Figure 3.45. There are different combinations of axles possible: some of them are grouped by two or three, as it was demonstrated in Table 3.4.

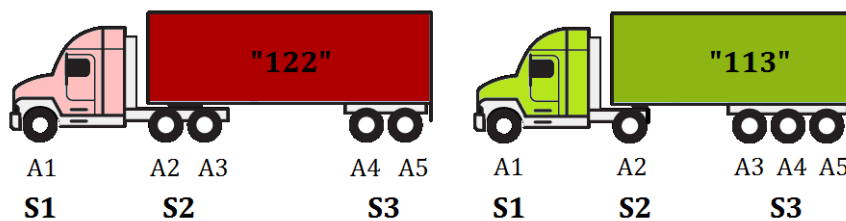


FIGURE 3.45 – Main types of axles groups and stresses from them

The value of the stress given by a group of axles is usually higher than the one caused by each axle separately and lower than their sum. For vehicles of type "113", to calculate

stress cycles, the common action of three axles have to be considered. Also for the types "112", "12", "122" and "1211", the group of two axles should be taken into account.

As it can be found on Figure 3.46, P_1 , P_2 and P_3 are point loads from each axle of the group of three axles, and P_1^* , P_2^* and P_3^* are moments that can be obtained theoretically if each axle would pass the span individually. So, it is necessary to take into account that for the response of the structure, there is an influence between axles in groups of two or three. It could be performed theoretically as two or three point loads, presenting on the 6-meter elements of the span at the same time.

Figure 3.46 is a schematic figure that is only made to explain the contribution of each axle load in a group. A 6-meter element of the first span of the deck is considered here, and influence lines are obtained as the ones for the simply supported beam. Real values of stresses from single axles and axle groups are obtained with the FE model \mathcal{M}_2 , see Section 3.5.1.

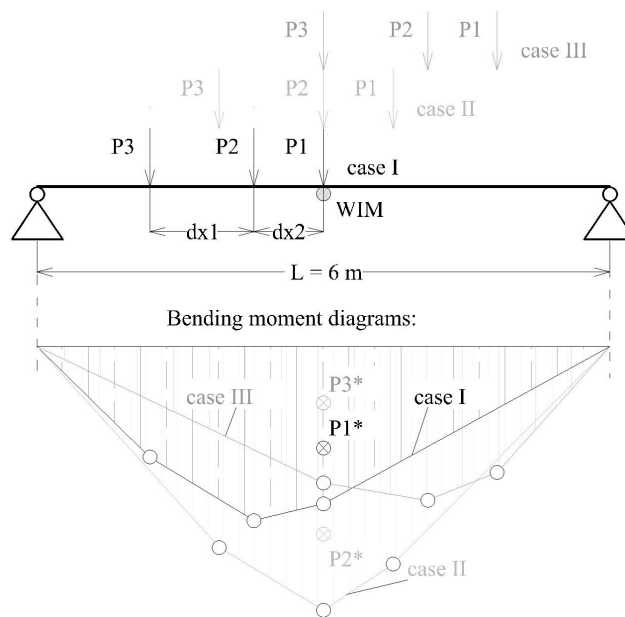


FIGURE 3.46 – Bending moment from a 3-axles group, [70]

This gives the absence of the bending moment (or the values are negligible) at "supports" – connections between each span. So, for large distances between single axles of vehicles, a weight of each axle can be taken separately as there is almost no influence in terms of stresses. However, for the groups of axles, different values of bending moments are considered as for two or three point loads.

As the most frequent vehicles are "113", "11" and "112", bending moments in the mid-span are calculated only for single, double and triple axles, as follows:

- Single point load P_I is considered if the distance between axle I and other axles is larger than $L_{span}/2=3\text{m}$,
- Double axles are presented by two point loads P_{II} , when the distance between them is smaller than 3m; the maximum moment is obtained from both positions: either P_{II-1} or P_{II-2} above the center,
- Triple axle load is given by three point loads P_{III} with three possible positions – each of them at the mid-span one by one.

Then, stress cycles in MPa are obtain for every axle or axle group, using the FEM \mathcal{M}_2 , Section 3.5.1, the histogram is shown on Figure 3.47.

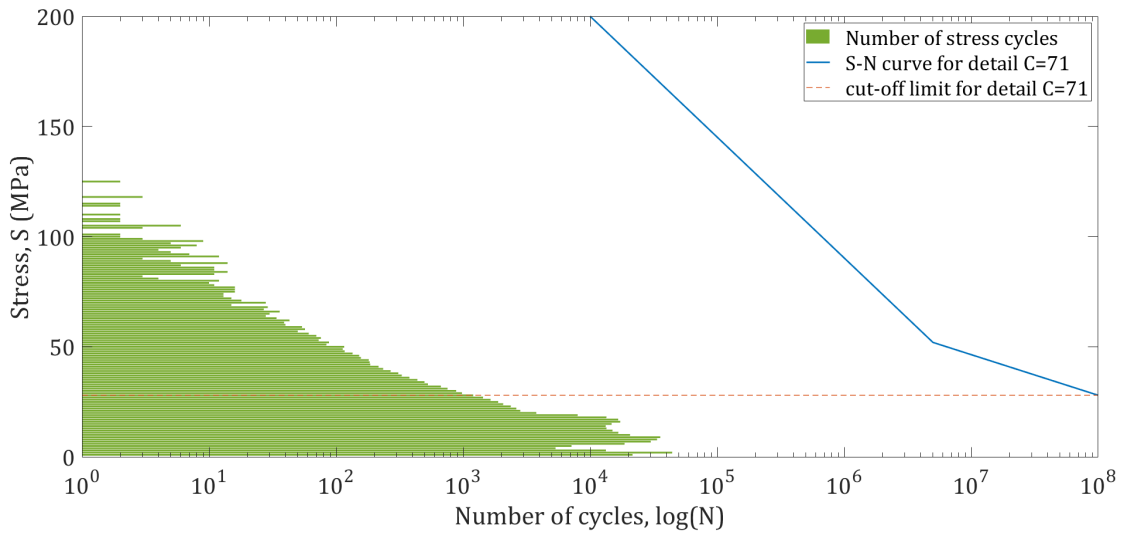


FIGURE 3.47 – Histogram of stress cycles, studied detail, deck of Millau viaduct

3.6.2 Fatigue load model according to standards

In order to assess fatigue in the structural detail of the deck with category $K = 71$, the corresponding S-N curve is used (EN [8], A.3). For the structural detail $K = 71$, according to Figure A.2 of A.3, the stress value at 2×10^6 of cycles is $S_K = 71$ MPa. The constant-amplitude fatigue limit (the point where the slope of the S-N curve changes from $m = 3$ to $m = 5$) is defined as $S_D = 0.738 \times S_K = 52$ MPa, and the cut-off limit as $S_L = 0.549 \times S_D = 28$ MPa. All stresses $S < S_L$ do not contribute to the fatigue damage accumulation.

Figure 3.48 shows the counted stress cycles in the chosen structural detail (it has category $K = 71$ according to Table A.2, Appendix A.3). The figure represents a more precise form of the graph in Figure 2.4, Section 2.5, that has shown possible damage in steel elements. Based on only a half a year of data, the values of stress cycles are far from the S-N curve.

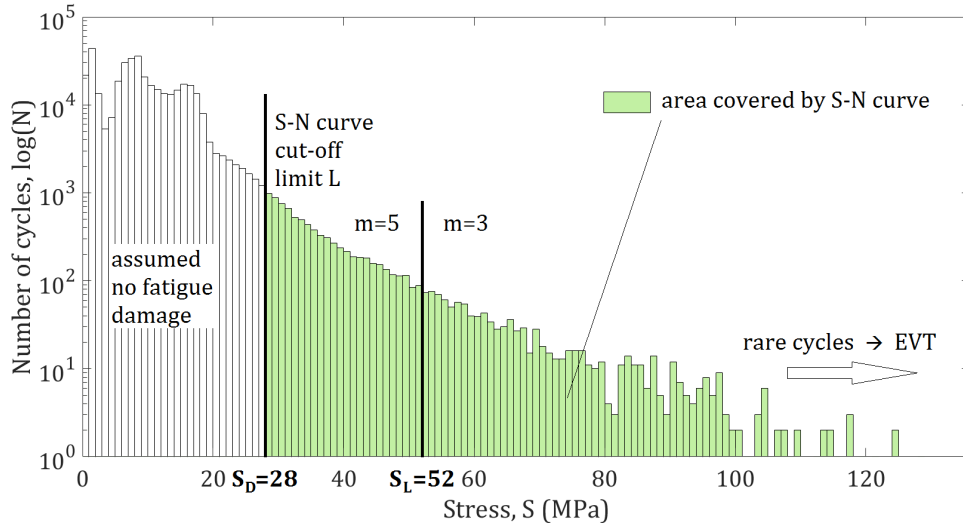


FIGURE 3.48 – Stress cycles histogram

Therefore, fatigue damage D_f is much smaller than its critical value:

$$D_f \ll D_{cr}. \quad (3.13)$$

In order to assess the damage D_f at the end of the operational life, an extrapolation is needed. When damage is estimated according to EN, a linear extrapolation of the damage is made. Let R_p be a reference value for the extrapolation in time with the desired number of years Y and monitored days d_m :

$$R_p = 365.25 \times \frac{Y}{d_m}. \quad (3.14)$$

The fatigue damage accumulation based on Palmgren-Miner's rule and two-slopes S-N curve can be written as:

$$D_f = R_p \left(\frac{1}{2 \times 10^6 (71^3)} \sum_{\geq 52 \text{ MPa}} dS_i^3 N_i + \frac{1}{5 \times 10^6 (52^5)} \sum_{28 \text{ MPa}}^{52 \text{ MPa}} dS_j^4 N_j \right) \quad (3.15)$$

where S_i is a considered stress range, such that $S_i \geq 0.74C$ with the corresponding number of cycles N_i , S_j is a considered stress range, such that $0.74C > S_j \geq 0.4C$ with the corresponding number of cycles N_j .

3.6.3 Peaks over threshold approach for the number of stress cycles

As it was briefly explained in Section 2.5, an alternative methodology is proposed to assess reliability of the deck element due to fatigue. The methodology is based on fitting

| stress range | threshold for $C^{(i)}$ | return level $C_r^{(i)}$ | confidence interval |
|-----------------|----------------------------|-----------------------------|------------------------|
| dS_1 | 1 | 6.0×10^3 | 1.3×10^5 |
| dS_2 | 53 | 4.0×10^3 | 5.8×10^5 |

TABLE 3.19 – Values of return level for daily number of fatigue cycles $C^{(1)}$ and $C^{(2)}$

the **GPD**, Eq. (2.5), with its shape and scale parameters to a number of fatigue cycles at different levels of stresses.

The algorithm of the proposed method is summarized in Figure 3.49. The return period $R_p = z \times dt$ corresponds to a number z of chosen time ranges dt during the period of interest. The array of stresses $S = [S_1, \dots, S_q, \dots, S_Q]$ recorded during J time ranges dt_j in the certain detail K is considered. It is subdivided into H stress ranges $\Delta^{(i)}$ in order to be studied separately. Firstly, the first chosen range $\Delta^{(1)}$ is taken. Secondly, for the first time range dt_1 is studied, a number of cycles $c_1^{(1)}$ is counted. Then, $c_j^{(1)}$ is obtained for every following time range dt_j until $j = J$. In that case, for the array $C^{(1)} = c_1^{(1)}, \dots, c_j^{(1)}, \dots, c_J^{(1)}$ that consist of J obtained numbers of cycles, the **POT** approach is used, see Sections 2.2, 3.3.5. It provides parameters of a fitted **GPD** $\mathcal{G}(u_i, \sigma_i, \xi_i)$ which are used to assess a return level of daily number of cycles $C_r^{(1)}$ for every $z = 1, \dots, Z$ so that $R_p = Z \times dt$. The procedure is repeated for all ranges $\Delta^{(i)}$ until $i = H$. The final step is to compute the fatigue damage according to Eq. (3.17) and to compare it with a critical value of damage accumulation.

The category of chosen detail is $K = 71$ that brings following values: $S_K = 71$ MPa, $S_D = 52$ MPa, and $S_L = 28$ MPa, see previous section and Figure 3.47. Therefore, stress ranges of $28 \leq dS_1 < 52$ and $dS_2 \geq 52$ defined according to the data set. It is done this way as the stress distribution is almost linear between S_L and S_D , Figure 3.47, and there not much data for values greater than S_D to divide this part into smaller ranges.

Let $C^{(1)}$ and $C^{(2)}$ be arrays of length J representing daily number of cycles counted for each range dS_1 and dS_2 , where $J = 129$ days of available data from monitoring. In a case of traffic loads, to respect weekly stationarity of the loading, weekdays must be counted separately from weekends and national holidays, so, not total 180 days are considered but 129 week days. Histograms for $C^{(1)}$ and $C^{(2)}$ are shown in Figure 3.50. Results of the application of **POT** approach (Section 2.2) are shown in Table 3.19 and Figure 3.51. The resulting value of P -years return level $C_r^{(i)}$ for each $\Delta^{(i)}$ is an updated value of number of stress cycles for the P -years return period.

The equivalent stresses are computed for ranges dS_1 and dS_2 to the stress ranges in order

Let $i = 1, \dots, H; j = 1, \dots, J; q = 1, \dots, Q, z = 1, \dots, Z$

set return period, $R_p = Z \times dt$

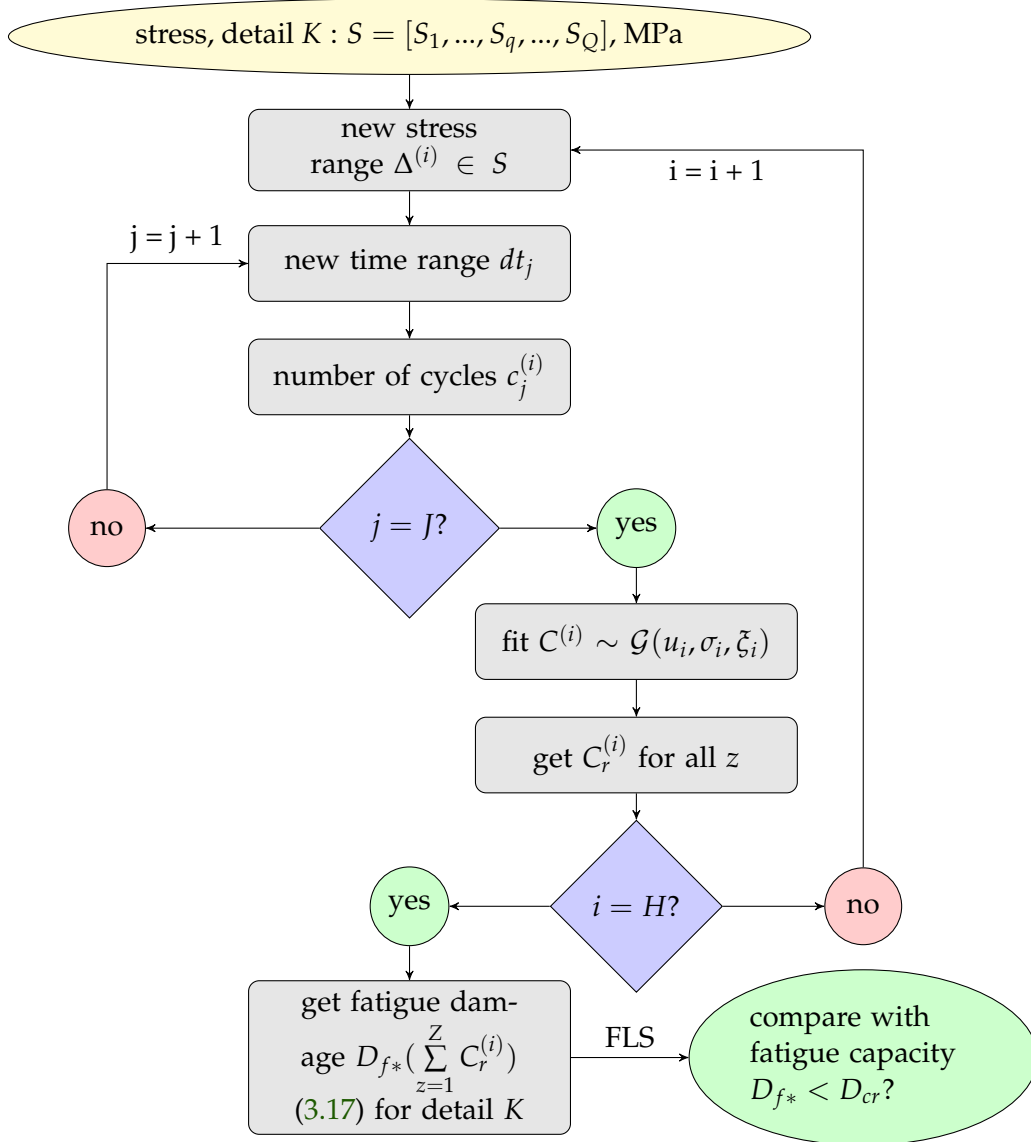


FIGURE 3.49 – Algorithm for the use of POT for the FLS

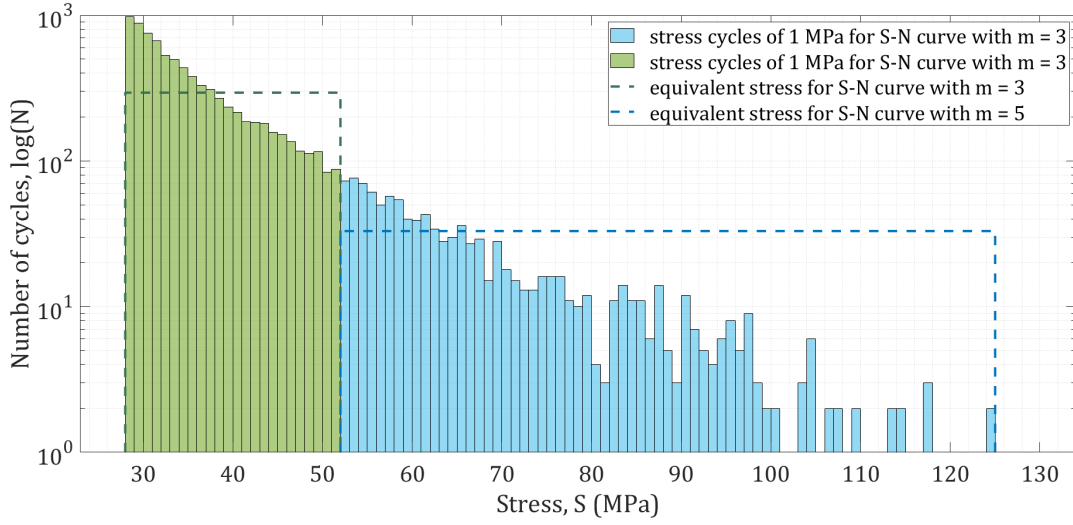


FIGURE 3.50 – Histogram of stress cycles with equivalent stresses of 65.7 MPa and 37.9 MPa

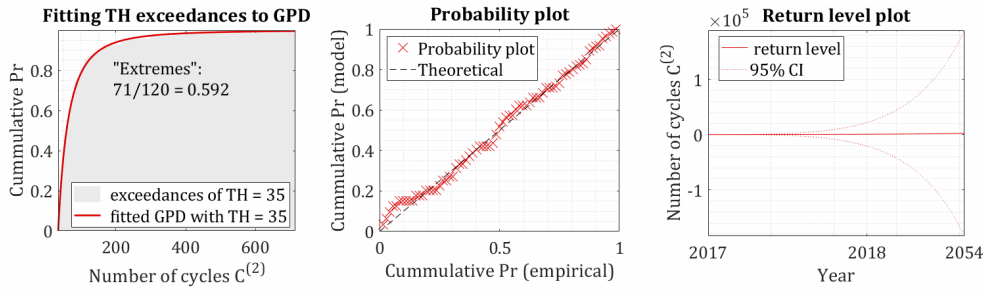


FIGURE 3.51 – Example of POT results for the range dS_2 : (i) fitting GPD to histogram of $C^{(2)}$, (ii) probability plot, (iii) return level plot

to apply the method. Let $s = s_1, \dots, s_i, \dots, s_{max}$ be the set of stress ranges of 1 MPa with the maximum recorded value s_{max} . Let $\eta = \eta_1, \dots, \eta_i, \dots, \eta_{max}$ be the set of corresponding number of cycles for s . Then, the equivalent stress is found as:

$$S^{eq} = \frac{\sum s_i \eta_i}{\sum \eta_i} \quad (3.16)$$

It is found that mean values for dS_1 and dS_2 equivalent stresses are respectively $S_1^{eq} = 37.9$ MPa, $S_2^{eq} = 65.7$ MPa. Finally, fatigue damage is computed according to EN [8], see Annex A.3 using updated values of $C_r^{(i)}$ for $i = 1, 2$, see Figure 2.6.

$$D_{f*} = \left(\frac{1}{A} \sum_{z=1}^Z (S_1^{eq})^3 C_{r,z}^{(1)} + \frac{1}{B} \sum_{z=1}^Z (S_2^{eq})^5 C_{r,z}^{(2)} \right) \quad (3.17)$$

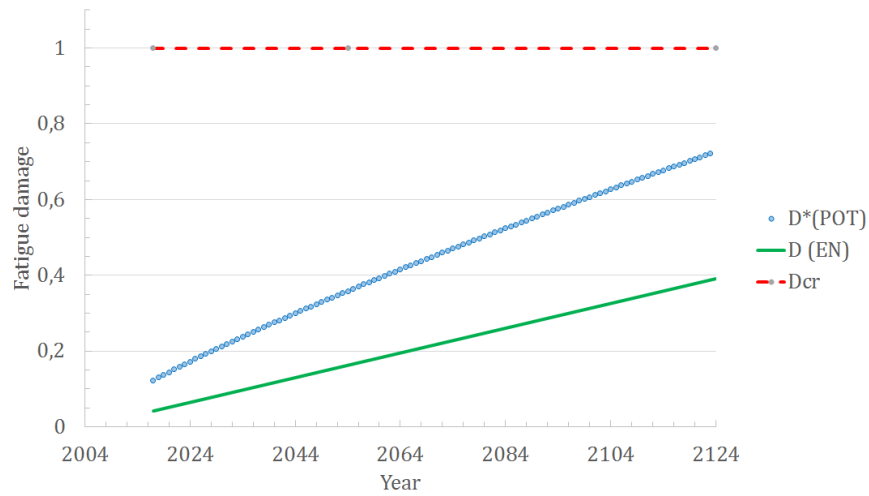


FIGURE 3.52 – Fatigue damage accumulation during the operational life of the viaduct, comparison of two methods

$$D_{f*} = \frac{1}{5 \times 10^6 (52^5)} (37.9^5 \times \sum_{z=1}^Z C_{r,z}^{(1)}) + \frac{1}{2 \times 10^6 (71^3)} (65.7^3 \times \sum_{z=1}^Z C_{r,z}^{(2)}) \quad (3.18)$$

3.6.4 Estimated fatigue damage and comparison with standards

Based on the obtained results, a comparison of damage accumulation assessed with both methods is presented in Table 3.20.

| method | D_0 , 180 days | D_f , 50 years | D_f , 120 years |
|-------------------------------|------------------|------------------|-------------------|
| linear extrapolation of D_0 | 0.002 | 0.163 | 0.348 |
| POT, fitting $C^{(i)}$ to GPD | 0.012 | 0.359 | 0.722 |

TABLE 3.20 – Fatigue damage obtained with linear extrapolation of D_0 and POT

The value of D_0 is the value of fatigue damage accumulation during available 180 days of monitoring. Years 50 and 120 correspond to the year 2054 and 2124 since the moment of the opening of the bridge. As it can be seen in Table 3.20, the values of fatigue damage are slightly higher when applying the EVT to the daily number of cycles, which brings attention to a possible grow in traffic volume with time, see Figure 3.52. In both cases, the values of fatigue damage D_f and D_{f*} are smaller than $D_{cr} = 1$. For both cases, the reliability analysis is performed in Section 3.7.3.

3.7 Reliability of the deck of the viaduct

The European road infrastructure includes a significant number of bridges with orthotropic decks, which are exposed to heavy traffic loads and unfavorable environmental influences. In order to estimate if a structure operates safely, such a structure needs to be assessed on a regular basis to verify the original design life. This can be done by reliability analysis (e.g. reliability index at the end of the operating life) of the most critical detail of the structure.

Following Sections 3.3.5, 3.4 and 3.6, this section summarizes the results obtained respectively for:

- extrapolated traffic load effects for ULS,
- combination of traffic and wind actions for ULS,
- extrapolated load effects for fatigue.

3.7.1 Comparison of reliability indexes based on several EVT approaches

The aim of this section is to compare predicted reliability levels at the end of design life based on a **limit state function (LSF)** defined with various approaches of the **EVT**. The **ULS** is studied since not only fatigue but also extreme values and serviceability have to be considered in the reliability analysis of bridges [47]. The stresses, derived from the **FE** model \mathcal{M}_2 based on 180 days of monitored by **BWIM** traffic data, are used. The model takes into account the self-weight of the bridge deck with its asphalt layer, the type of passing vehicle and amplitudes of axle loads from each axle, as well it considers the influence of vehicles queues. In order to perform the reliability analysis, limit state functions (3.19), (3.20) and (3.21) are defined for every method described in Section 2.4, **POT**, **BM** and **LCC**. Based on load effects estimated in Section 3.5, the three limit state functions take following forms:

$$G_{pot} = R - S_{pot}^{return}(u, \sigma, \xi, \zeta_u) = R - u + \frac{\sigma}{\xi} [(p\xi)^{-\xi} - 1], \quad (3.19)$$

where $\zeta_u \sim \mathcal{B}(\mu_{\zeta_u}; s_{\zeta_u})$ is the amount of load effects, that exceed the threshold, over a total amount of monitored events, $\sigma \sim \mathcal{L}(\mu_\sigma, s_\sigma)$ and $\xi \sim \mathcal{N}(\mu_\xi; s_\xi)$ are parameters of a fitted **GPD** (2.5), \mathcal{B} is Binomial distribution.

$$G_{bm} = R - S_{bm}^{return}(\mu_b, \sigma_b, \xi_b) = R - \mu_b - \frac{\sigma_b}{\xi_b} \left[1 - (d_{ref}/d_{return})^{-\xi_b} \right], \quad (3.20)$$

| Case | Random variable | | Distribution | Mean | CoV |
|------------|-----------------|------------|--------------|------------------------|-------|
| Resistance | steel strength | F_u | Log-normal | 400 MPa | 0.05 |
| | threshold | u | Constant | 64 | - |
| POT | shape | ξ | Normal | -0.2 | 0.28 |
| | scale | σ | Log-normal | 12.96 | 0.05 |
| | PE | ξ_u | Binomial | 0.003 | 0.05 |
| BM, day | location | μ_b | Normal | 67.84 | 0.02 |
| | scale | σ_b | Log-normal | 16.39 | 0.055 |
| | shape | ξ_b | Normal | -0.16 | 0.22 |
| BM, week | location | μ_b | Normal | 89.02 | 0.04 |
| | scale | σ_b | Log-normal | 18.9 | 0.12 |
| | shape | ξ_b | Normal | -0.26 | 0.27 |
| LCC | parameter | a_0 | Normal | 8.23 | 0.028 |
| | parameter | a_1 | Normal | -1.03×10^{-2} | 0.798 |
| | parameter | a_2 | Normal | -8.06×10^{-4} | 0.087 |

TABLE 3.21 – Random Variables for reliability modeling

where $\mu_b \sim \mathcal{N}(\mu_{\mu_b}; s_{\mu_b})$, $\sigma_b \sim \mathcal{N}(\mu_{\sigma_b}; s_{\sigma_b})$, $\xi_b \sim \mathcal{N}(\mu_{\xi_b}; s_{\xi_b})$ are location, scale and shape parameters of the fitted GEVD, and \mathcal{N} is the Normal distribution.

$$G_{lcc} = R - S_{lcc}^{return}(d_{return}, a_0, a_1, a_2) = R + \frac{a_1}{2a_2} - \sqrt{-\frac{a_0}{a_2} + \left(\frac{a_1}{2a_2}\right)^2 - \frac{\ln(d_{return})}{a_2}} \quad (3.21)$$

where d_{return} is the time reference that depends on a return period R_p and the reference period d_{ref} , a_0, a_1, a_2 are parameters used in order to fit Rice's formula to level up-crossings, see Table 3.18, Section 3.5.

The summary of random variables with their distribution functions, mean values and coefficients of variance for each LSF based on described approaches is given Table 3.21. They are used in the software UQLab to obtain the reliability indexes with First Order Reliability Method (FORM) method. Figures 3.53 to 3.56 show convergence of the reliability index β by FORM for each applied approach. The values of reliability indexes are found for the year of monitoring, the 50 years reference period and at the end of the promised operational life of the viaduct of 120 years. The results for every method are introduced in Table 3.22 and discussed in Section 3.7.4.

3.7.2 Reliability for wind and traffic actions and their combination

Based on results from Section 3.4, the current section compares the predicted reliability indexes β at several return periods p , Figure 3.57, for three possible cases: traffic actions

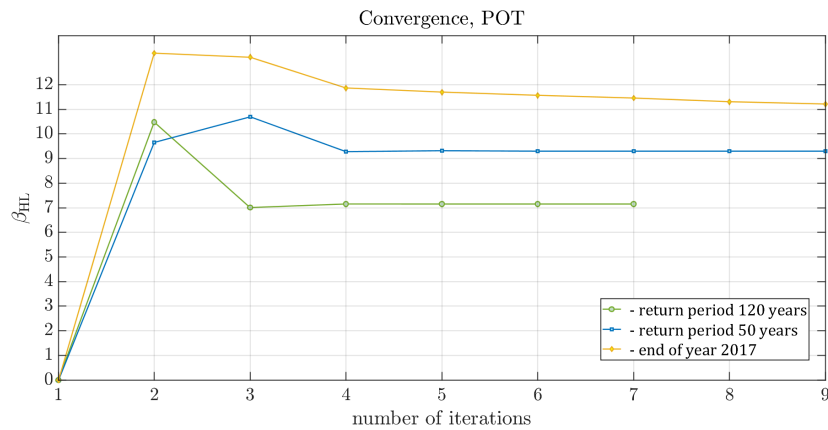


FIGURE 3.53 – Convergence of the reliability index by FORM, POT approach

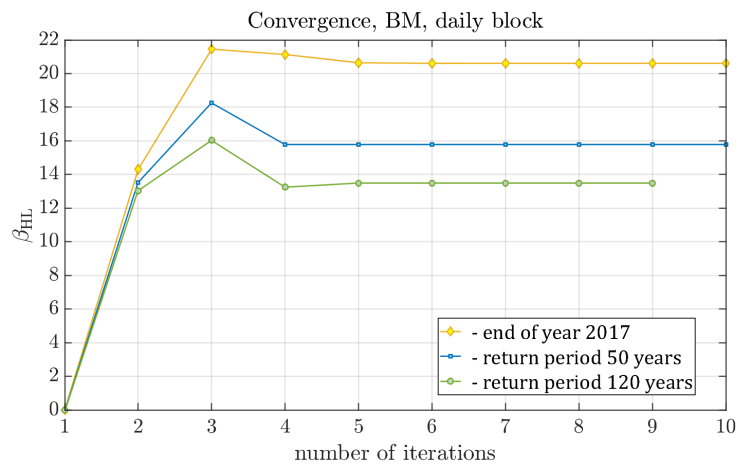


FIGURE 3.54 – Convergence of the reliability index, BM approach, daily

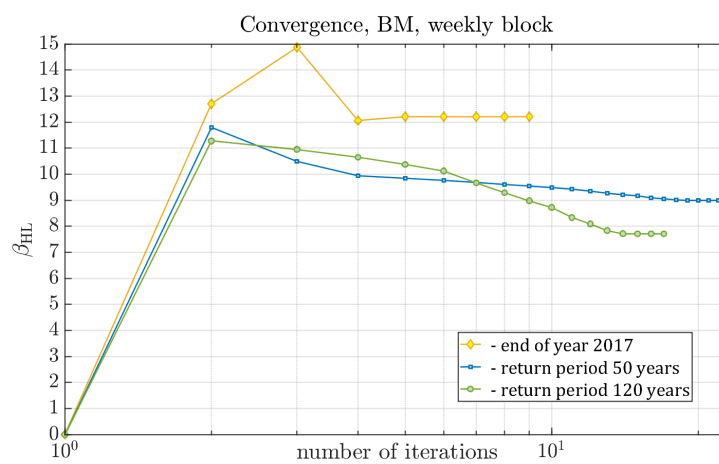


FIGURE 3.55 – Convergence of the reliability index, BM approach, weekly

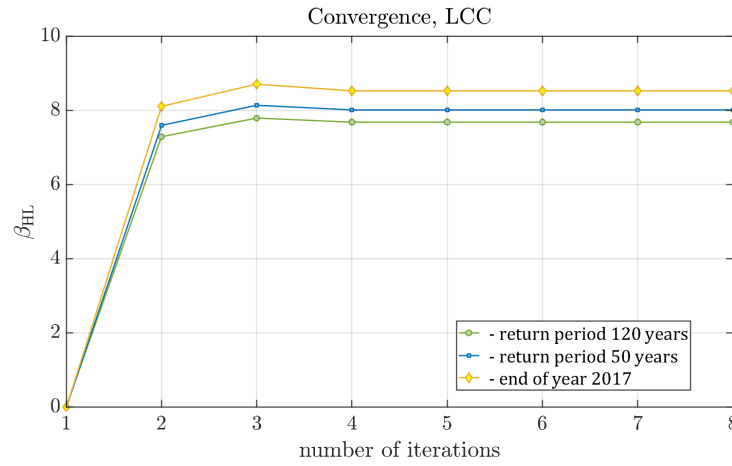


FIGURE 3.56 – Convergence of the reliability index, LCC approach

| reference | reliability | POT | BM, daily | BM, weekly | LCC | EN, LM1 [7] | β, EN [5], |
|-----------|----------------|-------------------|-------------------|-------------------|-------------------|-------------|-------------------------|
| 2017 | β | 11.1 | 20.6 | 12.2 | 9.6 | 21.8 ≈ 0 | 3.8 10 ⁻⁵ |
| | P _f | 10 ⁻²⁸ | 10 ⁻⁹⁴ | 10 ⁻³⁴ | 10 ⁻²¹ | | |
| 50 years | β | 8.9 | 15.7 | 8.9 | 8.0 | | |
| | P _f | 10 ⁻¹⁹ | 10 ⁻⁵⁶ | 10 ⁻¹⁹ | 10 ⁻¹⁵ | | |
| 120 years | β | 7.2 | 13.4 | 6.2 | 7.7 | | |
| | P _f | 10 ⁻¹³ | 10 ⁻⁴¹ | 10 ⁻¹⁰ | 10 ⁻¹⁴ | | |

TABLE 3.22 – Reliability index β for different studied cases

(I), wind actions (II), and combination of both (I+II).

The value of stress in the critical structural detail from each passing axle is obtained from **FEM** \mathcal{M}_2 of the part of the deck, Figure 3.30 by applying wind loads from Section 3.4. Therefore, the **LSF** G_t for traffic is based on the **POT** approach (see Eq. (3.19)):

$$G_t = R - S_t(u_t, \sigma_t, \xi_t, \zeta_t) = R - \begin{cases} u_t + \frac{\sigma_t}{\xi_t} [(p\zeta_t)^{\xi_t} - 1], & \xi_t \neq 0 \\ u_t + \sigma_t \log(p\zeta_t), & \xi_t = 0 \end{cases} \quad (3.22)$$

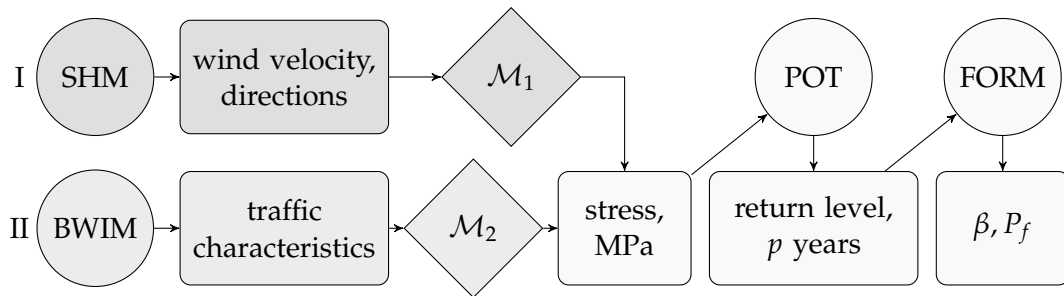


FIGURE 3.57 – Steps to be taken to access reliability based on data from monitoring

where u_t is a threshold for maximum values of stress from each passing vehicle, $\zeta_t \sim \mathcal{B}$ (0.001, 0.00008) is the amount of load effects, that exceed the threshold, over a total amount of monitored trucks, $\sigma_t \sim \mathcal{L}$ (9.62, 0.94) and $\xi_t \sim \mathcal{N}$ (-0.27, 0.065) are parameters of a fitted **GPD** (2.5), \mathcal{B} , \mathcal{L} and \mathcal{N} stand for Binomial, Log-normal, and Normal distributions.

In the case of wind actions, the values of stresses depend on the wind pressure $P = 0.5\rho v^2 A_{ref}$ that is a function of the wind velocity v [m/s]. Hourly maximum values of v are obtained from **SHM** together with the air temperature to evaluate the air density ρ . The pressure is applied to the computational model of the studied part of the viaduct in order to assess values of stresses in the considered structural detail. The computational model is built in Matlab software, which takes into account the geometry of the viaduct A_{ref} , the vertical variation of the wind pressure, and the stiffness of the deck. For the return values of stresses induced by the wind, **LSF** G_w for wind load effects is:

$$G_w = R - S_G - \begin{cases} u_w + \frac{\sigma_w}{\xi_w} [(p\zeta_w)^{\xi_w} - 1], & \xi_w \neq 0 \\ u_w + \sigma_w \log(p\zeta_w), & \xi_w = 0 \end{cases} \quad (3.23)$$

where S_G is the stress induced by the self weight of the structure, u_w is a threshold for stresses calculated from hourly wind velocities, $\zeta_w \sim \mathcal{B}$ (0.087, 0.00174) is the amount of extreme events (velocities that exceed the threshold) over a total amount of hours (24×180 days), $\sigma_w \sim \mathcal{L}$ (14.6, 3.36) and $\xi_w \sim \mathcal{N}$ (0.08, 0.0176) are parameters of the fitted **GPD**, (2.5). For the case when $\xi_t \neq 0$ and $\xi_w \neq 0$, the **LSF** G_C for the combination of loads is written as:

$$G_C = R - (u_t + \frac{\sigma_t}{\xi_t} [(p\zeta_t)^{\xi_t} - 1] + u_w + \frac{\sigma_w}{\xi_w} [(p\zeta_w)^{\xi_w} - 1]). \quad (3.24)$$

The list of the random variables for each **LSF**, (3.22), (3.23) and (3.24), based on the proposed approaches, is given in Table 3.23. Three failure modes are observed in the current study:

- extreme traffic load on one side of the deck (T),
- extreme static wind load normal to the deck (W),
- unfavorable combination of traffic and the wind.

Load effects from traffic are considered for: (i) only local traffic effects from one vehicle, (ii) all trucks on the deck (values in brackets, 3.23).

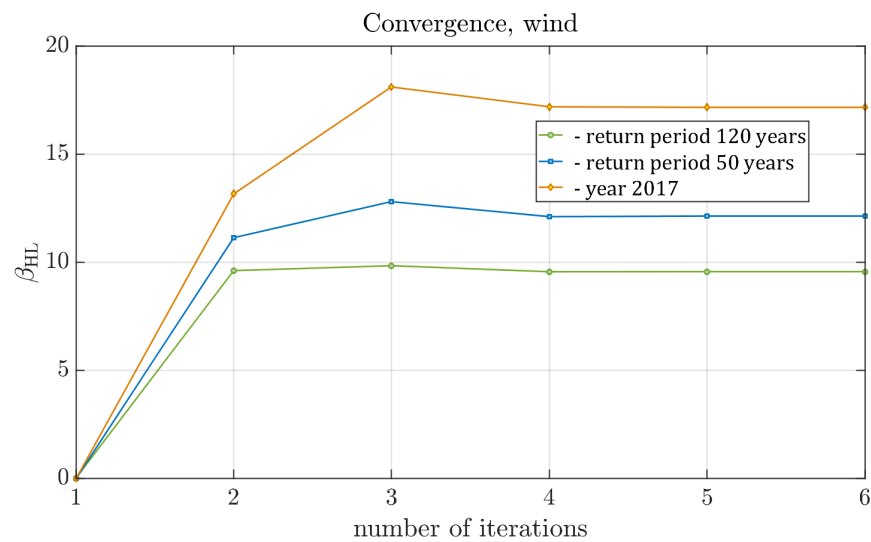


FIGURE 3.58 – Convergence of the reliability index by FORM, wind actions

First and Second Order Reliability Methods (FORM and SORM) method is also applied for this case. Figures 3.58 and 3.59 show convergence of the reliability index β by FORM for each applied approach. Reliability analysis for traffic only without taking wind into account has been demonstrated in the previous section, results from POT approach, see Figure 3.53, are used in the current section to combine with the wind.

The results of reliability analysis are listed in Table 3.24. It presents values of the reliability index β and the probability of failure P_f for three different return periods: one year, 50 years (in order to compare with EN return values), 120 years (the end of the design operational life of the viaduct). For the value of 50 years, it provides a comparison between reliability indexes derived from monitoring data with those from design load models. The last column shows reliability levels required by EN [5]. The results are discussed in Section 3.7.4.

| Case | Random variable | | Distribution | Mean | CoV |
|-------------|-----------------|-------------|--------------|---------------|-------------|
| resistance | steel strength | R , MPa | Log-normal | 400 | 0.05 |
| self-weight | stress | S_G , MPa | constant | 2.5 | 0 |
| traffic | threshold | u_t | constant | 36 (64) | 0 |
| | shape | ζ_t | Normal | -0.27 (-0.2) | 0.24 (0.28) |
| | scale | σ_t | Log-normal | 9.62 (12.96) | 0.1 (0.05) |
| | PE | ζ_t | Binomial | 0.001 (0.003) | 0.08 (0.05) |
| wind | threshold | u_w | constant | 38 | 0 |
| | shape | ζ_w | Normal | 0.08 | 0.22 |
| | scale | σ_w | Log-normal | 14.6 | 0.23 |
| | PE | ζ_w | Binomial | 0.087 | 0.02 |

TABLE 3.23 – Random variables for the reliability analysis

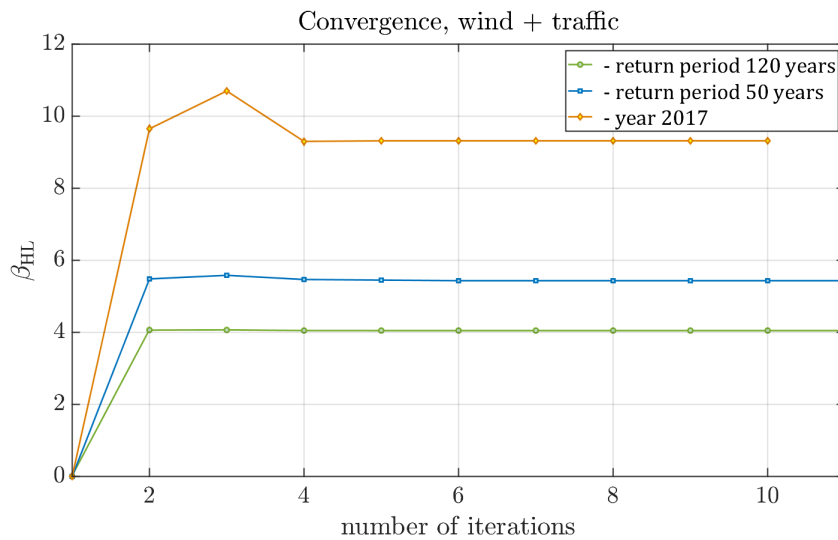


FIGURE 3.59 – Convergence of the reliability index by FORM, wind + traffic

| return period | Monitoring + EVT | | | | | Design models, [7, 6] | | | EN [5] value |
|---------------|------------------|-------------------|--------------------|-------------------|-------------------|-----------------------|------|------------------|-------------------------------|
| | | W | T _{local} | T _{all} | W+T | W | T | W+T | |
| 2017 | β | 17.1 | 21.8 | 11.1 | 9.3 | | | | 3.8 7.2 × 10 ⁻⁵ |
| | P _f | 10 ⁻⁶⁶ | ≈ 0 | 10 ⁻²⁸ | 10 ⁻²⁰ | | | | |
| 50 | β | 12.1 | 14.4 | 8.9 | 5.4 | 8.9 | 21.8 | 5.3 | |
| years | P _f | 10 ⁻³⁴ | ≈ 0 | 10 ⁻¹⁹ | 10 ⁻⁸ | 10 ⁻¹⁸ | ≈ 0 | 10 ⁻⁷ | |
| 120 | β | 9.6 | 11.4 | 7.2 | 4.0 | | | | |
| years | P _f | 10 ⁻²² | 10 ⁻³⁰ | 10 ⁻¹³ | 10 ⁻⁵ | | | | |

TABLE 3.24 – Results of the reliability analysis

3.7.3 Fatigue limit state

Fatigue verification is an essential topic to cover while evaluating a reliability of a given steel structure. Considering the same part of the deck of Millau viaduct, in addition to the **ULS** represented by extreme value analysis, also, the **FLS** is covered, Section 2.5.

This section summarizes the results for the reliability analysis based on traditional method of cycles counting and the approach, based on extrapolation, that is suggested in Section 2.5. Taking into account the results of the fatigue analysis made in Section 3.6, the limit state function for the traditional EN approach (see Eq. (3.15)) is written as:

$$G_f = D_{cr} - R_p \left(\frac{\Sigma_A}{5 \times 10^6 (52^5)} + \frac{\Sigma_B}{2 \times 10^6 (71^3)} \right) \quad (3.25)$$

and for the POT-based approach (see (3.18)) is written as:

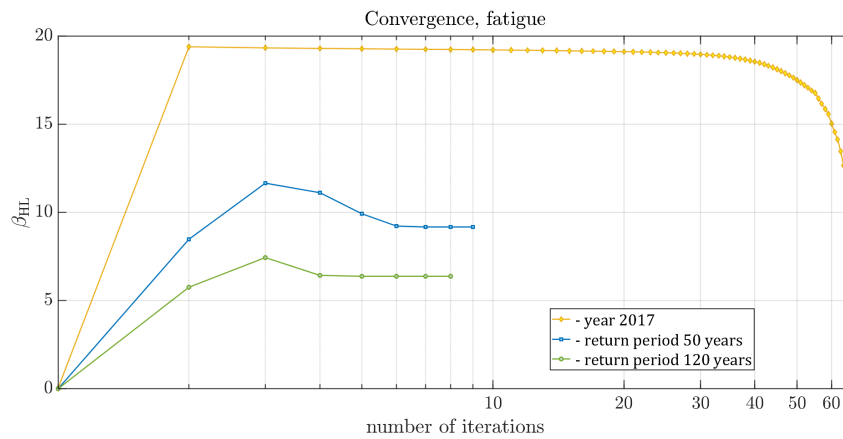
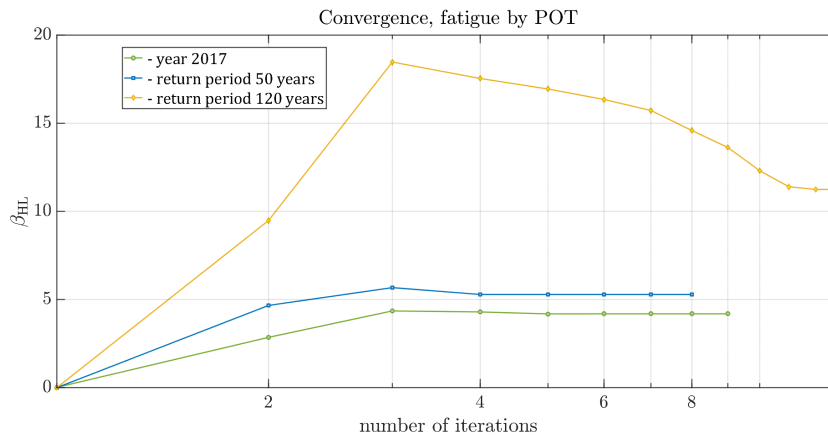
$$G_{f*} = D_{cr} - \frac{1}{5 \times 10^6 (52^5)} ((S_1^{eqv})^5 \Sigma_{S_1}) - \frac{1}{2 \times 10^6 (71^3)} ((S_2^{eqv})^3 \Sigma_{S_2}) - \frac{1}{5 \times 10^6 (52^5)} ((S_3^{eqv})^5 \Sigma_{S_3}), \quad (3.26)$$

where Σ_{S_1} and Σ_{S_2} are the random variables representing the sums of return levels for daily number of stresses during weekdays and Σ_{S_3} is a random variable representing the sum of return levels for daily number of stresses during weekends with the equivalent stress S_3^{eqv} . Table 3.25 lists all the random variables for each method. Second column gives the name of the reliability method to be used. In this case, FORM is also used to obtain the values of probability of failure P_f and reliability index β , Eq. (2.2) in Section 2 of Chapter 1. For the case of the traditional approach (Eq. (3.25)), the convergence for the reliability indexes β is shown in Figure 3.60, and for POT-based approach - in Figure 3.61.

For both reference periods of 50 and 120 years, reliability indexes obtained with the POT-based approach and with the traditional approach, see Table 3.26. The results are further discussed in Section 3.7.4.

| Case | Random variable | | Distribution | Mean | CoV |
|------|-------------------|-------------------------|--------------|-----------------------|-------|
| | critical damage | D_{cr} , MPa | Log-normal | 1 | 0.05 |
| | detail category | C , MPa | Normal | 71 | 0.05 |
| EN | sum A | Σ_A | constant | 4.05×10^{11} | 0 |
| | sum B | Σ_B | constant | 5.67×10^8 | 0 |
| POT | | $28 \leq dS_1 < 52$ MPa | | | |
| | equivalent stress | S_1^{eqv} | Normal | 37.9 | 0.076 |
| | sum S1 | Σ_{S_1} | Normal | 1.17×10^7 | 0.2 |
| | | $dS_2 \geq 52$ MPa | | | |
| | equivalent stress | S_2^{eqv} | Normal | 65.7 | 0.038 |
| | sum S2 | Σ_{S_2} | Normal | 3.87×10^7 | 0.1 |
| | | weekends | | | |
| | equivalent stress | S_3^{eqv} | Normal | 40.8 | 0.36 |
| | sum S3 | Σ_{S_3} | Normal | 1.43×10^8 | 0.3 |

TABLE 3.25 – Random variables for the fatigue reliability analysis

FIGURE 3.60 – Convergence for the reliability index β , fatigue by ENFIGURE 3.61 – Convergence for the reliability index β , fatigue by POT

| Case | β^1 | p_f^1 | β^{50} | p_f^{50} | β^{120} | p_f^{120} |
|------|-----------|------------|--------------|------------|---------------|-------------|
| EN | 19.9 | 10^{-88} | 9.1 | 10^{-20} | 6.4 | 10^{-10} |
| POT | 12.0 | 10^{-34} | 5.2 | 10^{-7} | 4.8 | 10^{-6} |

TABLE 3.26 – Results of the fatigue reliability analysis

3.7.4 Conclusions

Two limit states were covered by Section 3.7 - ultimate limit state, represented by extreme events of traffic actions and environmental actions, and fatigue. The results are represented by reliability indexes and probabilities of failure of the considered critical structural detail in the orthotropic deck of the Millau viaduct. Three figures (Figure 3.62 to 3.64) summarize the results of this chapter.

First, limit state functions have been based on traffic actions, recorded by the BWIM system, and on three different extreme value approaches in order to compare them. Figure 3.62 shows three curves: reliability index β_{pot} based on POT approach, reliability

index β_{bm} based on **BM** method, and reliability index β_{lcc} based on level up-crossings to Rice's formula. As it can be observed from this graph, two methods, **POT** and **LCC**, give similar curves, which are less optimistic than the curve based on **BM** approach. This may mean that the **BM** method, in this case, is too sensitive to a choice of a block size and to the fact that only one "extreme" data per block is considered. The positive point is that the curve β_{pot} (**POT**-based) is similar (just a little bit below) to β_{lcc} that represent fitting level up-crossings to Rice's formula that is one of the methods suggested in the background works on **EN**. It is not investigated further in work, but **POT** is used as an alternative approach.

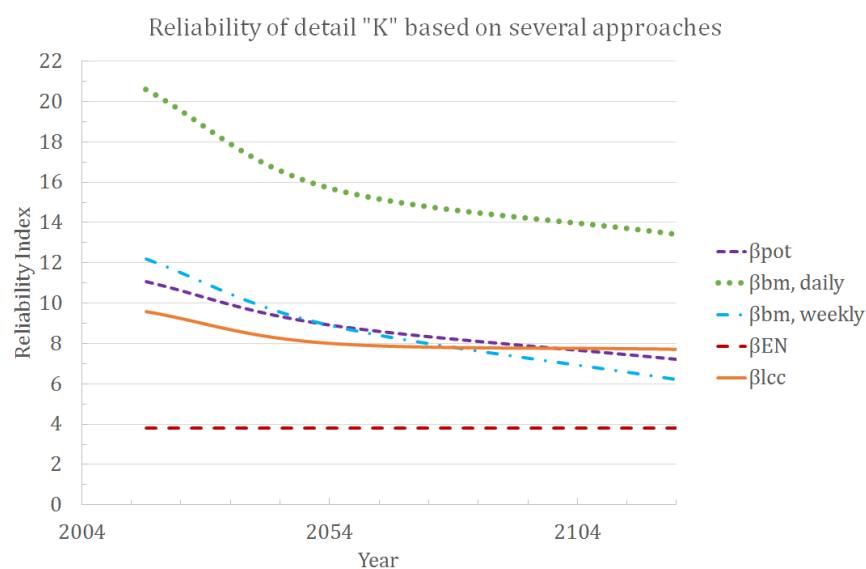


FIGURE 3.62 – Evaluation of reliability index with time, EVT approaches

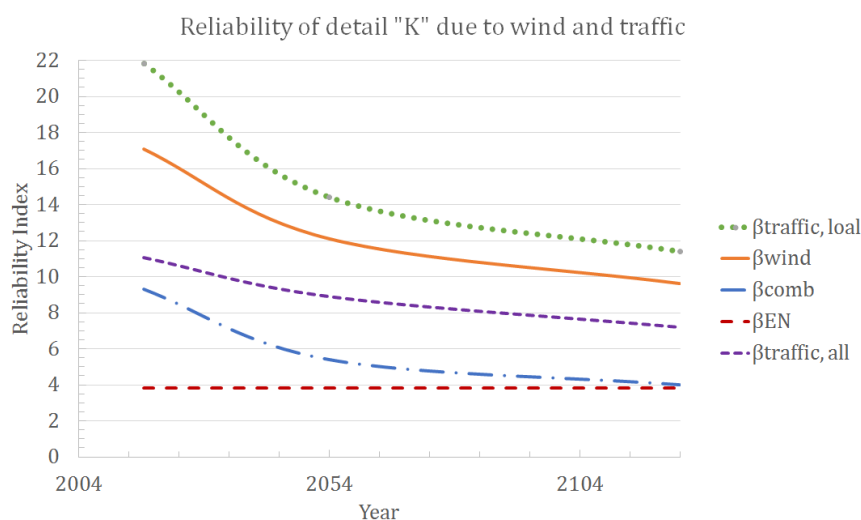


FIGURE 3.63 – Evaluation of reliability index with time, traffic and wind

The second graph (Figure 3.63) pictures results of the application of the (POT) for predictions of load effects from traffic queues, high-speed static wind, and their combination. The comparison with the design load models from European standards is made. Again, three curves can be observed: β_{traf} , β_{wind} and β_{comb} that show reliability due to traffic actions, due to the wind and due to their combination.

Finally, the fatigue damage has been computed based on 180 days of monitoring data and extrapolated both linearly (as it is usually done), and by POT-based approach. Figure 3.64 shows two curves, β_f shows reliability based on linear extrapolation of damage accumulated during monitoring period and β_{f*} demonstrates the POT-based extrapolation of the same data. Both curves prove that reliability of the structural detail due to fatigue is higher than required by EN [5] at the end of the design life of the viaduct. The probabilistic approach to extrapolate data gives a slightly lower reliability level. It can be explained not only by the variance of random variables but also by the change of traffic in volume and weight over the measured period.

The final table (Table 3.27) brings together all the results in order to conclude on reliability of the studied structural detail. All the reliability indexes and probabilities of failure are listed here and compared with design load models and the values required by norms. The main conclusions are following:

- chosen method for extrapolation of loads or load effects affects the final result,
- for some methods (as BM), monitoring period of several months is not enough to have reliable results,
- static wind actions on large bridge structure in combination with traffic may affect critical structural details of an orthotropic deck and decrease their reliability,
- in case of an orthotropic deck, fatigue reliability is lower than extreme events reliability (ULS),
- extrapolation of fatigue cycles in time is not necessarily linear but can be negatively affected by traffic growth in volume or in weight.

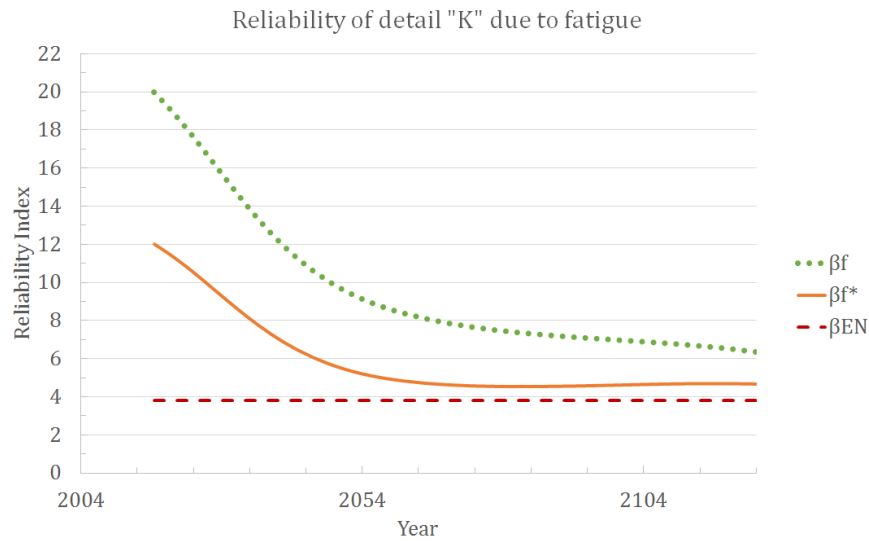


FIGURE 3.64 – Evaluation of reliability index with time, fatigue

| case | 2017 | | 50 years | | 120 years | |
|---------------------|---------|------------|----------|----------------------|-----------|------------|
| | β | P_f | β | P_f | β | P_f |
| EN [5], minimum | | | 3.8 | 7.2×10^{-5} | | |
| EN [7], traffic LM1 | | | 21.3 | ≈ 0 | | |
| EN [6], wind LM | | | 8.9 | 10^{-19} | | |
| EN [5], combination | | | 5.3 | 10^{-7} | | |
| BM, day, Traffic | 20.6 | 10^{-94} | 15.7 | 10^{-56} | 13.4 | 10^{-41} |
| BM, week, Traffic | 12.2 | 10^{-34} | 8.9 | 10^{-19} | 6.2 | 10^{-10} |
| LCC, Traffic | 9.6 | 10^{-21} | 8.0 | 10^{-15} | 7.7 | 10^{-14} |
| POT, Traffic | 11.1 | 10^{-28} | 8.9 | 10^{-19} | 7.2 | 10^{-13} |
| POT, Wind | 17.1 | 10^{-66} | 12.1 | 10^{-34} | 9.6 | 10^{-22} |
| POT, Combination | 9.3 | 10^{-20} | 5.4 | 10^{-8} | 4.0 | 10^{-5} |
| EN [8], FLS | 19.9 | 10^{-89} | 9.1 | 10^{-20} | 6.4 | 10^{-11} |
| POT, FLS | 12.0 | 10^{-34} | 5.2 | 10^{-7} | 4.7 | 10^{-6} |

TABLE 3.27 – Summary of reliability indexes β and probabilities of failure P_f

Chapter 4

Conclusions and perspectives

4.1 Summary of conclusions

This Doctoral Thesis is devoted to the estimation of reliability of the orthotropic deck of Millau viaduct, a cable-stayed bridge located in Southern France. For decks of such bridges, traffic is not necessarily the leading action, but the wind can have similar or superior effects. The goal was to observe how the reliability of the deck exposed to traffic and wind actions changes within the remaining operational life of the viaduct. **Structural health monitoring (SHM)** provides a large amount of data that may be difficult to analyze, especially in complex structures such as Millau viaduct. This Thesis demonstrates a possibility to use limited-time and accessible monitoring data for predictions of load effects.

Extrapolation in time of load effects caused by traffic actions is made using the data from a **bridge Weigh-in-Motion (BWIM)** system, installed for 180 days. For static wind actions, a week of **SHM** and data from the nearest weather station are used. Due to the absence of the direct measurements of stresses in the deck, two **finite element model (FEM)** have been developed for analyzing the traffic and wind actions. The study of the influence of a duration of monitoring on confidence intervals for return levels of traffic and wind actions show that a longer period of monitoring significantly influences the values of confidence intervals for the return levels of actions. For example, for traffic weights, a three times longer period of monitoring decreases the confidence intervals by 65%.

A choice of an appropriate extreme value method is important for each studied case. One of the objectives was to compare reliability indexes based on extrapolation of load effects in time with three different approaches. This part of work is based only on load effects from monitored traffic actions in a chosen structural detail of the deck. Limit state functions have been based on three different approaches: (i) **Peaks Over Threshold (POT)**

with fitting threshold exceedances to a **generalized Pareto distribution (GPD)**, (ii) **Block Maximum (BM)** with fitting events with maximum values of stresses to a **generalized extreme value distribution (GEVD)** and (iii) **Level Crossing Counting (LCC)** with fitting Rice's formula to up-crossings of chosen load effects. The results show that **POT**, **LCC**, and **BM** with weekly blocks give quite similar reliability indexes. They stay above the required reliability index of 3.8 during the operational life of the viaduct. The reliability index based on **BM** approach with the daily block are almost twice higher than results from all other methods. This means that the **BM** method, in this case, is too sensitive to a choice of the block size. It also confirms the weekly stationarity of traffic loads, what has been assumed in this work. The positive point is that the **POT**-based reliability index is similar to the one based on the **LCC** approach that is one of the methods suggested in the background works on **European Norms (EN)**. Some of the obtained reliability indexes are not representative due to their order. They are used for the comparison of different models. For the best results, several extrapolation theories should be compared in every particular case. In this Thesis, for further extreme value analyses, **POT** is used as a method that is easy to apply.

One of the drawbacks of the **POT** method is the estimation of the threshold parameter. A contribution to existing methods for threshold choice has been made. A graphical is proposed way for choosing the most appropriate value of the threshold. It is based on a comparison of several values of thresholds based on the confidence intervals for a return level of analyzed load effects and on the probabilities of threshold exceedance. In most of the studied cases, chosen thresholds give good distribution fitting.

Static wind load obtained from **SHM** of the viaduct are considered in combination with queues of traffic lorries. A probabilistic model is made to observe occurrences of extreme cases for both actions and their combination, and their effect on the deck. The first conclusion shows that, for the **ultimate limit state (ULS)** and **serviceability limit state (SLS)**, the wind action contributes more than the traffic action to bending moments in the studied part of the deck. Separately, these loads do not bring much damage to the stiff deck of Millau viaduct, even at the end of the expected operational life, the reliability in each case stays quite high (twice higher than required by **EN**). On the other hand, the combination of them yields the reliability index close to the critical value (for the reference of 50 years). Although, in terms of actions themselves, the probabilistic model for the combination of extreme traffic and extreme wind actions show that critical case, which would endanger the entire structure, is unlikely to arrive during the design life of the bridge.

Moreover, a comparison has been performed between the reliability indexes derived from

statistical models with design load models from European standards. For the 50 years return period, design load model LM1 for traffic gives a low probability of failure. However, in practice, the presence of several heavy vehicles on the deck (LM3 of EN) negatively affects the reliability index. It shows the importance of structural monitoring for updating the design load models during the operational life of the structure. The probability of failure due to wind loads from monitored actions is lower than the value obtained with the design load models (for the reference period of 50 years). It confirms that the European design standards for wind actions stay on the safe side. Reliability indexes from a combination of both loads, derived from the extreme value model and from the design load model (for ULS), are almost the same. So, both types of action, traffic and climatic, should be considered together in the reliability analysis of the orthotropic deck.

Not only ULS is important in orthotropic decks, but also fatigue of steel structural details. The values of stress cycles are composed of local effects caused by passing vehicles and global effects from traffic queues on both lanes and from the wind. Usually, fatigue damage accumulated in a detail during a monitoring period is linearly extrapolated in time. A methodology has been proposed for extrapolating the numbers of fatigue cycles in time with the POT approach. It accounts for a traffic change in volume and in weight with time. Comparison of the proposed approach with the classical method has been carried out and used in the fatigue reliability analysis. The fatigue damage has been computed, based on 180 days of monitoring data, and has been extrapolated both, linearly (as it is usually done) and by POT-based approach. Both methods prove that at the end of the design life of the viaduct, reliability of the structural details due to fatigue is higher than required by EN value for the reference period of 50 years. The suggested statistical approach to extrapolate data gives a slightly lower reliability level. It can be explained by the change of traffic in volume and weight over the measured period.

4.2 Short-term perspectives

First of all, it is necessary to highlight that monitoring data, which have been used in this Thesis, is limited. For example, the records of the traffic have been assumed to be continues, however, they included several breaks in time. A study based on longer monitoring data could be made in order to observe not only seasonal traffic growth but also the increase in volume and weights over several years.

Here, FEM has been contracted in order to compute stresses in the deck from the monitored actions. An analysis, based on a direct monitoring of the stresses inside the deck of

the Millau viaduct, could be performed in order to compare the predictions of the load effects (based on monitored actions) with monitored load effects extrapolated in time by the same statistical approaches.

Due to the lack of data for the transversal position of each vehicle, the passage in the center of the lane has been assumed for simplicity. Thus, it would be more correct to record the exact positions of vehicles if only traffic actions are monitored.

Finally, static wind actions have been studied, although, the influence of dynamic effects plays a crucial role in some cases. Dynamic wind actions affect cables of the bridge, which have not been investigated in this Thesis. Reliability indexes of other structural parts of the viaduct could be assessed, as well, in order to complete the picture.

4.3 Long-term perspectives

For large scale bridges, not only combination of traffic and wind actions is important but also other actions. Therefore, more similar structures in various environments could be investigated in order to take into account probabilistic combinations of traffic with earthquakes, waves, temperature variations, etc.

Several additional analyses could also confirm or contradict the proposed probabilistic method for extrapolating fatigue damage in time. If it works well for other structures with different traffic flow and for other structural elements of decks, then it can be applied in engineering as an additional tool for studying fatigue of structural details in existing bridges.

European design standards stay on the safe side in most cases. However, a set of rules for existing structures (i.e. bridges) is yet missing in European design standards. It could include a methodology for reassessment of the reliability of bridges, that targets to a longer operational life of important structures.

4.4 Scientific production

- M. Nesterova, F. Schmidt and C. Soize. Probabilistic analysis of the effect of the combination of traffic and wind actions on a cable-stayed bridge. *Journal of Bridge Structures*, accepted for publication, 2019.
- M. Nesterova, F. Schmidt and C. Soize. Estimation of remaining life of a bridge with an orthotropic deck exposed to extreme traffic and wind actions. *12th International Workshop on Structural Health Monitoring (IWSHM)*, Stanford, USA, 10-12 September 2019.
- M. Nesterova, M. Nowak, F. Schmidt and O. Fischer. Reliability of a bridge with an orthotropic deck exposed to extreme traffic events. *11th International Conference on Mathematical Methods in Reliability (MMR)*, Hong-Kong, 3-7 June 2019.
- M. Nesterova, F. Schmidt, E. Brühwiler and C. Soize. Generalized Pareto Distribution for reliability of bridges exposed to fatigue. In *Proceedings of the Ninth International Conference on Bridge Maintenance, Safety and Management (IABMAS 2018): Maintenance, Safety, Risk, Management and Life-Cycle Performance of Bridges*, 2477-2484, Melbourne, Australia, July 2018.
- B. Sawicki, E. Brühwiler and M. Nesterova. Fatigue safety verification of a steel railway bridge using short term monitoring data. In *Proceedings of the Sixth International Symposium on Life-Cycle Civil Engineering (IALCCE 2018)*, Ghent, Belgium, October 2018.
- M. Nesterova, F. Schmidt, C. Soize and D. Siegert. Extreme effects on bridges caused by traffic and wind. *23ème Congrès Français de Mécanique (CFM 2017)*, Lille, France, 28 August - 01 September 2017.

References

Norms and Standards

- [1] ASCE/SEI-7-10. *Minimum Design Loads for Buildings and Other Structures*. New York, 2010 (p. 10).
- [2] AS/NZS-1170.1:2002. *General design requirements and loading on structures*. Sydney, Australia, Wellington, New Zealand, 2002 (p. 10).
- [3] ASTM-E1049-85. *Standard Practices for Cycle Counting in Fatigue Analysis*. West Conshohocken, Pensilvania, 2017 (p. 78).
- [4] COST-323. *Post-proceedings of the second European Conference on Weigh-in-Motion of Road Vehicles: Lisbon, 14th-16th September*. Brussels, 1998 (pp. 10, 40).
- [5] EN1990. *Eurocode: Basis of structural design*. Brussels, 2002 (pp. 8, 10, 28, 65, 89, 91, 92, 96, 97).
- [6] EN1991-1-4. *Eurocode 1: Actions on structures - Part 1-4: General actions - Wind actions*. Brussels, 2005 (pp. 2, 17, 28, 60, 65, 92, 97, 114).
- [7] EN1991-2. *Eurocode 1: Actions on structures - Part 2: Traffic loads on bridges*. Brussels, 2003 (pp. 2, 12, 14, 17, 28, 64, 65, 67, 89, 92, 97).
- [8] EN1993-1. *Eurocode 3: Design of steel structures - Part 1-9: Fatigue*. Brussels, 2005 (pp. xix, 17, 31, 32, 80, 84, 97).
- [9] EN1993-1-3. *Eurocode 3: Design of steel structures - Part 1-3: General rules - Supplementary rules for cold-formed members and sheeting*. Brussels, 2006 (p. 38).
- [10] ISO2394:2015. *General principles on reliability for structures*. Geneve, 2015 (pp. xix, 1, 3).
- [11] NBCC. *National Building Code of Canada*. Ottawa, 2010 (p. 10).
- [12] R312-10. *Code de la route. Partie réglementaire. Livre III: Le véhicule. Titre Ier: Dispositions techniques. Chapitre II: Poids et dimensions. Section 2: Dimensions des véhicules. Article R312-10*. France, 2016 (p. 52).
- [13] R312-4. *Code de la route. Partie réglementaire. Livre III: Le véhicule. Titre Ier: Dispositions techniques. Chapitre II: Poids et dimensions. Section 1: Poids. Article R312-4*. France, 2016 (p. 51).

Books

- [14] S. Coles. *An Introduction to Statistical Modeling of Extreme Values*. London: Springer Science & Business Media, 2001 (pp. 2, 12, 15, 16, 23, 24, 29, 53, 54, 73).
- [15] C. Cremona. *Structural Performance: Probability-based Assessment*. Hoboken, USA: John Wiley & Sons, Inc., 2013 (p. 53).
- [16] P. Embrechts, C. Kluppelberg, and T. Mikosch. *Modelling Extremal Events for Insurance and Finance*. Berlin: Springer Verlag, 2012 (pp. 16, 25).
- [17] E. J. Gumbel. *Statistics of extremes*. New York: Columbia University Press, 1958 (p. 12).
- [18] C. Klüppelberg, D. Straub, and I. Welpé. *Risk - A Multidisciplinary Introduction*. Berlin: Springer, 2014 (pp. 7, 22).
- [19] H.-H. Lee. *Finite Element Simulations with ANSYS Workbench 17*. SDC Publications, 2017 (p. 11).
- [20] M. Lemaire. *Fiabilité des structures: Couplage mécano-fiabiliste statique*. Paris: Hermes Science Publications, 2005 (p. 7).
- [21] A. McNeil, P. Embrechts, and R. Frey. *Quantitative Risk Management: Concepts, Techniques, and Tools*. Princeton, USA: Princeton University Press, 2005 (pp. 16, 25).
- [22] L. Sanpalesi and P. Croce. *Handbook 4. Design of Bridges. Guide to basis of bridge design related to Eurocodes supplemented by practical examples*. Ed. by L. D. V. P. Project. Pisa, Italy, 2005 (p. 12).
- [23] C. Soize. *Uncertainty Quantification. An Accelerated Course with Advanced Applications in Computational Engineering*. Berlin: Springer, 2017 (p. 69).
- [24] C. Soize and P. Kree. *Mathematics of Random Phenomena: Random Vibrations of Mechanical Structures (Mathematics and Its Applications)*. Berlin: Springer, 1986 (pp. 15, 41).

Articles

- [25] N. D. Adasooriya. "Fatigue reliability assessment of ageing railway truss bridges: Rationality of probabilistic stress-life approach". *Case Studies in Structural Engineering* 6, 1–10, 2016. (p. 9).
- [26] P. Agarwal and L. Manuel. "Simulation of offshore wind turbine response for long-term extreme load prediction". *Engineering Structures* 31, 2236–2246, 2009. (p. 16).
- [27] A. Balkema and L. de Haan. "Residual life time at great age". *Annals of Probability* 2, 792–804, 2003. (p. 12).

- [28] G. Box and D. Cox. "An Analysis of Transformations". *Journal of the Royal Statistical Society B*, 211–264, 1964. (p. 15).
- [29] M. Buonomo et al. "The design and the construction of the Millau Viaduct". *Steel-bridge 2004*, 2004. (p. 60).
- [30] C. Caprani and E. O'Brien. "Estimating extreme highway bridge traffic load effects". *International Conference on Structural Safety and Reliability (ICOSSAR 2009)*, Osaka, Japan, September 2009. (pp. 14, 15).
- [31] C. Caprani and E. O'Brien. "The use of predictive likelihood to estimate the distribution of extreme bridge traffic load effect". *Structural Safety*, 138–144, 2010. (p. 14).
- [32] C. Caprani, E. O'Brien, and A. Lipari. "Long-span bridge traffic loading based on multi-lane traffic micro-simulation". *Engineering Structures* 115, 207–219, 2016. (p. 9).
- [33] C. Caprani, E. O'Brien, and G. McLachlan. "Characteristic traffic load effects from a mixture of loading events on short to medium span bridges". *Structural Safety* 30, 394–404, 2008. (p. 15).
- [34] A. Cetin, A. Naess, and A. Härkegård. "A physically based extreme value characterization of material fatigue". *International Journal of Fatigue* 47, 216–221, 2013. (p. 9).
- [35] S. Chen et al. "Research of long-span bridge and traffic system subjected to winds: A system and multi-hazard perspective". *International Journal of Transportation Science and Technology* 6, 184–195, 2017. (p. 10).
- [36] C. Cremona. "Optimal extrapolation of traffic load effects". *Structural Safety* 23, 31–46, 2001. (pp. 15, 30, 75).
- [37] C. Crespo-Minguillon and J. Casas. "A comprehensive traffic load model for bridge safety checking". *Structural Safety* 19, 339–359, 1997. (p. 23).
- [38] L. D'Angelo and A. Nussbaumer. "Reliability based fatigue assessment of existing motorway bridge". *Structural Safety* 57, 35–42, 2015. (p. 8).
- [39] A. Davenport. "The generalization and simplification of wind loads and implications for computational methods". *Journal of Wind Engineering and Industrial Aerodynamics* 46, 409–417, 1993. (p. 10).
- [40] P. Dissanayake and P. Karunananda. "Reliability Index for Structural Health Monitoring of Aging Bridges". *Structural Health Monitoring: An International Journal* 7, 175–183, 2008. (p. 7).
- [41] A. Eslami, S. H. Golafzani, and R. J. Chenari. "Assessment of Babolsar Concrete Pedestrian Bridge Failure for 1964 Flood Event and Retrofitting Practice". *Engineering Failure Analysis* 68, 101–112, 2016. (p. 8).

- [42] J. Eymard. "Un nouveau logiciel: le programme CASTOR pour le calcul des actions et sollicitations du trafic dans les ouvrages routiers". *Bulletin de liaison des laboratoires des ponts et chaussées* 164, 64–77, 1989. (p. 11).
- [43] I. Farreras-Alcover, M. K. Chryssanthopoulos, and J. E. Andersen. "Data-based models for fatigue reliability of orthotropic steel bridge decks based on temperature, traffic and strain monitoring". *International Journal of Fatigue* 95, 104–119, 2017. (pp. 8, 9).
- [44] I. Farreras-Alcover, P. L. Sørensen, and N. Bitsch. "Fatigue life prediction of New Little Belt Bridge steel deck under a cracked pavement section. Comparison between a monitoring-based and a FE modelling approaches". *Eurosteel*, 2017. (p. 67).
- [45] S. Gallice and H. Lancon. "Dix années de monitoring structurel du viaduc de Millau". *Travaux (Paris)*, 108–117, 2013. (p. 41).
- [46] T. Garcia-Segura et al. "Lifetime reliability-based optimization of post-tensioned box-girder bridges". *Engineering Structures*, 381–391, 2017. (p. 8).
- [47] S. H. Ghasemi and A. Nowak. "Target reliability for bridges with consideration of ultimate limit state". *Engineering Structures* 152, 226–237, 2017. (pp. 8, 86).
- [48] F.-I. Giskea et al. "Long-term extreme response analysis of a long-span pontoon bridge". *Marine Structures*, 154–171, 2018. (p. 7).
- [49] J. Gorse. "Calcul des effets du trafic routier sur les ponts par le programme TRAF-MUL". *Bulletin de liaison des laboratoires des ponts et chaussées* 96, 41–48, 1978. (p. 11).
- [50] T. Guo, D. Frangopol, and Y. Chen. "Fatigue reliability assessment of steel bridge details integrating weigh-in-motion data and probabilistic finite element analysis". *Computers and Structures* 112–113, 245–257, 2012. (p. 8).
- [51] T. Haugen et al. "Weigh-in-Motion Equipment – Experiences and Challenges". *Transportation Research Procedia* 14, 1423–1432, 2016. (p. 11).
- [52] J. Hosking and J. Wallis. "Parameter and Quantile Estimation for the Generalized Pareto Distribution". *Technometrics* 29 339, 1987. (p. 25).
- [53] C. Huang et al. "Force-based and displacement-based reliability assessment approaches for highway bridges under multiple hazard actions". *Journal of Traffic and Transportation Engineering (English Edition)* 2, 223–232, 2015. (p. 8).
- [54] B. Jacob, E. J. O'Brien, and W. Newton. "Assessment of the accuracy and classification of weigh-in-motion systems. Part 2: European specification". *International Journal of Heavy Vehicle Systems* 7, 2000. (p. 40).
- [55] S. Kameshwar and J. Padgett. "Multi-hazard risk assessment of highway bridges subjected to earthquake and hurricane hazards". *Engineering Structures* 78, 154–166, 2014. (p. 8).

- [56] M. Kratz. "Level crossings and other level functionals of stationary Gaussian processes". *Probability Surveys* 3, 230–288, 2006. (p. 75).
- [57] I. Kusano et al. "The importance of correlation among flutter derivatives for the reliability based optimum design of suspension bridges". *Engineering Structures* 173, 416–428, 2018. (p. 9).
- [58] K. Kwon and D. Frangopol. "Bridge fatigue reliability assessment using probability density functions of equivalent stress range based on field monitoring data". *International Journal of Fatigue* 32, 1221–1232, 2010. (p. 8).
- [59] C. Leahy, E. O'Brien, and A. O'Connor. "The Effect of Traffic Growth on Characteristic Bridge Load Effects". *Transportation Research Procedia* 14, 3990–3999, 2016. (p. 9).
- [60] J. Leander. "Reliability evaluation of the Eurocode model for fatigue assessment of steel bridges". *Journal of Constructional Steel Research* 141, 1–8, 2018. (p. 8).
- [61] Y. Liu et al. "Fatigue reliability assessment for orthotropic steel deck details under traffic flow and temperature loading". *Engineering Failure Analysis* 71, 179–194, 2017. (p. 8).
- [62] I. Lukačević, B. Androić, and D. Dujmović. "Assessment of reliable fatigue life of orthotropic steel deck". *Central European Journal of Engineering* 1, 306–315, 2011. (p. 8).
- [63] F. Massey. "The Kolmogorov-Smirnov Test for Goodness of Fit". *Journal of the American Statistical Association* 253 46, 68–78, 1951. (pp. 55, 77).
- [64] F. Miao and M. Ghosn. "Reliability-based progressive collapse analysis of highway bridges". *Structural Safety* 63, 33–46, 2016. (p. 7).
- [65] J. Morio et al. "A survey of rare event simulation methods for static input-output models". *Simulation Modelling Practice and Theory* 49, 287–304, 2014. (p. 7).
- [66] F. Moses. "Weigh-in-Motion System Using Instrumented Bridges". *Transportation Engineering Journal of ASCE* 105, 233–249, 1979. (p. 11).
- [67] M. Nesterova, F. Schmidt, and C. Soize. "Estimation of remaining life of a bridge with an orthotropic deck exposed to extreme traffic and wind actions". *12th International Workshop on Structural Health Monitorin (IWSHM2019)*, Stanford, USA, September 2019. (pp. 18, 67).
- [68] M. Nesterova, F. Schmidt, and C. Soize. "Probabilistic analysis of the effect of the combination of traffic and wind actions on a cable-stayed bridge". *Journal of Bridge Structures*, 2019. (pp. 16, 18).
- [69] M. Nesterova et al. "Extreme effects on bridges caused by traffic and wind". *23ème Congrès Français de Mécanique*, Lille, France, August 2017. (p. 18).

- [70] M. Nesterova et al. "Generalized Pareto Distribution for reliability of bridges exposed to fatigue". *Maintenance, Safety, Risk, Management and Life-Cycle Performance of Bridges: Proceedings of the Ninth International Conference on Bridge Maintenance, Safety and Management (IABMAS 2018)*, 2477–2484, Melbourne, Australia, July 2018. (pp. 18, 79).
- [71] M. Nesterova et al. "Reliability of a bridge with an orthotropic deck exposed to extreme traffic events". *11th International Conference on Mathematical Methods in Reliability (MMR2019)*, Hong-Kong, June 2019. (p. 18).
- [72] M. Nowak, D. Straub, and O. Fischer. "Extended extrapolation methods for robust estimates of extreme traffic load effects on bridges". *Proceedings for the Sixth International Symposium on Life-Cycle Engineering (IALCCE 2018)*, Ghent, Belgium, October 2018. (p. 15).
- [73] E. O'Brien et al. "A review of probabilistic methods of assessment of load effects in bridges". *Structural Safety* 53, 44–56, 2015. (pp. 12, 15, 16, 24).
- [74] E. O'Brien and B. Enright. "Modeling same-direction two-lane traffic for bridge loading". *Structural Safety* 33, 296–304, 2011. (p. 9).
- [75] M. Ovetto et al. "Vulnerability to failure of cable-stayed bridges for beyond-design basis wind events". *Engineering Failure Analysis* 91, 182–200, 2018. (p. 10).
- [76] J. Pickands. "Statistical Inference Using Extreme Order Statistics". *The Annals of Statistics* 3, 119–131, 1975. (pp. 12, 16, 23).
- [77] S. Rice. "Mathematical analysis of random noise". *Bell System Technical Journal* 23, 282–332, 1944. (pp. 15, 30).
- [78] J. Richardson, S. Jones, and A. Brown. "On the use of bridge weigh-in-motion for overweight truck enforcement". *International Journal of Heavy Vehicle Systems* 21, 83–104, 2014. (p. 11).
- [79] M. Roth et al. "Projections of precipitation extremes based on a regional, non-stationary peaks-over-threshold approach: A case study for the Netherlands and north-western Germany". *Weather and Climate Extremes* 4, 1–10, 2017. (p. 16).
- [80] B. Sawicki, E. Brühwiler, and M. Nesterova. "Fatigue safety verification of a steel railway bridge using short term monitoring data". *Proceedings of the Sixth International Symposium on Life-Cycle Civil Engineering (IALCCE 2018)*, Ghent, Belgium, October 2018. (p. 18).
- [81] T. Schendel and R. Thongwichian. "Confidence intervals for return levels for the peaks-over-threshold approach". *Advances in Water Resources* 99, 53–59, 2017. (p. 25).
- [82] S. Shiri, M. Yazdani, and M. Pourgol-Mohammad. "A fatigue damage accumulation model based on stiffness degradation of composite materials". *Materials and Design* 88, 1290–1295, 2015. (p. 9).

- [83] C. Sigauke and A Bere. "Modelling non-stationary time series using a peaks over threshold distribution with time varying covariates and threshold: An application to peak electricity demand". *Energy* 119, 152–166, 2017. (p. 16).
- [84] H. Tello et al. "Weigh-in-Motion Equipment – Experiences and Challenges". *Transportation Research Procedia* 14, 1423–1432, 2016. (p. 11).
- [85] V.-H. Truong and S.-E. Kim. "An efficient method of system reliability analysis of steel cable-stayed bridges". *Advances in Engineering Software*, 295–311, 2017. (p. 7).
- [86] H. Wang, J.-X. Mao, and B. F. Spencer. "A monitoring-based approach for evaluating dynamic responses of riding vehicle on long-span bridge under strong winds". *Engineering Structures* 189, 35–47, 2019. (pp. 9, 10).
- [87] W. Wang and G. Morgenthal. "Reliability analyses of RC bridge piers subjected to barge impact using efficient models". *Engineering Structures* 166, 485–495, 2018. (p. 8).
- [88] H. Xie, Y. Wang, and R. Zou. "Reliability analysis of RC T-beam highway bridges in China based on a virtual bridge dataset". *Engineering Structures* 104, 133–140, 2015. (p. 8).
- [89] G. Yiming et al. "A novel Bayesian extreme value distribution model of vehicle loads incorporating de-correlated tail fitting: Theory and application to the Nanjing 3rd Yangtze River Bridge". *Engineering Structures* 59, 386–392, 2017. (pp. 14, 15).
- [90] Y. Yu et al. "Prediction of bridge maximum load effects under growing traffic using non-stationary bayesian method". *Engineering Structures* 185, 171–183, 2019. (p. 9).
- [91] W. Zhang et al. "Fatigue life estimation of existing bridges under vehicle and non-stationary hurricane wind". *Journal of Wind Engineering and Industrial Aerodynamics* 133, 135–145, 2014. (pp. 9, 10).
- [92] X.-Y. Zhou, F. Schmidt, and B. Jacob. "Extrapolation of traffic data for development of traffic load models: assessment of methods used during background works of Eurocode". *6th Conference on Bridge Maintenance, Safety and Management (IABMAS 2012)*, Lac de Come, Italy, July 2012. (p. 12).
- [93] X.-Y. Zhou et al. "A mixture peaks over threshold approach for predicting extreme bridge traffic load effects". *Probabilistic Engineering Mechanics* 43, 121–131, 2016. (pp. 12, 16, 23).

Other references

- [94] I. F. Alcover. "Data-based models for assessment and life prediction of monitored civil infrastructure assets." PhD thesis. University of Surrey, 2014 (p. 9).
- [95] E. Bommier. "Peaks-Over-Threshold Modelling of Environmental Data". MA thesis. Uppsala University, Applied Mathematics and Statistics, 2014, 39 (p. 26).
- [96] M. Jacob. *Methods for the prediction of extreme vehicular loads and load effects on bridges*. 1990, 31 (p. 12).
- [97] S. Mohammadi and R. Mukherjee. "Wind Loads on Bridges: Analysis of a three span bridge based on theoretical methods and Eurocode 1". MA thesis. KTH, School of Architecture and the Built Environment (ABE), 2013 (p. 2).
- [98] G. Sedlacek et al. *Background document to EN 1991 Part 2 - Traffic loads for road bridges - and consequences for the design*. 2008, 105 (p. 12).
- [99] J. D. Sørensen. *Notes in Structural Reliability Theory And Risk Analysis*. Aalborg University. Aalborg, Denmark, 2004 (pp. 3, 26, 55).
- [100] X. Y. Zhou. "Statistical analysis of traffic loads and their effects on bridges". PhD thesis. Université Paris-Est, 2013 (pp. 9, 11, 16, 23, 24).

Software

- [101] *Ansys Workbench*. Version 19.2. Southpointe, USA, 2018. URL: <https://ansys.com> (p. 11).
- [102] Cestel. *SiWim software*. Slovenia, 2003. URL: <https://www.cestel.eu> (p. 11).
- [103] *MATLAB and Statistics Toolbox*. Version 2017.a. Natick, USA, 2017. URL: <https://mathworks.com> (p. 11).
- [104] C. Moler, J. Little, and S. Bangert. *MATLAB*. USA, 1984. URL: <https://mathworks.com> (pp. 11, 60, 69).
- [105] J. Swanson. *Ansys*. Version 2. Southpointe, USA, 1971. URL: <https://ansys.com> (pp. 11, 68).

Appendix A

Adapted methodologies

A.1 Wind load model according to European Standards

The general expression of a wind force F_w acting on a structure:

$$F_w = 0.5\rho v_b^2 c_e c_f A_{ref}, \quad (\text{A.1})$$

Where:

ρ is the air density, $\rho = 1.25 \text{ kg m}^{-3}$ is the recommended value,

v_b is the basic wind velocity, , see Eq. (A.5),

c_e is the exposure factor, that can be found from Eq. (A.2),

c_f is the force coefficient wind actions on bridge decks in the x-direction, recommended value $c_f = 1.3$),

A_{ref} is the reference area reference area of all the elements of the considered part of the bridge (the pylon, pile, deck, and cables) correspond to actual dimensions of the studied Millau viaduct.

$$c_e = \frac{(1 + 7I_v(z))0.5\rho V_m^2(z)}{0.5\rho v_b^2} \quad (\text{A.2})$$

where:

V_m is the mean wind velocity at a height z above the ground, see Eq. (A.4).

$I_v(z)$ is the turbulence intensity at height z :

$$I_v(z) = \frac{\sigma_v}{v_m(z)} = \frac{k_1}{c_0(z) \ln(z/z_0)} \quad (\text{A.3})$$

k_1 is the turbulence factor, recommended value is 1.0,

$c_0(z)$ is the oreography factor,

z_0 is the roughness length.

The mean wind velocity:

$$V_m(z) = c_r(z) c_0(z) v_b, \quad (\text{A.4})$$

where: $c_r(z) = 0.19(z_0/z_{0,II})^{0.07} \times \ln(z/z_0)$ is the roughness factor with z_0 - the roughness length, $z_0 = z_{0,II} = 0.05m$ in the case of Millau, $z_{min} = 2m$,

The basic wind velocity:

$$v_b = c_{prob} c_{dir} c_{season} v_{b,0} \quad (\text{A.5})$$

$v_{b,0}$ is the fundamental value of the basic wind velocity, defined as the characteristic 10 minutes mean wind velocity at 10 m above ground level in open country with low vegetation and few isolated obstacles (distant at least 20 obstacle heights), in the area of Millau the value $v_{b,0} = 24m/s$ as it is stated in National Annex, [6].

c_{dir} and c_{season} are the directional and seasonal factors, with recommended values 1.0,

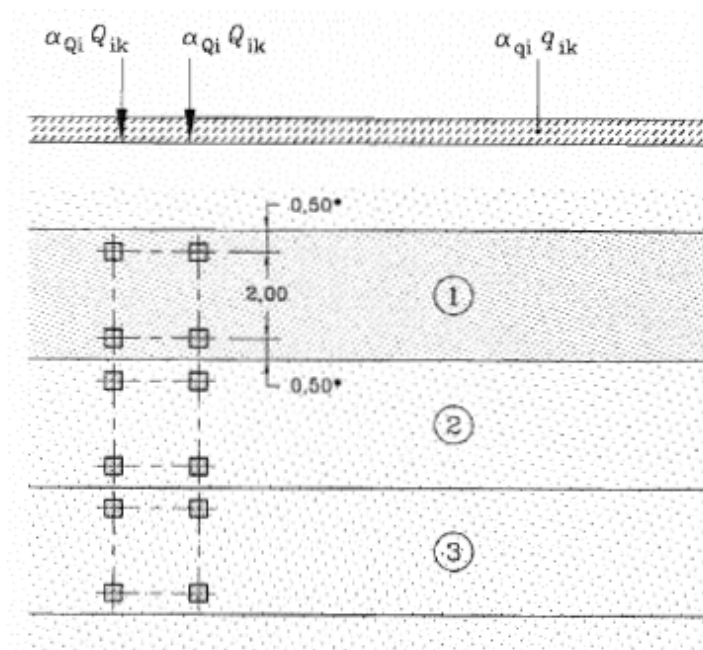
c_{prob} is a probability factor that should be used as the return period for the design of the Millau viaduct defers from $T = 50$ years. Considering a 2-% value of annual probability p of exceedance, parameters $K = 0.2$ and $n = 0.5$, then, $c_{prob} = 1.33$.

A.2 Traffic load model according to European Standards

Table A.1 and Figure A.1 show the extract from EN1991-2 "Eurocode 1: Actions on structures - Part 2: Traffic loads on bridges" that represents the traffic load model LM1.

| Location | Tandem system <i>TS</i> | <i>UDL</i> system |
|-----------------------------|--------------------------|--|
| | Axle loads Q_{ik} (kN) | $\boxed{\text{AC1}} q_{ik}$ (or q_{ik}) (kN/m ²) $\boxed{\text{AC1}}$ |
| Lane Number 1 | 300 | 9 |
| Lane Number 2 | 200 | 2,5 |
| Lane Number 3 | 100 | 2,5 |
| Other lanes | 0 | 2,5 |
| Remaining area (q_{ik}) | 0 | 2,5 |

TABLE A.1 – EN 1993-2 : 2003. Table 4.2. Load model 1 : characteristic values



Key

- (1) Lane Nr. 1 : $Q_{1k} = 300 \text{ kN}$; $q_{1k} = 9 \text{ kN/m}^2$
- (2) Lane Nr. 2 : $Q_{2k} = 200 \text{ kN}$; $q_{2k} = 2,5 \text{ kN/m}^2$
- (3) Lane Nr. 3 : $Q_{3k} = 100 \text{ kN}$; $q_{3k} = 2,5 \text{ kN/m}^2$

$\boxed{\text{AC1}}$ Tandem axle spacing = 1,2 m $\boxed{\text{AC1}}$

* For $w_l = 3,00 \text{ m}$

FIGURE A.1 – EN 1993-2 : 2003. 4.3.2 (3) Figure 4.2a. Application of load Model 1

A.3 Fatigue load model according to European Standards

Table A.2 and Figure A.2 show the extract from EN1993-1 "Eurocode 3: Design of steel structures - Part 1-9: Fatigue" that represents detail category 71 of the orthotropic deck.

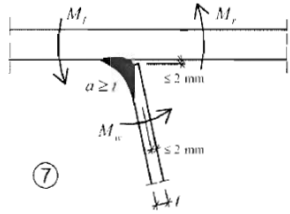
| Detail category | Constructional detail | Description | Requirements |
|-----------------|---|---|---|
| 71 |  | <p>$\Delta\sigma = \frac{\Delta M_w}{W_w}$</p> <p>Weld connecting deck plate to trapezoidal or V-section rib</p> <p>7) Partial penetration weld with $a \geq t$</p> | 7) Assessment based on direct stress range from bending in the plate. |

TABLE A.2 – EN 1993-1-9 : 2005. Table 8.8. Orthotropic decks - closed stringers

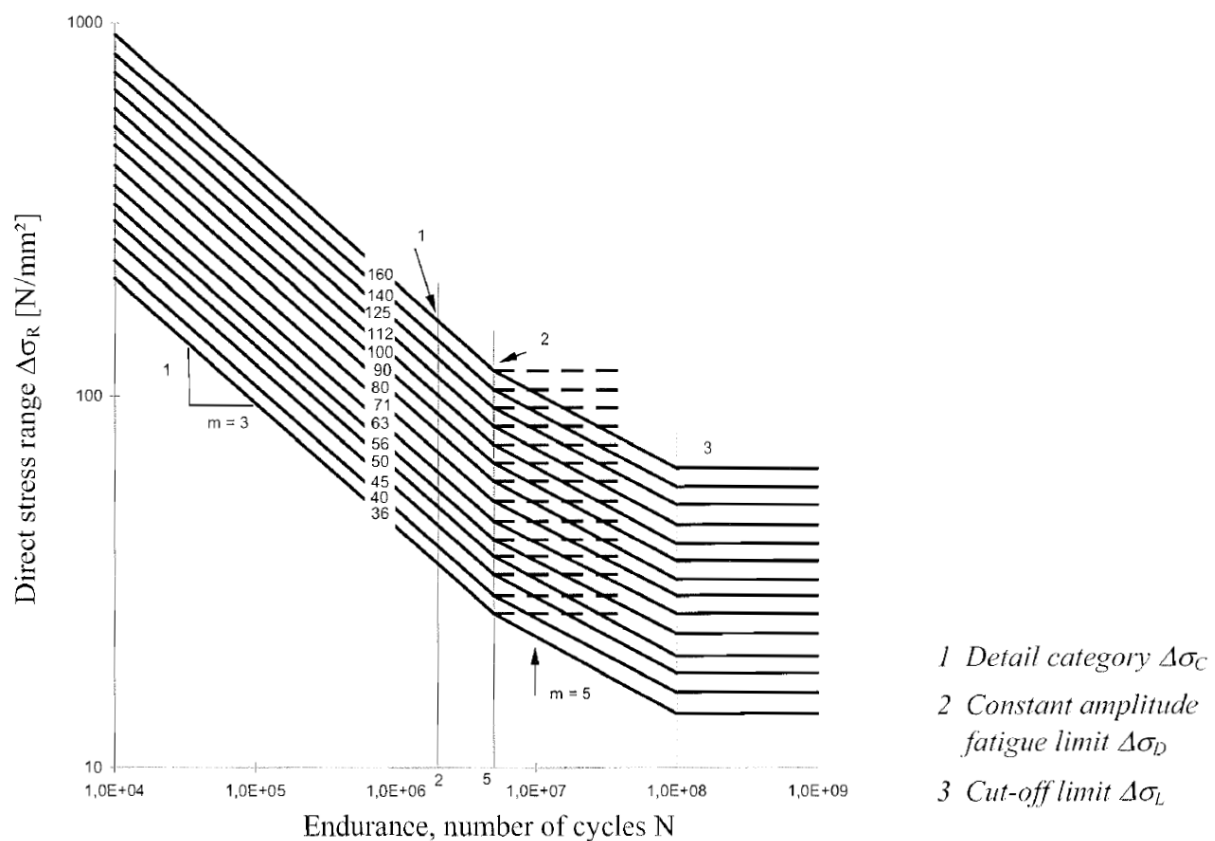


FIGURE A.2 – EN 1993-1-9 : 2005. 7.1 (3) Figure 7.1. Fatigue strength curves for direct stress ranges